

**STRUCTURAL BEHAVIOUR OF HIGH STRENGTH SELF
COMPACTING CONCRETE DEEP BEAMS**

MOHAMMAD MOHAMMADHASSANI

**THESIS SUBMITTED IN FULFILMENT
OF THE REQUIREMENTS
FOR THE DEGREE OF DOCTOR OF PHILOSOPHY**

**FACULTY OF ENGINEERING
UNIVERSITY OF MALAYA
KUALA LUMPUR**

2012

UNIVERSITY MALAYA

ORIGINAL LITERARY WORK DECLARATION

- (1) Name of Candidate: Mohammad Mohammadhassani
- (2) Registration/Matric. No: KHA080035
- (3) Name of Degree: Doctor of Philosophy

(4) Title of Thesis:

**“STRUCTURAL BEHAVIOUR OF HIGH STRENGTH SELF COMPACTING
CONCRETE DEEP BEAMS”**

Field of Study: Structural Engineering

I do solemnly and sincerely declare that:

- (1) I am the sole author/ writer of this work;
- (2) This work is original;
- (3) Any use of any work in which copyright exists was done by way of fair dealing and for permitted purposes and any excerpt or extract form, or reference to, or reproduction of any copyright work has been disclosed expressly and sufficiently and the title of the work and its authorship have been acknowledged in this work;
- (4) I do not have any actual knowledge nor do I reasonably know that the making of this work constitutes an infringement of any copyright work;
- (5) I hereby assign all and every rights in the copyright to this work to the University of Malaya (‘UM’), who henceforth shall be owner of the copyright in this work, and that any reproduction or use in any form or by any means whatsoever is prohibited without the written consent of UM having been first had and obtained;
- (6) I am fully aware that if in the course of making this work I have infringed any copyright whether intentionally or otherwise, I may be subject to legal action or any other action as may be determined by UM.

Candidate’s Signature

Date:

Subscribed and solemnly declared before,

Witness’ Signature

Date:

Name:

Designation:

Abstract

This study is motivated by the lack of clear design provisions for the design and behaviour of deep beams. The behaviour of deep beam is significantly different from normal beams. In deep beams, the plane section does not remain planar after deformation. Presented in this study are the results of serviceability and design criteria of eight simply supported high strength self compacting concrete (HSSCC) deep beams tested to failure with variation in web reinforcement and tensile reinforcement ratios. The deflection at two points along the beam length, the web strains, tensile bars strains and the strain at concrete surface at the height of mid span section were recorded in the experimental phase. Effective input data and the corresponding deflection and strain in tie section as output data were recorded in analytical phase at all loading stages up to failure load for all the deep beams. Adaptive Network-based Fuzzy Inference System (ANFIS) and Artificial Neural Network (ANN) were applied in this study as modelling tools to predict deflection and strain in tie section for HSSCC deep beams. The complexities and difficulties to predict the accurate behaviour of deep beams can be overcome by the use of these latest tools in the area of artificial intelligence and computational intelligence. Finite element modelling was used to determine the strain and neutral axis depth variation at the height of mid span section. The results clearly show that the distribution of horizontal strains and the stresses in deep beams are nonlinear and completely different from the linear distribution in normal beams. At the ultimate limit state, the stress distribution in concrete surface located in mid-span is no longer parabolic as in normal beams. Deep beams develop several neutral axes before ultimate failure is reached. The number of neutral axis decreases as load increases and reduces to one at failure load. The failure of deep beams with longitudinal tensile steel reinforcement less than that suggested by ACI codes is flexural with large deflections

and no inclined cracks. As the longitudinal tensile steel reinforcement increases, failure due to crushing of concrete at nodal zones was clearly observed. The appearance of first inclined crack in compression strut trajectory is independent of tensile and web reinforcement ratio variations. The modulus of rupture for HSSCC deep beams is close to the ACI 318-95 code. The first crack appeared at a load over 13 percent of the ultimate load in deep beams. ACI code provisions for the prediction of shear capacity of reinforced HSSCC deep beams are conservative. The Artificial neural network (ANN) displayed a superior ability in predicting mid span deflection with 10-10-4-1 and predicting strain in tie section of deep beam with 10-11-10-1 architectures. The suitability of ANN and ANFIS techniques in deflection prediction and tie strain prediction was evident when compared to Linear Regression (LR). ANN is more flexibility in training data compared to ANFIS while in term of incomplete data, ANFIS has proper response to unseen data. Finite element modeling shows a very good agreement with experimental data analysis and confirms the strain and neutral axes depth variation at the mid span section. Based on finite element modeling, the compressive strains were much less than 0.0025 in extreme compression fiber and less than 0.002 along the inclined compression struts.

Abstrak

Kajian ini didorong oleh kekurangan peruntukan reka bentuk yang jelas untuk reka bentuk dan tindakan rasuk tebal. Rasuk tebal mempunyai perbezaan tindakan yang ketara berbanding dengan rasuk biasa. Dalam rasuk tebal, keratan yang rata tidak kekal rata selepas perubahan bentuk. Kajian ini mempersembahkan hasil kajian kebolehhidmatan dan kriteria reka bentuk bagi lapan rasuk tebal Konkrit Tanpa Mampatan Berkekuatan Tinggi (HSSCC) disokong mudah yang diuji sehingga gagal dengan variasi dalam nisbah tetulang web dan tetulang tegangan. Pesongan bagi dua titik sepanjang rasuk, tegangan web, tegangan bar, dan tegangan di permukaan konkrit pada ketinggian keratan pertengahan rentang direkodkan pada fasa eksperimen. Data input yang efektif berserta dengan pesongan dan tegangan pada keratan gabungan sebagai data output telah direkodkan pada fasa analitikal di semua peringkat beban sehingga beban kegagalan untuk kesemua rasuk tebal. Rangkaian Ubah Suai berasaskan Sistem Inferens Kabur (ANFIS) dan Rangkaian Neutral Buatan (ANN) telah diaplikasikan dalam kajian ini sebagai peralatan-peralatan model untuk meramalkan pesongan dan tegangan bagi rasuk tebal HSSCC di keratan gabungan. Kerumitan dan kesukaran untuk meramalkan tindakan rasuk tebal yang tepat boleh diatasi dengan menggunakan peralatan-peralatan yang terkini ini dalam bidang kecerdasan buatan dan kecerdasan perkomputeran. Model unsur terhingga digunakan untuk mengenal pasti variasi tegangan dan kedalaman paksi neutral pada ketinggian keratan pertengahan rentang. Keputusan dengan jelasnya menunjukkan bahawa taburan tegangan mendatar dan tegangan dalam rasuk tebal adalah tak linear dan berbeza sama sekali dengan taburan linear dalam rasuk normal. Dalam keadaan had muktamad, taburan tegangan di permukaan konkrit yang terletak pada pertengahan rentang tidak lagi parabolik seperti yang terdapat dalam rasuk biasa. Rasuk tebal menyebabkan beberapa paksi neutral sebelum kegagalan muktamad dicapai. Bilangan paksi neutral berkurangan apabila

beban bertambah dan ia berkurang sehingga satu dalam keadaan beban kegagalan. Kegagalan rasuk tebal yang bertetulang keluli memanjang adalah lebih rendah daripada yang disyorkan dalam kod ACI dengan terdapatnya kelenturan dan pesongan yang besar serta tidak mempunyai retakan condong. Apabila tetulang keluli memanjang bertambah, kegagalan yang disebabkan oleh kehancuran konkrit pada zon pusat dapat diperhatikan dengan jelas. Kemunculan retakan condong pertama dalam trajektori topang mampatan adalah tidak bergantung pada variasi nisbah tegangan dan tetulang web. Pepecahan modulus bagi rasuk tebal HSSCC adalah berhampiran dengan yang terdapat dalam kod ACI 318-95. Retakan yang pertama wujud pada tahap beban 13 peratus daripada beban muktamad dalam rasuk tebal. Peruntukan kod ACI untuk meramalkan kapasiti ricih bagi rasuk tebal HSSCC yang bertetulang adalah konservatif. Rangkaian Neutral Buatan (ANN) menunjukkan kebolehan yang tinggi dalam meramalkan pesongan pertengahan rentang dengan 10-10-4-1 dan meramalkan tegangan di keratan gabungan bagi rasuk tebal dengan reka bentuk 10-11-10-1. Kesesuaian teknik ANN dan ANFIS dalam meramalkan pesongan dan tegangan gabungan adalah jelas apabila dibandingkan dengan Regresi Linear (LR). ANN adalah lebih fleksibel dalam melatih data berbanding dengan ANFIS, sementara daripada segi data yang tidak lengkap, ANFIS mempunyai respons yang lebih wajar bagi data yang tidak kelihatan. Model unsur terhingga menunjukkan hasil yang memuaskan dalam analisis data eksperimen dan mengesahkan variasi tegangan dan kedalaman paksi neutral pada keratan pertengahan rentang. Berdasarkan model unsur terhingga, tegasan mampatan adalah lebih rendah daripada 0.0025 dalam mampatan serat lampau dan rendah daripada 0.002 sepanjang topang mampatan yang condong.

ACKNOWLEDGEMENTS

First, I would like to extremely thank Prof Ir. Dr. Mohd Zamin Bin Jumaat for being my supervisor, for his encouragement, accompany, valuable advices and guidance during the time of study in University of Malaya.

Secondly, I would like to thank Dr Mohammed Jameel for his immense assistance which enables me successfully completes my thesis.

I would like to thank Dean of the faculty of engineering, Prof. Dr. Mohd Hamdi Bin Abd Shukor, Head of the civil engineering department, Prof Ir. Dr. Mohd Zamin Bin Jumaat, and the administrative staffs of the faculty and department.

I would also like to convey thanks to the University of Malaya for providing the financial means and laboratory facilities.

TABLE OF CONTENT

LIST OF TABLES.....	xiii
LIST OF FIGURES.....	xvi
LIST OF SYMBOLS.....	xxiii
1.0 Introduction	1
1.1 Scope	6
1.2 Objectives.....	6
1.3 Aims	7
1.4 Layout of thesis	7
2.0 Literature Review	8
2.1 Introductions	8
2.2 Failure mode of deep beams.....	9
2.3 Neutral Axis Depth (NAD) variation.....	12
2.3.1 Modulus of Rupture and First Bending Crack.....	15
2.4 Material properties and their effect.....	16
2.4.1 High-Strength-Self-Compacting-Concrete (HSSCC)	16
2.4.2 High Strength Steel (HSS) reinforcement.....	17
2.5 Strain variation.....	19
2.5.1 Strain variation in tie section.....	19
2.6 Shear strength of deep beams.....	24
2.7 Numerical studies	27
2.7.1 Artificial Neural Network (ANN).....	28
2.7.2 Adaptive Network-based Fuzzy Inference System (ANFIS)	30

2.7.3	Review on related works by comparing ANFIS and ANN models	31
3.0	Material and Method	33
3.1	Test program.....	33
3.2	Materials and material properties	33
3.2.1	Steel properties.....	33
3.2.2	High Strength Self Compacting Concrete.....	36
3.3	Deep Beam Details.....	41
3.3.1	Individual Beam Testing Details.....	43
3.3.1.1	Detail of specimen B1.....	43
3.3.1.2	Detail of specimen B2.....	44
3.3.1.3	Detail of specimen B3.....	45
3.3.1.4	Detail of specimen B4.....	46
3.3.1.5	Detail of specimen B5.....	47
3.3.1.6	Detail of specimen B6.....	48
3.3.1.7	Detail of specimen B7.....	49
3.3.1.8	Detail of specimen B8.....	50
3.4	Test setup and loading process.....	51
3.5	Instrumentation	52
3.5.1	Overview.....	52
3.5.2	Strain gauges.....	53
3.5.3	Data acquisition system.....	57
3.6	Methodology of Numerical Study.....	57
3.6.1	Adaptive Network-based Fuzzy Inference System (ANFIS).....	57
3.6.1.1	Data availability.....	58
3.6.1.2	System Modeling.....	59
3.6.1.3	Fuzzy Expert System.....	60

3.6.1.4 Fuzzy Inference System (FIS).....	62
3.6.1.5 Adaptive network-based fuzzy inference system (ANFIS).....	65
3.7 ANNs structure and definition.....	67
3.7.1 Evaluation.....	68
3.7.2 Training and testing of Neural Networks	68
3.7.3 Variants of Back-propagation Learning Algorithm.....	71
4.0 Results and discussion.....	72
4.1 Experimental study and discussion.....	72
4.1.1 Horizontal strain distribution at the height of mid-span in HSSCC deep beams.....	72
4.1.2 Modulus of Rupture.....	80
4.1.3 Failure Modes and Serviceability of HSSCC Deep Beams.....	94
4.1.3.1 Flexural failure in deep beams.....	95
4.1.3.2 Shear failure in deep beams.....	96
4.1.3.3 Combined flexural and Shear failure in deep beams.....	98
4.1.3.4 Local failure of deep beams.....	99
4.1.3.5 Compression failure of deep beams	100
4.1.4 Serviceability of deep beams.....	100
4.1.5 Behaviour and shear resistance of HSSCC deep beams reinforced with HSS	102
4.1.6 Experimental assessment of shear capacity and comparison with ACI code approaches.....	113
4.1.7 Ductility and performance assessment in HSSCC deep beams: An experimental investigation.....	119
4.1.7.1 Ductility measurement by curvature method.....	120

4.1.7.2 Ductility index based on deflection measurements.....	128
4.2 Numerical Study	130
4.2.1 Application of artificial neural network (ANN) and linear regressions (LR) in predicting the deflection of concrete deep beams	130
4.2.1.1 The Best learning function and optimum architecture of MLFFNN.....	128
4.2.2 Application of Adaptive Network-based Fuzzy Inference System for Prediction of deflection in HSSCC deep beams.....	138
4.2.2.1 Development of ANFIS model for the prediction of deflection of deep beam.....	139
4.2.3 Comparison of ANN and ANFIS in deflection prediction.....	143
4.2.4 Application and Comparison of (ANN), ANFIS and (LR) in predicting the strain in tie section of concrete deep beams	143
4.2.4.1 Introduction.....	143
4.2.4.2 Experimental Result.....	145
4.2.4.3 The Best learning function and optimum architecture of MLFFNN.....	148
4.2.4.4 Developing the ANFIS model for the prediction of strain in tie section of deep beam.....	155
4.3 Application of ANFIS in shear strength prediction of deep beams.....	159
5.0 Nonlinear finite element analysis.....	166
5.1 Introduction.....	166
5.2 Material properties.....	166
5.2.1 Concrete.....	166
5.2.2 Steel.....	167
5.3 Elements	169
5.3.1 Plane stress element.....	169
5.3.2 Beam element.....	170

5.4 Finite Element Models.....	170
5.5 Finite Element results.....	171
5.6 Summary.....	181
6.0 Conclusion.....	184
7.0 References	189

University of Malaya

LIST OF TABLES

Table caption	page
Table 3.1 Bar specifications.....	34
Table 3.2 HSSCC mix design.....	37
Table 3.3 Specification of tested deep beams.....	40
Table 3.4 Bar schedule specification of deep beams.....	42
Table 3.5 Different parameters of the eight HSSCC deep beams for deflection prediction.....	58
Table 3.6 Different parameters of the eight HSSCC deep beams for tie strain prediction.....	59
Table 3.7 BPs learning functions used in this study.....	71
Table 4.1 Corresponding load to first flexural crack	91
Table 4.2 Corresponding experimental moment and the modulus of rupture of deep beams	92
Table 4.3 Comparison of the various modulus of rupture.....	93
Table 4.4 Ratio of first inclined crack load to ultimate load.....	97
Table 4.5 Strain in extreme compression fiber of concrete and along the tensile bar.....	106
Table 4.6 Reserve strength of tested HSSCC deep beams.....	110
Table 4.7 Absorbed energy of tested deep beams.....	113
Table 4.8 Comparison of experimental and theoretical shear strength of tested HSSCC	

deep beam.....	115
Table 4.9 Shear stress of tested HSSCC deep beam correspond to first inclined crack.....	117
Table 4.10 Strain distribution at the mid span height of beam length at yield and ultimate loading state.....	122
Table 4.11 Tensile reinforcement ratio of the code limit and the bars used	126
Table 4.12 Web reinforcement ratio for tested deep beams.....	128
Table 4.13 Ductility assessment of tested deep beams.....	129
Table 4-14 Performance of different type of BPs on prediction of deflection.....	132
Table 4-15 Performance of different type of BPs on prediction of deflection.....	132
Table 4.16 The optimum network specification.....	136
Table 4.17 Comparison of MSE and R values from ANN and Linear Regression.....	137
Table 4.18 Comparison of MSE and R values from ANFIS and Linear Regression..	140
Table 4.19 Performance of different type of BP on prediction of tie strain	149
Table 4.20 Performance of different type of BP on prediction of tie strain.....	150
Table 4.21 The optimum network specification.....	153
Table 4.22 Comparison of MSE and R values from ANN and LR.....	154
Table 4.23 Comparison of MSE and R values from ANFIS and LR.....	156
Table 4.24 Datasets of published works.....	160
Table 4.25 Different parameters of the eight HSSCC deep beams.....	163

Table 4.26 Comparison of MSE and R values in ultimate shear prediction of deep beams using ANFIS and LR.....	164
Table 5.1 Comparison of experimental and FE measured value of failure loads of the test samples.....	182

University of Malaya

LIST OF FIGURES

Figure Caption	page
Figure 2.1: Variation of strain and stress along bottom length of deep beams (GEER, 1960).....	13
Figure 2.2: Concrete strain variation at mid-span and plane of rupture of a typical deep beam with web openings (Ray 1980, 1982.).....	14
Figure 2.3: Definition of struts and tie in strut and tie model (STM).....	19
Figure 2.4: STM model for ACI code design.....	21
Figure 3.1: Deformed and non-deformed steel bar in beam B2.....	34
Figure 3.2: Stress strain curve for NSS reinforcing bar (Ø9mm).....	35
Figure 3.3: Comparison of typical stress-strain curves for HSS and NSS reinforcing steel. [After EI-Hacha and rizkalla, 2002].....	36
Figure 3.4: Workability slump value.....	38
Figure 3.5: Splitting test of used HSSCC.....	39
Figure 3.6: Casting arrangement of deep beam.....	40
Figure 3.7: General geometrical specifications of deep beams.....	42
Figure 3.8: Detail of beam tested B1.....	43
Figure 3.9: Detail of beam tested B2.....	44
Figure 3.10: Detail of beam tested B3.....	45
Figure 3.11: Detail of beam tested B4.....	46
Figure 3.12: Detail of beam tested B5.....	47
Figure 3.13: Detail of beam tested B6.....	48

Figure 3.14: Detail of beam tested B7.....	49
Figure 3.15: Detail of beam tested B8.....	50
Figure 3.16: Experimental setup for HSSCC deep beams.....	51
Figure 3.17: Strain gauges location of beam B1.....	53
Figure 3.18: Strain gauges location of beam B2.....	54
Figure 3.19: Strain gauges location of beam B3.....	54
Figure 3.20: Strain gauges location of beam B4.....	55
Figure 3.21: Strain gauges location of beam B5.....	55
Figure 3.22: Strain gauges location of beam B6.....	56
Figure 3.23: Strain gauges location of beam B7.....	56
Figure 3.24: Strain gauges location of beam B8.....	57
Figure 3.25: System modelling using an adaptive intelligent system.....	60
Figure 3.26: An example of: (a) classical Boolean set, and (b) Fuzzy Logic set.....	62
Figure 3.27: A flow diagram of a fuzzy inference system (FIS).....	63
Figure 3.28: ANFIS architecture.....	65
Figure 3.29: Neuron model with n-element in the input model.....	69
Figure 3.30: Single-layer and Multi-layer networks.....	70
Figure 4.1: NAD variation at mid-span at different loading stage for B1.....	73
Figure 4.2: NAD variation at mid-span at different loading stages for B2.....	74
Figure 4.3: NAD variation at mid-span at different loading stages for B3.....	75

Figure 4.4: NAD variation at mid-span at different loading stages for B4.....	76
Figure 4.5: NAD variation at mid-span at different loading stages for B5.....	77
Figure 4.6: NAD variation at mid-span at different loading stages for B6.....	78
Figure 4.7: The principle of St-Venant: (a) zone of a body affected by self-equilibrating forces at the surface; (b) application to a prismatic bar (beam) loaded at one face. [(Schlaich and Schäfer, 1991) and (Schlaich et al., 1987)].....	81
Figure 4.8: B-regions and D-regions.....	82
Figure 4.9: Load transferring mechanism in deep beams.....	83
Figure 4.10: Common types of strut, (a) Prism (b) Bottle (c) Fan.....	85
Figure 4.11: Crack progressions in B1.....	86
Figure 4.12: Crack progressions in B2.....	87
Figure 4.13: Crack progression in B3.....	87
Figure 4.14: Crack progression in B4.....	88
Figure 4.15: Crack progressions in B5.....	88
Figure 4.16: Crack progressions in B6.....	89
Figure 4.17: The (a) shear diagram and (b) moment diagram of tested deep beams.....	90
Figure 4.18: general crack progress in tested deep beams (Rigotti, 2002).....	94
Figure 4.19: Typical crack pattern of deep beams with two point loading.....	95
Figure 4.20: Crack pattern for beam B2.....	97
Figure 4.21: Crack pattern for beam B5.....	98
Figure 4.22: Load-deflection curve of tested deep beams.....	101
Figure 4.23: Comparison of steel bar behaviour by different strength.....	103
Figure 4.24: Comparison of stress and strain behaviour of ductile and brittle materials.....	104

Figure 4.25: Stress–strain relationships of NSC and HSC (following (Kani, 1966))...	105
Figure 4.26: Failure of beam B7.....	111
Figure 4.27: Failure of beam B8.....	112
Figure 4.28: Comparison of shear strength component and ACI code provision.....	116
Figure 4.29: Definition of ductility.....	120
Figure 4.30: Yield curvature (ϕ_y) and ultimate destructive curvature (ϕ_{uf}) in bending section.....	121
Figure 4.31: The MSE value for different number of neurons in first hidden layer.....	133
Figure 4.32: The R value for different number of neurons in first hidden layer.....	134
Figure 4.33: The MSE values for different number of neurons in second hidden layer.....	135
Figure 4.34: The R values for different number of neurons in second hidden layer.....	135
Figure 4.35. Deflection prediction performance from a) LR b) ANN.....	138
Figure 4.36. Deflection prediction performance from a) Linear regression b) ANN....	141
Figure 4.37: Fuzzy surface: Tensile reinforcement ratio and yield strength of tensile bar vs. deflection prediction.....	142
Figure 4.38: Fuzzy surface: Tensile reinforcement ratio and load vs. deflection prediction.....	142
Figure 4.39: Strut and Tie model for design using appendix A of ACI code.....	144
Figure 4.40: Strain variation along the Tie section of B1.....	145
Figure 4.41: Strain variation along the Tie section of B2.....	146

Figure 4.42: Strain variation along the Tie section of B3.....	146
Figure 4.43: Strain variation along the Tie section of B4.....	147
Figure 4.44: Strain variation along the Tie section of B6.....	147
Figure 4.45: Strain variation along the Tie section of B7.....	148
Figure 4.46: The MSE value for different number of neurons in first hidden layer.....	151
Figure 4.47: The R value for different number of neurons in first hidden layer.....	151
Figure 4.48: The MSE values for different number of neurons in second hidden layer.....	152
Figure 4.49: The R values for different number of neurons in second hidden layer.....	153
Figure 4.50: Tie strain prediction performance from (a) ANN, (b) LR.....	155
Figure 4.51: Tie strain prediction performance from a) LR b) ANFIS.....	157
Figure 4.52: Fuzzy surface: Tensile bar percentage and yield strength of tensile bar versus strain in Tie prediction.....	158
Figure 4.53: Fuzzy surface: Tensile bar percentage and load versus strain in Tie prediction.....	158
Figure 4.54: Ultimate shear prediction performance from a) ANFIS b) LR.....	165
Figure 5.1: Concrete stress-strain curve used in the finite element analysis.....	167
Figure 5.2: Methods of steel reinforcement modeling in concrete.....	168
Figure 5.3: Eight node three dimensional element.....	169
Figure 5.4: Two node beam element used to model the steel reinforcement.....	170
Figure 5.5: The finite element modeling.....	171

Figure 5.6: Comparison of experimental and FE analysis of deflection for beam B1..	172
Figure 5.7: Comparison of experimental and FE analysis of deflection for beam B2..	172
Figure5.8: Comparison of experimental and FE analysis of deflection for beam B6..	173
Figure 5.9: Deflection of beam B1 as determined by the FE analysis at a loading of 215Kn.....	173
Figure5.10: Deflection of beam B1 as determined by the FE analysis at a loading of 402kN.....	174
Figure 5.11: Deflection of beam B1 as determined by the FE analysis at a loading of 510kN.....	174
Figure 5.12: Deflection of beam B2 as determined by the FE analysis at a loading of 743kN.....	175
Figure5.13: Deflection of beam B6 as determined by the FE analysis at a loading of 1100kN.....	175
Figure 5.14: NAD variations at mid-span at different loading stage for beam B1 using FE modeling.....	176
Figure 5.15: NAD variations at mid-span at different loading stage for beam B2 using FE modeling.....	177
Figure 5.16: NAD variations at mid-span at different loading stage for beam B6 using FE modeling.....	178
Figure 5.17: Compressive stresses at a loading of 215.8kN for beam B1.....	179
Figure 5.18: Compressive stresses at a loading of 401kN for beam B1.....	179

Figure 5.19: Compressive stresses at a loading of 510kN for beam B1.....180

Figure 5.20: Compressive stresses at a loading of 743kN for beam B2.....180

Figure 5.21: Compressive stresses at a loading of 1100kN for beam B6.....181

University of Malaya

LIST OF SYMBOLS

l/h = Span/depth ratio

a/h = Shear-span/depth ratio

f_y = Strength of tensile bar at yielding condition

f_{yv} = Yield strength of vertical web reinforcement

f_{yh} = Yield strength of horizontal reinforcement

ρ = Tensile reinforcement percentage

ρ_{\min} = Minimum Tensile reinforcement percentage

ρ_b = Balance reinforcement ratio

f_{cu} = Concrete cylinder strength

b_w = Beam width

d = Effective depth

f'_c = Concrete compressive strength of cube samples

A_s = Area of longitudinal main reinforcement

I_g = Moment of inertia of gross concrete section

f_u = Ultimate strength of bars

E_s = Modulus of elasticity of bars

$\emptyset =$ Diameter

$f_t =$ Tensile strength of splitting test of cylinder samples

$f_r =$ Modulus of rupture

$P =$ Applied load

$y_t =$ Distance of extreme tension fibre from the neutral axis

$l_0/d =$ Ratio of effective span to effective depth of beams

$A_v =$ Area of vertical bar

$s_v =$ Vertical bar distance

$A_h =$ Area of horizontal bar

$s_h =$ Horizontal bar space

$\Delta =$ Deflection at the mid-span

$\varepsilon =$ Strain in Tie section

$\varepsilon_y =$ Strain in the tie section at the yield of tensile bar

$\varepsilon_{cy} =$ Strain in extreme compression fiber when tensile bar reaches yield state

$\varepsilon_{su} =$ Strain in tie section at ultimate yield state

$\varepsilon_{cu} =$ Strain in extreme compression fiber at ultimate state

$\phi_u =$ Ultimate curvature when the concrete compression strain reaches a specified limit

ϕ_y = the curvature amount when the tension reinforcement first reaches its the yield strength

$y(k)$ = Noisy output of the actual system

$\hat{y}(k)$ = The adaptive intelligent system output

$d(k)$ = The desired output

L = The number of instances

X = Input Vector

University of Malaya

1.0 INTRODUCTION

Reinforced concrete (RC) is a non-homogeneous and elastic material (British Standards Institution, 1985). However, in current design practice the structural analysis of RC elements is generally based on the conventional assumption that plane sections remain planar after loading and that the material is homogeneous and elastic; linear elastic methods of analysis are adopted for the design of reinforced concrete beams. Design engineers of concrete structures often encounter sections of a structure that are subject to significant shear stresses. The conventional design assumption is not applicable to such locations. One such structure is the deep beam. Deep beams are widely used as structural elements and have many structural applications such as transfer girders, offshore structures, pile caps, foundation walls and in nuclear power plant containment structures. The change in behaviour from a normal beam to that of a deep beam is imprecise, and in terms of design it occurs at a span/depth ratio of about 2.5 (Kong, 2003). In the past, deep beams were defined using its span/depth ratio (l/h) and shear-span/depth ratio (a/h) (Kong & Singh, 1972).

Existing design codes have varying definitions of a deep beam. The ACI318-05 code (American Concrete Institute, 2005), CEB-FIP model code (1978) and CIRIA Guide 2 (1997) use a span/depth ratio limit to define RC deep beams, but CSA 94 (1994) employs the concept of a shear span/depth ratio. ACI defines deep beams as beams with clear span to effective depth ratios less than 5. The CEB-FIP model code treats simply supported beams of span/depth ratios less than 2.0 as deep beams. The CEB-FIP model code also recognises continuous beams of span/depth ratios less than 2.5 as deep beams. The CIRIA Guide (1977) applies to beams with an effective span/depth ratio l/h of less than 2.0 for single-span beams and less than 2.5 for continuous beams.

Due to the inconsistencies in the definition of a deep beam, existing design codes of practice are lacking. For example, the British code, BS8110 (1985), explicitly states that, for the design of deep beams, reference should be made to specialist literature. Other codes such as the ACI (ACI 318-05), the Canadian code (CSA A23.3-04) and the CIRIA guide No. 2b (CIRIA, 1997) present some design guidelines based solely on experimental data, with no theory explaining it. These varying definitions, the lack of clear design provisions and uncertainty over the behaviour of deep beams are the motivation behind this study.

It is common design practice to first design an RC beam for flexure and prevent any other types of failure that might occur once the flexural capacity is attained. The flexural capacity is assessed on the basis of the plane sections theory, the Euler-Bernoulli theory. Based on this theory, the main assumption for normal beams is that 'plane sections remain plane after bending'. In other words, any deformation due to shear (common in deep beams) is not accounted for in this theory because a plane section after shear deformation is no longer planar.

To identify the internal force distributions in beams, the beams are divided into regions B and D, where the B-region is the Beam or Bernoulli region and the D-region is the Disturbed or Discontinuity. The ACI code defines B and D regions in deep beams based on the Saint-Venant strain distribution which states that a localised disturbance such as a concentrated load will dissipate within one beam height from the load point. The discussion of these regions is vital in understanding the internal distribution of forces and stresses in a RC elements. ACI code defined D-regions (Disturbed or Discontinuity) as regions adjacent to the concentrated load points that are affected by abrupt change in load and reactions points or adjacent to abrupt changes in geometry, such as internal holes or changes in cross-section. In D-regions, the strain distributions are not linear.

For structural members where plane sections are non-planar after bending, i.e. deep beams, the strain distribution is nonlinear and therefore the linear approach does not apply. The elastic stress distribution in a D-region is difficult to determine and it changes as cracks progress. Schlaich et al. (1987) introduced a design method based on plasticity theory using a Strut and Tie Model (STM).

In structural elements such as deep beams, shear deformation is a significant main deformation that occurs before flexural capacity is attained. Thus the serviceability and failure pattern of these structural elements are different from normal beams. Investigation on the failure mode of deep beam has gained importance with the discovery of latest innovation in material technology.

There are two types of steel reinforcement, NSS and HSS. In the past, design methods and analysis for concrete elements involved normal strength concrete (NSC) with normal steel strength (NSS) as reinforcement. With the recent developments in material technology, the application of HSC and HSS are in practice as they reduce the quantity of raw material and reinforcement needed. HSS and NSS are different in terms of mechanical properties; NSS has a clear yield point but for HSS, which is more brittle, the yield point is unclear.

High-strength-self-compacting-concrete (HSSCC) is a type of high strength concrete (HSC). In HSSCC, the difference between the elastic modulus and the strength of aggregates and matrix are relatively small compared to NSC. Moreover, in NSC the behaviour is linear up to 40 percent of the maximum stress, while it is about 85 percent in HSSCC sections (Iravani, 1996; Mohammadhassani et al., 2011b). Compared to NSC, the behaviour of HSSCC is linear elastic with a brittle failure mode. The use of HSS to reinforce HSSCC affects its structural performance and failure modes. Recently research has been carried out to study the behaviour of concrete elements reinforced

with HSS. Malhas (2002) and Vijay et al. (2002) validated the current design method for flexure-critical slender beam with HSS. Since the current design code provisions are based on studies focused on NSC and NSS, ACI 318-05 sets a limit for the yield strength of bar (f_y) of 550 MPa for longitudinal reinforcement and 410 MPa for shear reinforcement. For HSS, these current design code provisions have to be investigated for higher values of f_y .

Due to their geometry and dimensions, deep beams behave two-dimensionally rather than one-dimensionally, and are thus subjected to a two-dimensional state of stress. Thus it is important to investigate the neutral axis depth variation and the modulus of rupture in deep beams. The appearance of the first crack is indicative of when the concrete in deep beams changes from elastic to plastic behaviour in the tension zone. In this regard, the stress and strain distribution along the deep beam length is different from that in normal beams.

The stress and strain distributions in deep beams are nonlinear; hence the prediction of stress, strain and design parameters is not simple. With the ongoing development in the field of computer science in artificial intelligence and computational intelligence, researchers are able to apply them successfully in the construction industry. Given the complexities in deep beam behaviour and the difficulties in the accurate evaluation of its deflection, the use of artificial intelligence is highly preferred. Artificial Neural Network (ANN) has been established and acknowledged as a powerful tool in pattern recognition, signal processing and control and complex mapping, because of its excellent learning capacity and high tolerance to errors (Kao & Hung, 2003 and Masri et al, 2002). In structural engineering, ANNs have been successfully applied to various applications. ANNs are applied to solve these aforementioned problems, especially in modelling, curve fitting, forecasting, prediction, approximation and system

identification that are not easily solved using conventional engineering calculations. ANNs are able to model engineering systems using only the input/output observed data without requiring additional assumptions. The main characteristics of ANNs are their adaptive ability. This means that they can provide surprising results to unseen data after good training.

Fuzzy-neural systems are part of an intelligent system which combines significant characteristics of ANNs and fuzzy inference systems (FIS) to construct powerful tools for computing. ANFIS (Adaptive Network-based Fuzzy Inference System) uses ANN theory in order to determine the properties (fuzzy membership functions and fuzzy rules) of data samples in the learning of a fuzzy inference system. In ANFIS, a fuzzy inference system is implemented through a feed-forward network and a hybrid learning method including back propagation theory from ANNs, and the recursive least square (RLS) method and clustering techniques are used together to construct the FIS according to data appropriately. In other words, ANFIS combines fuzzy logic and ANNs, by utilising the mathematical properties of ANNs in tuning rule based fuzzy inference systems that approximate the way the human brain processes information. ANFIS has shown significant promise in modelling nonlinear systems where it is able to learn features of the data set and adjusts the system characteristics accordingly to a given error criterion (Jang, 1993). Like ANN, ANFIS is capable of mapping unseen inputs to their outputs by learning the rules from the previously seen data. The determined values of physical parameters (input) and the real values of deflection and strain in tie sections (output) are used to train the fuzzy neural network.

In order to study the strain distribution across the height of mid span section the Finite element model is created using the finite element software. The finite element analysis determined that the horizontal strain distribution in the height of mid-span were

nonlinear before ultimate load. However, the stresses in tension area were uniformly disturbed.

1.1 Scope

The scope of this work is to study the serviceability and design criteria of HSSCC deep beams by experimental and analytical methods.

1.2 Objectives

The following below are the objectives of present research work.

- i) To investigate the non-linear strain distribution across mid-span section of HSSCC deep beams so that a designer can use appropriate maximum strain values for designing important elements of deep beams such as horizontal strut, inclined struts, tie sections, etc. Further to study the variation of neutral axis depth for understanding the tension behaviour in web region of deep beams.
- ii) To understand all the failure modes and crack progress of HSSCC deep beams having wide range of tensile and web reinforcement ratios.
- iii) To study the load deflection behavior of HSSCC deep beams reinforced with HSS bars
- iv) To investigate the shear capacity of HSSCC deep beams reinforced with HSS and validate the applicability of ACI code provisions.
- v) To employ AI as modelling tool for predicting strains and deflections of HSSCC deep beams due to its ability as a machine to learn and think from experience and perform tasks attributed to human intelligence for complex behaviour of deep beams.

- vi) To develop and validate mathematical model for deep beam using finite element method. The model can be used to predict the behaviour of deep beams having complex geometry, various loading conditions, different materials and boundary conditions.

1.3 Aim

With the objectives highlighted in Subchapter 1.2, this study aims to contribute towards the better understanding of strain distribution in HSSCC deep beams, and develop a numerical prediction for strain and deflection at the mid-span using artificial intelligence and the modelling of deep beams using FE software.

1.4 Layout of Thesis

This thesis comprises six chapters describing a research project focused on the behaviour and analysis of HSSCC deep beams reinforced with HSS.

Chapter 2 presents the literature review on previous research and applications for reinforced concrete members with HSSCC and HSS, strain distribution and failure modes. Also included is a literature review on applying artificial intelligence in predicting civil engineering problems and related issues.

Chapter 3 presents the methodology and descriptions of the experimental program carried out in this project. It contains the detailing, fabrication, instrumentation and test setup of the specimens. The properties of the steel bar and concrete used in this project are also presented in this chapter.

Chapter 4 reports the results and discussion of the experimental and numerical analysis.

Chapter 5 provides the results and discussion on the FE modelling of the deep beams tested. Chapter 6 concludes the findings of this study.

2.0 LITERATURE REVIEW

This chapter will outline some of the significant studies conducted on reinforced concrete deep beams, focusing on the strain distribution at the height of the mid-span section and along the tie section of HSSCC deep beams, the neutral axis depth, failure modes, shear capacity and use of ANN and ANFIS.

2.1 Introduction

Deep beams are very common construction components, which are often used in civil and maritime engineering to carry loads over a wide area. These components have practical applications in many structures such as tall buildings, foundations, offshore structures. Floor slabs under horizontal loading and some shear walls are also examples of deep beam applications. They are sometimes used for load distribution, for example as transfer girders, pile caps, folded plates and foundation walls. They are often designed to carry bending moments about the strongest axis only. These elements are loaded similarly to normal beams, but differ in terms of shear span/depth ratio. Compared to normal beams (NB), deep beams have relatively smaller span/depth ratios. In NBs, the beam can collapse after a diagonal tension failure but in deep beams the beams are able to carry more loading even after diagonal cracking. This is due to the formation of arch action. When a deep beam fails, crushing of concrete is noted around the loading points or supports.

Deep beam sections usually have two moments of inertia axes, and one is a much stronger-axis than the other. Traditional design assumptions, especially regarding the plane section remaining planar after bending for NBs, do not apply to deep beams. The transition from reinforced concrete NB behaviour to that of deep beams is imprecise (Kong, 2003). For example, while the ACI code (ACI318-83, 2008), CEB-FIP (1978) model code and CIRIA Guide 2 (1977) use a span/depth ratio limit to define RC deep

beams, the Canadian codes (CAN/CSA A23.3-04) employ the concept of shear span/depth ratio. ACI (ACI 318-83, 2008) defines beams with clear span to effective depth ratios less than 5 as deep beams, whereas the CEB-FIP (1978) model code treats simply supported and continuous beams with span/depth ratios less than 2 and 2.5 respectively as deep beams. However, their design is not yet covered by BS8110 (1985), which explicitly states that 'for the design of deep beams, reference should be made to specialist literature'. Currently, the main design documents applied to deep beams are ACI 318-08, CAN-A23.3-04, the CEB-FIP model code (1978) and CIRIA Guide 2 (1977). The CIRIA Guide gives the most comprehensive recommendations and is the only one that covers the buckling strength of slender beams.

Usually, RC beams that have a shear span to effective depth ratio not exceeding 2.50 are commonly referred to as short beams or deep beams. Due to their geometric proportions, the capacity of these RC beams is mainly governed by shear strength rather than flexure. During shear failure, a tied-arch forms after diagonal cracking.

2.2 Failure Mode of Deep Beams

The failure behaviour of deep beams is significantly different from that of NBs due to the difference in geometry and load transfer mechanism. Shear action in deep beams lead to compression in the diagonal direction and tension in the perpendicular direction. It is this difference in the load transferring mechanism that leads to different behaviour in deep beams. The serviceability and failure pattern of these structural elements is not reported extensively due to the lack of clear procedure for behaviour prediction. Several possible modes of failure in deep beams have been identified from physical tests, and the shear failure mode appears to be most significant due to the deep beams' geometrical dimensions. The disturbance of internal stresses due to heavy concentrated loads causes a drop in the load-carrying capacity of the deep beams and results in

sudden shear failure as the overall depth of beam section increases. The shear action leads to compression in a diagonal direction and tension in a perpendicular direction.

De Paiva and Siess (1965) investigated 19 small-scale deep beams with depths varying from 178 mm to 330 mm with a span of 610 mm (span to depth ratios between 3.43 and 1.85). Positive anchorage was provided to the tension reinforcement by welding of steel plates to the end of the bars, thus eliminating anchorage failure. From their work, the following observations were made:

a) Increasing the concrete strength had a negligible effect on beam failure as a result of yield in the tension reinforcement and increased the load capacity of beams failing in shear, and in some cases changed the mode of failure from shear to flexure.

b) Increasing the amount of tension reinforcement increased the load capacity of the beams and changed the mode of failure from flexure to shear.

Leonhardt and Walther (1966) showed that for top loaded beams with $l/d \leq 2$, failure is caused by the crushing of concrete near the supports (in the bearing zone). As part of their experimental investigations, Leonhardt and Walther (1966) also measured the deflection along the bottom chord of their deep beams. The results showed that at ultimate loads, the deflection of the beams was small, and thus compared to NBs deep beams were inflexible, i.e. brittle. Small differences in support settlements may lead to a large redistribution of internal forces. Consequently movements caused by secondary effects such as foundation movements or axial shortening of columns, normally acceptable in structures with NBs, may prove more critical for structures with deep beams.

Ramakrishnan and Ananthanarayana (1968) tested 26 single span simply supported reinforced concrete deep beams with a span of 686 mm and depths of 381, 508, 572 and 762 mm (span to depth ratios of 1.8, 1.35, 1.2 and 0.9 respectively). The most dominant

mode of failure was diagonal tension (shear). In this mode, a clean break occurred between the load and outside edge of the reaction plate. Other failure modes included diagonal compression, splitting of the compression zone and flexure-shear.

Smith and Vantsiotis (1982) indicated that the strain in the region of maximum bending moment in deep beams are almost uniform at each loading levels, and that failure occurred with the yielding of the main longitudinal bars.

Ansley (2002) compared the behaviour of NBs of same geometry reinforced by NSS and HSS. It was concluded that at the time of failure, based on an area below the load-deflection response, the beams reinforced with HSS resisted 76% additional load and ductility increased by 40% compared to the beams reinforced with NSS. For beams designed to fail in shear, the HSS stirrup played a minor role in the shear capacity of the sections with an increase in capacity of only 9%. Yang et al. (2007) proposed a numerical technique to assess the load capacity of continuous deep beams based on the upper bound analysis of plastic theory. Chemrouk and Kong (2004a, 2004b) found that the current codes and design manuals covering continuous deep beams were lacking, and if followed could lead to severe cracking and unsafe structural members, e.g. buckling in slender deep beams. Ashour and Yang (2008) stated that the strut-and-tie model and mechanism analyses are more rational, adequately accurate and sufficiently simple for estimating the load capacity of RC deep beams.

Garay-Moran and Lubell (2008) tested ten reinforced concrete deep beams containing HSS reinforcement. Their conclusion was that the failure mechanisms of deep beams reinforced with high-strength reinforcing steel were similar to those reinforced with normal strength reinforcing steel. Zhang and Tan (2010) concluded that for continuous deep beams with three support points, the settlement at the mid support significantly affected the serviceability load, crack pattern and failure mode.

2.3 Neutral Axis Depth (NAD) Variation

The neutral axis is an imaginary line along the horizontal length of a beam where there is no longitudinal stress or strain. In NBs, before bending occurs the neutral axis is at the geometric centre if the section is symmetrical and not curved, and any variation in strain (due to a variation in loading) will result in the change of the neutral axis location; this can be mathematically determined. BS 8110 imposes a minimum neutral axis depth of $0.11d$ (where d is the effective depth to the tension steel). The failure of a beam section is always initiated by the crushing of the concrete in compression, by reaching the ultimate concrete strain in the extreme compression fibre. In NBs, the concrete's ultimate strain and tensile yield strain is used to mathematically determine the neutral axis depth. In a deep beam, it needs further investigation because the conventional design assumptions that are applicable for NB are not applicable for deep beams, e.g. the theory of linear elastic behaviour that is valid for NBs is invalid for deep beams and other structural elements, where shear failure dominates over flexural behaviour due to cracking and the development of plastic deformation. Deep beams are classified as regions of discontinuity.

In terms of strain, deep beams behave two-dimensionally rather than one-dimensionally, and are thus subject to a two-dimensional state of stress and strain. The stress and strain distribution along the deep beam length is different from that in NBs. Dischinger (1932) used a trigonometric series to determine the stresses in continuous NSC deep beams. Geer (1960) stated that the maximum tensile stress for a beam was independent of the location of the load (Figure 2.1); loading directly over the supports and loading at the central portion results in similar maximum stresses. Geer also concluded that the maximum stress is dependent on the reaction to the loading. Compression stress in the top fibre increases as load is added near the centre of the span but decreases when load is added in the outer one-third of the top; tension is caused in the upper compression

fibres. In much deeper beams, with loading over the entire upper length, the maximum compressive stress occurs below the mid-height of beam. Also, a triple neutral axis is seen in the deeper beams with central loading. The location of the lowest neutral axis is fairly constant for any given ratio of depth to length, but is proportionately lower in deeper beams. Based on Geer's findings, the general rule of thumb is to assume that the tension exists in a depth equal to a third of the clear span. Geer (1960) also stressed that the greatest tensile stress is not at the mid-span but is near the face of the support; the maximum tensile stress is independent of the location of the load; only loads placed directly over the supports results in maximum stress similar to loads placed at the centre of the beam. The tension at the top of the beam is equal to the tension at the bottom of the beam. The horizontal stress variation along the span and variation in load length showed sudden changes from conventional flexural theory.

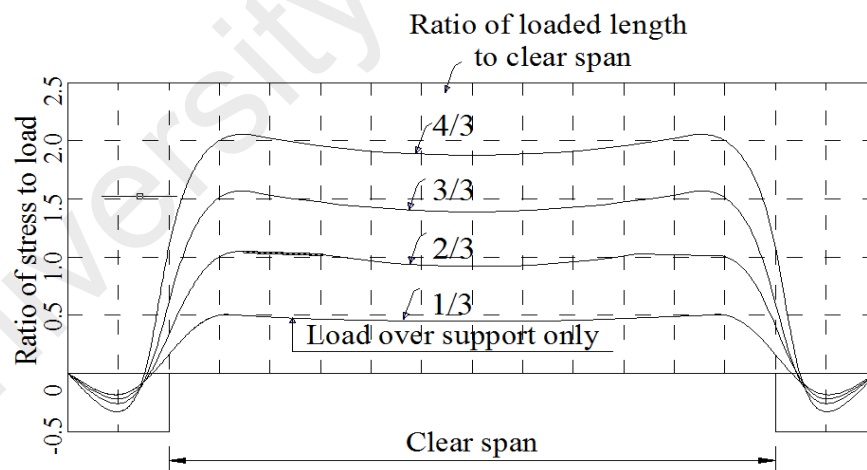


Figure 2.1: Variation in strain and stress along bottom length of deep beams (Geer, 1960).

Chow (1952) used finite difference equations to solve simple span deep beam problems and concluded that a considerable amount of error existed because of the coarseness of the net, the inherent rounding off of peak values and the behaviour of deep beams that is

different from NBs. Ray and Reddy (Ray & Reddy, 1979; Ray, 1980, 1982) concluded that the concrete strain variation at mid-span of a deep beam indicates that prior to the first crack the beam behaves elastically and shows nonlinear distribution of strain and the presence of more than one neutral axis (Figure 2.2).

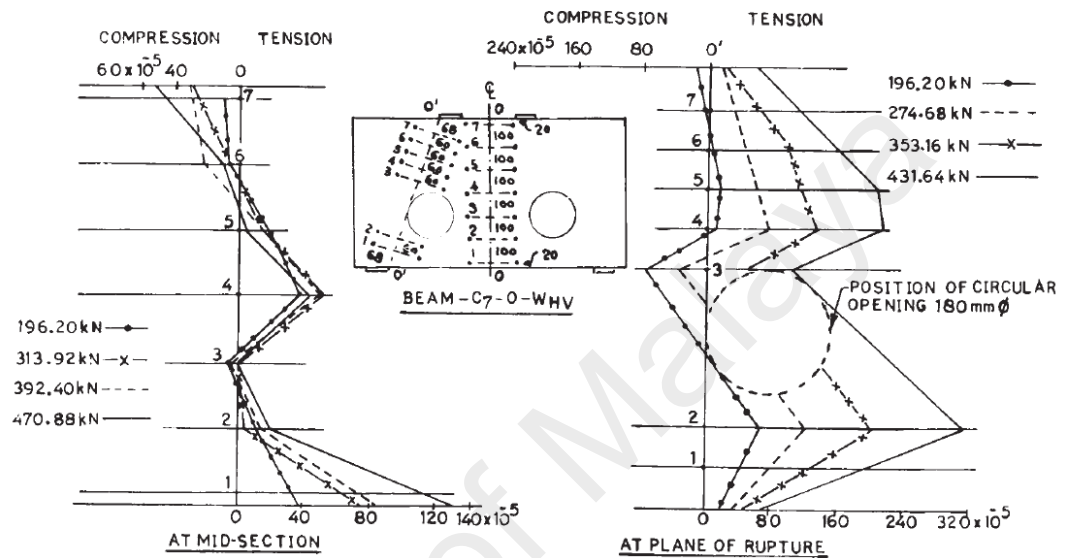


Figure 2.2: Concrete strain variation at mid-span and plane of rupture of a typical deep beam with web openings (Ray, 1980, 1982)

Ray and Reddy (1979) and Ray (1980) concluded that the number of neutral axes decreases with an increase in load, and that at ultimate load only one neutral axis exist. The variation in concrete strain at the rupture plane is indicative of deep beam behaviour before cracking and the existence of diagonal tension which persists until failure. The crack width and deflection do not affect service loads. Should the crack width be limited to 0.3 mm, a corresponding 60–70% of the ultimate load is expected.

Schlaich et al (1987) identified deep beams as a discontinuity region, where the strain distribution is significantly nonlinear compared to NBs and so requires a new design method to be developed.

To evaluate the behaviour of a reinforced concrete deep beam with HSS reinforcement, Garay-Moran and Lubell (2008) tested ten large-scale specimens under four-point bending with variables such as the shear span to depth ratio, main longitudinal steel ratio, and type of longitudinal reinforcement. They found that the shape of the strain distribution along the bottom bar of main tension reinforcement varied for different a/d ratios. The strain distribution along the beam span was uniform at the early stage of loading for beams with $a/d \leq 1.8$. At higher load levels, the strain close to the supports became larger than the strain at mid-span due to the wider cracks near to the support.

2.3.1 Modulus of rupture and first bending crack

Typically, deep beams are designed to include some shear reinforcement for serviceability and crack control. The appearance of the first bending crack is important in the design of concrete beams in relation to serviceability; the first crack exposes the steel reinforcements to the environment and possible corrosion. Some research by Shin (1986), Paulson et al (1989), Lambotte and Taerwe (1990), Khaloo (1995), Shah and Ahmad (1998), Ashour (2000), Rashid and Mansur (2005), and code provisions such as CSA94 and ACI318-95 refer to the first crack and modulus of rupture in normal strength and HSC beams as a percentage of ultimate load and a fraction of concrete compressive strength respectively. Rigoti (2002), who researched the first flexural crack in deep beams, defined it as a percentage of the ultimate load without a mention of modulus rupture. In this regard the application of the modulus of rupture is most urgent in structures for which safety concerns are particularly high, e.g. concrete dams and nuclear reactor vessels or containers. Recent work by Chemrouk and Kong (2004b), Ashour and Yang (2008), Park and Kim (2008), Lu et al (2010) and Pimentel et al (2008) investigated the design and behaviour of concrete deep beams in shear. The

appearance of the first crack is indicative of when the concrete in deep beams changes from elastic to plastic behaviour in the tension zone. There have been many studies on the mechanical properties and application of HSC (Khaloo & Hoseini, 2005; Seow & Swaddiwudhipong, 2005; Roth et al, 2010; Hashemi et al, 2008; Bechtoula et al, 2009; Mohammadhassani et al., 2011b) but none on HSSCC, the modulus of rupture and the first crack in deep beams.

2.4 Material Properties and Their Effects

Three main materials were used in this study. They are High-Strength-Self-Compacting-Concrete (HSSCC), High-Strength-Steel (HSS) and Normal-Strength-Steel (NSS).

2.4.1 High-strength-self-compacting-concrete (HSSCC)

HSSCC is a type of high-strength-concrete (HSC). Compared to a typical normal-strength-concrete (NSC) the difference in strength and modulus of elasticity of the aggregate and matrix are relatively smaller (Khaloo & Kim, 1996). In NSC, the behaviour is linear till 40% of the maximum stress, while it is the case till 85% in HSSCC sections (Iravani, 1996). An experimental study by Mohammadhassani et al (2011b) confirmed the need for an evaluation of the modulus of elasticity at higher stress values than $0.5 f_c'$ in stress-strain curves. The behaviour of HSSCC is close to linear elastic with brittle failure compared to the behaviour of the same structure made from NSC. By varying different parameters such as concrete compressive strength, tensile reinforcement ratio and web reinforcement percentages, different failure modes and serviceability are expected.

De Paiva and Siess (1965) investigated the effect of concrete strength and tension reinforcement on the behaviour of concrete beams. From their work the following observations were made:

- a) Increasing the concrete strength increased the load capacity of beams failing in shear and in some cases changed the mode of failure from shear to flexure.
- b) Increasing the amount of tension reinforcement increased the load capacity of the beams and changed the mode of failure from flexure to shear.

Other studies by Selvam and Tomas (1987) and Oh and Shin (2001) found that concrete strength and reinforcement ratio are the two most effective parameters on the capacity of deep beams.

2.4.2 High-strength steel (HSS) reinforcement

The use of high-strength steel (HSS) reinforcement in concrete structures is encouraged due advantages such as its higher effective yield strength and better corrosion resistance. This type of reinforcing bar shows good behaviour under high temperatures, in comparison to NSS (Darwin et al, 2002; El-Hacha & Rizkalla, 2002). The mechanical properties of HSS reduce steel usage, and the weight of the structures as a design reinforcement requirement. The improved corrosion resistance with the use of HSS makes it ideal for reinforcement in highly-hazardous corrosion areas, such as foundations, bridges and offshore structures, etc. (Darwin et al, 2002). However, due to the design stress limitations in current design code provisions, the full capacity of HSS is not realised. The behaviour of HSS and NSS are similar until the yielding of NSS. After this yield point, the main differences include the nonlinear stress-strain response

in HSS and the lack of a clear yield point and its corresponding yield plateau for HSS. Based on the traditional method using the 0.2% strain offset, yielding strains in HSS are twice the yielding strains of NSS. Research on the performance and behaviour of concrete members with HSS has only been carried out for the flexural and shear behaviour of NBs. Malhas (2002) tested 22 NBs under four-point bending using HSS and NSS as reinforcing steel. These beams were designed using concrete compressive strengths of 40 MPa and 60 MPa. The reinforcement ratios were between 0.21% and 1.0%. Findings showed that all specimens exhibited ductile behaviour prior to flexural behaviour. It was also concluded that the ultimate strength of the beams and their serviceability and other design requirements conform to the ACI318 code provisions. Furthermore, after flexural cracks the stiffness of beams reinforced with HSS reduced in comparison to the beams reinforced with NSS. The overall conclusion was that using HSS was effective in NB sections. Vijay (2002) carried out a series of tests on the flexural behaviour of NBs reinforced with HSS. Concrete strengths varied from 55 MPa to 77 MPa and the reinforcement ratio varied between 0.4% to 0.8%; the conclusion was that the ACI318 code provision is applicable to predict the flexural behaviour of NBs reinforced with HSS.

Ansley (2002) compared the behaviour of NB reinforced with HSS and NB reinforced with NSS with similar geometry; the contribution of the shear strength of stirrups made with HSS and NSS were also compared. Beams were tested in flexure and it was found that the behaviour of both types of reinforcement was similar until the yield point of NSS. After the yield point, the load-deflection curve for beams reinforced with HSS maintained the same path, while for beams reinforced with NSS, the deflection rates increased due to the yielding of the tension reinforcement.

Garay-Moran and Lubell (2008) tested ten large-scale specimens under four-point bending to study the behaviour of reinforced concrete deep beams with HSS reinforcement. They concluded that for specimens containing HSS as the main tension reinforcement, the common serviceability deflection limits of $l/360$ and $l/180$ were achieved at loads greater than 60% and 90% of P_{max} , respectively.

2.5 Strain Variation

Two main strain areas in deep beams are considered in this study. They are the strain along the tie section in the tension zone and the strain in the mid-span compression zone. The strain along the tie section in the tension zone is studied to determine the serviceability, the design of the tie section and the strut-and-tie model. The strain in the mid-span compression zone is studied to determine the width of the horizontal strut and the design of the horizontal strut. The locations of these strut and tie are shown in Figure 2.3.

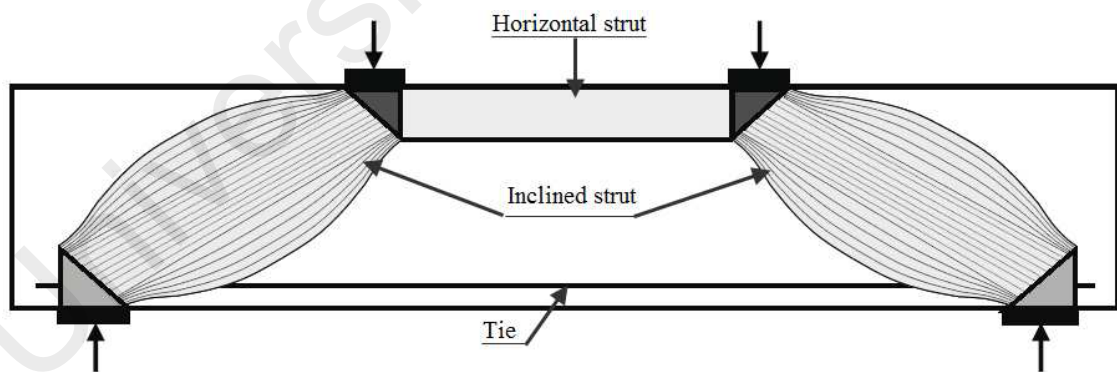


Figure 2.3: Definition of struts and tie in strut and tie models (STM)

2.5.1 Strain variation in tie section

The strain distribution at the tie section of deep beams is important for tie section design as well as flexural design and serviceability prediction. To transfer a large loads

throughout the tie section to create a uniform strain distribution, design codes suggest a minimum limit on the anchorage for tensile bars to prevent bonding failure and to control crack width. For example, Sections 12.10.6 and 12.11.4 of ACI 318-99 indicate that in flexural areas, positive moment-tension reinforcement must be anchored to achieve yield strength (f_y) in tension at the face of the support and to achieve the ultimate deep beam capacity.

Nowadays, a common method in the design of these elements is using a collection of simple stress paths. The forces within a strut-and-tie model (STM) can be calculated using a static equilibrium if the truss is statically determinate. With the forces in each strut and tie determined from basic statics and any necessary compatibility conditions, only the stresses within these elements (struts, ties, and nodes) need be compared with permissible stresses. Based on the definition of STM models in the ACI code, a major portion of the load is transferred directly to the supports by in-plane compressive forces in the concrete and tensile forces in the reinforcement. In addition to the strut's importance in deep beam design, it is also important in the failure of deep beams. For instance, STMs are assumed to fail due to yielding of the tie, anchorage failure of the ties, failure of nodal zones connecting the strut and ties and crushing of the concrete. Ties play an important role in controlling cracks and crack widths. For controlling cracks in aggressive and normal environments, attention should be given to the percentage of tensile bars. The CIRIA guide No. 2b(CIRIA, 1997) suggests that in a tension zone, the steel ratio ρ , calculated as the ratio of the total steel area to the local area of the concrete in which it is embedded, should satisfy the condition of

$$\rho \geq \left(0.52 \sqrt{f_{cu}}\right) / (0.87 f_y) .$$

Ties are the elements within a STM that carry tension, and are generally confined to reinforcing steel. The geometry of a tie is simple. The tie is geometrically confined to elements that can carry high tensile forces, and the allowable force is generally given as a fraction of the yield force. With the forces in each of the truss members known, the appropriate amount of reinforcing steel can be determined very simply by dividing the force in the tie by the yield stress of the steel and the appropriate strength reduction factor. Once the necessary amount of reinforcement has been determined, the truss geometry can be refined. For example, if more reinforcing steel is needed than the amount initially expected, the location of the tie is changed in order to accommodate the increased amount of steel. The centres of the reinforcement that will act as the tie should coincide with the location of the tie in the STM. Once the ties have been designed and the truss model refined to include the final tie positions, the struts and nodes can be checked for the required strength. Based on ACI code provision (Appendix A), the main load-carrying mechanism in the STM approach consists of single diagonal struts between the loading and the support plates as shown in Figure 2.4.

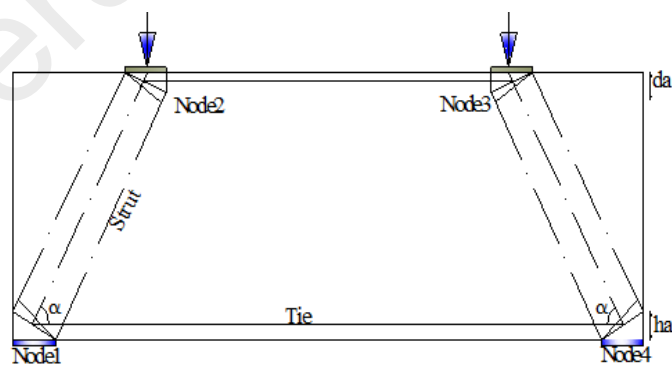


Figure 2.4: STM model for ACI code design

The tied arch model is predominantly used in the design of short beams with an a/d less than 1, on the assumption that the load is transferred directly from the point of the load to the support through the formation of the concrete strut. The horizontal component of

each strut at the support is set to equilibrium by a horizontal tie extending the full length of the beam (refer to Figure 2.4). The tie force in the model is constant throughout the span, and as a result the longitudinal bar forming the ties should be anchored at the face of the node over each support to develop the yield stress and prevent bond failure. Some researchers that have studied the importance of stress transfer in tensile bars, such as Thompson (2002), focused on the details required for proper anchorage and confinement in nodal zones. Smith and Vantsiotis (1982) indicated that the strains in the region of maximum bending moment are almost uniform at every level, and failure of tests beams occurred near the yielding of the main longitudinal bars. Tensile steel strains increased at almost a constant rate with no sudden increase observed at or after major inclined crack formation. Leonhardt and Walther (1966) showed that deep beams behave like tied arches, with the tension force in the flexural reinforcement more or less uniform along the span. If the flexural reinforcement is bent up to cross approximately perpendicularly to the shear plane, a loss in capacity for the top loaded beams is noted. The resulting loss in strength is due to inadequate tie reinforcement near the supports and stress concentrations occurring at the bends in the bars. No attempt was made to measure steel strain near the supports, where the major inclined cracks are located. Also a study by Yang et al (2007) showed that the variation in strain along the main longitudinal top and bottom bars is dependent on the shear span-to-depth ratio. The lower the shear span to depth ratio, the less variation is observed.

Any STM is a combination of a strut as a compression element, a tie section against tension loads and their intersection as nodes. When the AASHTO LRFD specifications are used for STM modelling, the strength of a strut is calculated based on the strain of the tie which adjoins the strut in question. The effect of the tie section is important on the serviceability of deep beams and its effect on the strut design by the equilibrium of internal forces. The effects of longitudinal reinforcement as the tie section in deep

beams were discussed by researchers such as Moody et al(1954), Watstein and Mathey (1958), Rajagopalan and Ferguson (1968), Tan et al (1997), and Oh and Shin (2001). Moody et al. (1954) demonstrated that after diagonal cracking at shear-critical zone, the stiffness in the deep beam decreased compared to a beam failing in flexure. Sudden shear failures were observed at the location where the longitudinal bars ended, and this location is where the anchorage of tie reinforcement is important.

Watstein and Mathey (1958) concluded that in a deep beam the strain in the longitudinal reinforcement is approximately uniform along the length due to a tied arch mechanism. Rajagopalan and Ferguson (1968) developed a relationship between the concrete contribution to shear strength and the longitudinal reinforcement ratio. The empirical relationship was linear, and had a maximum value of shear stress equal to $2 f_c'$ at a reinforcement ratio of 1.2%; it also provided a safe lower bound for the design of beams with shear span-to-depth ratios greater than 2.75. Oh and Shin (2001) and Tan et al. (1997) agreed with Rajagopalan and Ferguson (1968) in that the shear strength of concrete beams is a function of the flexural reinforcement ratio. However, both Oh and Shin (2001) and Tan et al. (1997) concluded that the effects of shear span-to-depth ratio are much more critical than the effects of longitudinal reinforcement ratio. Nevertheless,

ACI 318-05 Section 10.5.1 suggests a minimum of $200 \frac{b_w d}{f_y}$ rather than $3 \frac{\sqrt{f_c'}}{f_y} b_w d$ as the tensile reinforcement ratio.

The importance of the tensile bar is more in serviceability assessment of a structure and the ductility of this element is a vital requirement in seismic hazard areas.

2.6 Shear Strength of Deep Beams

The major concern related to deep beams is its shear capacity. These structural elements usually fail in shear at the ultimate limit state. Shear failure in deep beams is different from shear failure in NBs. In deep beams, the applied load is transferred to the supports directly through the compression struts formed between the load and supports. Many studies have been carried out on the shear prediction of deep beams. Nielsen (1971) and Braestrup and Nielsen (1983) used the plasticity concept for the shear strength prediction using plastic method for deep beam problems. Their solutions and also the design codes differed from elastic design which uses the STM to better explain deep beam behaviour. STM is very useful when dealing with structures with planar sections that become non-planar when a load is applied, as is the case with deep beams. STM analyses deep beams with the plastic truss analogy which internally transfers the load forces from the loading points to the support points through both horizontal and inclined concrete struts and steel reinforcing ties acting in tension (Schlaich et al. 1987 and Möller et al. 2008).

Smith and Vantsiotis (1982) analysed the shear strength of deep beams to identify the effect of vertical and horizontal web reinforcement and shear span-to-effective depth ratio on ultimate shear strength. Their results indicated that web reinforcement moderately affects the ultimate shear strength, and that the addition of vertical web reinforcement of 0.18–1.25% shows a significant improvement in the ultimate shear strength of deep beams. But the addition of horizontal web reinforcement of 0.23–0.91% had little or no influence on the ultimate shear strength. Also observed was the considerable increase in load-carrying capacity when concrete strength was increased and shear span-to-effective depth ratio decreased.

Tan et al. (1995) tested 19 reinforced concrete deep beams with compressive strengths of 41–59 MPa under two-point top loading. All beams were reinforced with a $\rho_t = 1.23\%$ with a nominal shear reinforcement of 0.48%. The beams were tested for seven shear span-depth ratios (a/d) from 0.27–2.70, and four effective span-depth ratios (le/d) from 2.15–5.38. The results showed that le/d had an insignificant effect on the failure load. But for beams with $a/d \geq 1.00$, the flexural failure was dominant with increasing le/d . When compared to the ACI predictions, the results showed that the ACI code provisions are more suited for deep beams with higher strength. The ACI code is also more conservative compared to the Deep-Beam Design Guide by the Construction Industry Research and Information Association (CIRIA Guide 2, 1977).

Tan et al. (1997) studied the shear prediction of 18 HSC deep beams, and the results showed that the ACI code provisions for deep beams overestimated the contribution of the horizontal web steel to shear strength; a revision to the ACI equations (11–31) for web steel contribution was suggested. The Canadian code, though more consistent, was conservative for deep beams with different web reinforcement, while the UK CIRIA Guide was un-conservative for beams with horizontal web reinforcement.

Tan and Lu (1999) tested 12 specimens to failure with a total main-steel-and-strand ratio (ρ_c) maintained close to 2.50%, a beam height (h) of 500–1750 mm, and a shear-span-to-height ratio (a/h) of 0.50–1.00. The specimens were deep beams with concrete cylinder strengths of about 40 MPa without any web reinforcement; they were tested to study the effect of beam size on concrete shear strength. The results revealed ultimate shear stress as being size-dependent, but not the diagonal cracking stress that occurred. Compared to current design codes, the CSA was found to be more suitable for large- and medium-sized beams, while both the ACI and CIRIA predictions become less conservative with an increase in the h and a/h ratio.

Oh and Shin (2001) studied the shear strength of reinforced HSC deep beams with 53 beams with compressive strengths of 23–74 MPa and geometrical variations such as an effective span-depth ratio l_e/d of 3.0–5.0 and a shear span-effective depth ratio a/d of 0.5–2.0. All the beams were reinforced, with ρ_t ratios of 0.0129–0.0156 and ρ_v ratios of 0–0.0034, and ρ_h ratios of 0–0.009. The results showed that the ultimate shear strength of deep beams was predominantly determined by a/d , and the ACI code Equations (11–29) and (11–30) are conservative and underestimated the effects of both the concrete compressive strength f'_c and longitudinal steel reinforcement ρ_t . The addition of horizontal shear reinforcement did not improve the ultimate shear strength when a/d was increased.

Yang et al. (2003) tested 21 beam specimens to investigate their shear characteristics whilst the concrete strength, shear span/depth ratio, and overall depth were varied. The decrease in shear span/depth ratio and the increase in overall depth while the shear span/depth ratio remain unchanged led to more brittle failures with wide diagonal cracks and high energy release. The ACI code gave similar safety factors on the shear strength when the first diagonal crack appeared, but did not specify a maximum limit for the safety factor in terms of ultimate strength and the effect of beam size.

Arabzadeh et al. (2011) tested sixteen reinforced concrete deep beams with compressive strengths in range 59 MPa $< f'_c < 65$ MPa under two-point top loading. The shear span-to-effective depth ratio a/d was 1.10; all the specimens were simply supported and reinforced by vertical, horizontal and orthogonal steel bars in various arrangements. The test specimens were composed of five series based on their arrangement of shear reinforcement. Observations were made on mid-span and loading point deflections, crack formation, failure modes and shear strength. The test results indicated that both vertical and horizontal web reinforcement are efficient in the shear capacity of deep

beams, also orthogonal shear reinforcement was the most efficient when placed perpendicular to the major axis of diagonal cracks. The test results were then compared with the predicted ultimate strengths using the ACI 318-08 provisions; ACI code tended towards either unsafe or scattered results. The investigations performed deduced that the ACI code provisions need to be revised.

2.7 Numerical Studies

From knowledge of the nonlinear strain and stress distribution, the serviceability, strain and stresses of deep beams can be predicted. There are many parameters that affect serviceability, strain and stress in deep beams. Amongst these parameters are the concrete compressive strength, web reinforcement percentage, tensile reinforcement ratio, length and shear span/depth ratio. There has not been any effort until now to address the theoretical modelling of a deep beam's serviceability in terms of deflection and the prediction of strain and stress. One of the key problems in modelling the deflection and prediction of strain and stress using classical methods is the lack of valid design provision due to excessive parameters. Collecting data on these excessive parameters is costly as it involves casting, curing and testing procedures of deep beams. An inexpensive new tool is desired by Structural Engineers for the modelling of deep beam behaviour, such as deflection, crack width, etc. This involves the use of the latest intelligent technology such Artificial Intelligence.

Artificial Intelligence (AI) is an area of computer science focusing on creating 'smart' machines that are similar to human intellect in terms of 'thinking' capacity. With 50 years of research in AI programming techniques and the latest developments in computers, the dream of smart machines is becoming a reality. AI systems such as Neural Networks (NN), Fuzzy Inference Systems (FIS), and Neuro-Fuzzy/fuzzy-neural

systems (NF) have been used successfully for modelling in many engineering applications as well as in agriculture (Mazlounzadeh et al, 2010; Alavi et al, 2010), soil science (Yilmaz & Kaynar, 2011) , analysis (Swaddiwudhipong et al, 2008) and the stability of structures (Bilgehan, 2011).

2.7.1 Artificial neural network (ANN)

An artificial neural network (ANN) or NN is a computational model inspired by the structure and/or functional aspects of biological neural networks. A neural network consists of an interconnected group of artificial neurons, and it processes information using a connectionist approach to computation. Due to the ANN's excellent learning capacity and high tolerance to errors, these techniques have been established and acknowledged as powerful tools in pattern recognition, signal processing, control and complex mapping (Kao & Hung, 2003; Masri et al, 2002). ANN is an adaptive system that changes its structure based on external or internal information that flows through the network during the learning phase. Modern neural networks are nonlinear statistical data modelling tools. They are usually used to model complex relationships between inputs and outputs or to find patterns in data.

ANN simulates the human brain. It learns from existing designs and actual behaviour during the training process. ANNs are able to process incomplete and noisy data as is the case with many engineering applications. Much of ANN's achievement is due to its nonlinear and parallel processing characteristics.

ANN is also known as parallel distribution processor, adaptive system, self organising system, connectionism, neurocomputer and NN (neural network). Though ANN is based on simple principles, its mathematical talent is in terms of nonlinear iteration that is practical in the prediction of deep beam's deflection and strain prediction. The use of

the ANN technique began when ANN was used to predict the ultimate shear strength of reinforced concrete deep beams (Sanad & Saka, 2001). Sanad and Saka (2001) showed that the shear strength of NBs and deep beams are better predicted using multi-layered feed forward ANNs than other existing formulas and code provisions. Moreover, some researchers (Rajasekaran & Vijayalakshmi Pai, 2004; Davis, 1991) published the main principle of neural networks that are based on the aforementioned principles.

The use of this technology has been successful in areas of civil engineering such as structural analysis and design (Flood & Kartam, 1994; Sakr & Sakla, 2009; Möller et al, 2008; Mashreia et al, 2010; Kang et al, 2009; Rosales et al, 2009 and Saridakis et al, 2008), structural damage assessment (Hakan Arslan, 2010; Gonzalez & Zapico, 2008; Lee, 2003), concrete technology (Ni & Wang, 2000; Yeh, 1999; Lai & Serra, 1997; Ozcan et al, 2009; Naderpour et al, 2010 and Lautour & Omenzetter, 2009), shear strength prediction of reinforced concrete beams (Sobhani et al, 2010; Cladera & Mari, 2004; Flood et al, 2001), compressive strength of columns (Tang et al, 2003; Caglar, 2009), non-destructive strength assessment (Hola & Schabowicz, 2005), and concrete deep beam elements (Pal & Deswal, 2011).

ANNs are applied to solve such aforementioned problems (especially modelling, curve fitting, forecasting, prediction, approximation, system identification) that are not easily solved the using conventional calculations that engineers use. ANNs are able to model engineering systems using only the input/output observed data without requiring additional assumptions. The main characteristics of ANNs are their adaptive ability that can provide surprising results to unseen data following good training. In this study, ANN will be applied to predict the deflection and strain in the tie section of deep beams.

2.7.2 Adaptive-neuro-fuzzy-inference-system (ANFIS)

Fuzzy logic systems are particularly suited for modelling the relationship between variables in environments that are either ill-defined or very complex, and provides a more precise alternative. The use of qualitative variables and mathematical relationships in this technique results in a more accurate decision-making process. Fuzzy logic, which was first introduced by Zadeh (1965), is a self-learning technique that provides a mathematical tool to convert linguistic evaluation variables based on expert knowledge into an automatic evaluation strategy. Fuzzy-neural systems are part of an intelligent system which combines the characteristics of ANNs and fuzzy inference system (FIS) to construct powerful tools for computing.

ANFIS is based on the Takagi-Sugeno fuzzy model (Takagi & Sugeno, 1985). In this study it is applied to model the deflection amount and strain in tie sections. In ANFIS, a fuzzy inference system is implemented through a feed-forward network and a hybrid learning method including back propagation theory from ANN, and the recursive least square (RLS) method and clustering techniques are used appropriately together to construct the FIS according to the data. In other words, ANFIS combines fuzzy logic and ANNs, by utilising the mathematical properties of ANNs in tuning rule based fuzzy inference system that approximates the way a human brain processes information. ANFIS has shown significant promise in modelling nonlinear systems, where it is able to learn features of the data set and adjusts accordingly the system characteristics to a given error criterion (Jang, 1993).

Like ANN, ANFIS is capable of mapping unseen inputs to their outputs by learning the rules from the previously seen data. The determined values of physical parameters (input) and the real values of deflection (output) are used to train the fuzzy neural network. Today, neural networks and fuzzy sets are the answers to high-tech solutions.

Neural networks can solve problems that cannot be solved using standard or common calculations. These networks are used when the data necessary for the interpretation is insufficient and/or not available.

Fuzzy logic is not very efficient in learning but presents the advantage of approximate reasoning. The combination of these two techniques appears in a neuro-fuzzy (NF) system without having any of their disadvantages (Vassilopoulos & Bedi, 2008). NF systems are the most widely studied hybrid systems as a combination of two very popular modelling techniques – neural networks (NNs) and fuzzy logic (Mendel, 1995). These systems combine the learning capability of ANNs with the linguistic interpretation power offered by fuzzy systems.

2.7.3 Review of Related Works Comparing ANFIS and ANN Models

This study aims to explore the feasibility of the potential use of NN and NF for the prediction of deflection and strain in tie sections in deep beams. In this regard, the performance of ANN and ANFIS are compared in terms of the accuracy in deflection prediction and strain in tie sections of deep beams. To the knowledge of the author, no literature has addressed the application of the ANNs and ANFIS approach to the deflection prediction and strain in tie sections in deep beams, and more specifically for HSSCC deep beams.

In recent years, many researchers have reported using ANFIS in the field of concrete element related fields. Bilgehan and Turgut (2010) used ANFIS and ANN models for the buckling analysis of slender prismatic columns with a single non-propagating open-ended crack subjected to axial loads. The main focus of their work was to study the feasibility of using ANFIS and ANN trained with the non-dimensional crack depth and the non-dimensional crack location parameters to predict the critical buckling load of

different end-supported condition in axially loaded compression rods. Bilgehan and Turgut (2010) concluded that the ANFIS architecture with Gaussian membership functions performed better than the multilayer-feed-forward ANN learning by back-propagation-algorithm. Bilgehan (2011) compared an application of ANFIS and ANN in concrete compressive strength estimation; it was concluded that the proposed ANFIS architecture with Gaussian membership function is found to perform better than the multilayer feed-forward ANN learning by the back-propagation- algorithm.

University of Malaya

3.0 MATERIALS AND METHODS

3.1 Test Program

Eight HSSCC deep beams have been designed and cast, with the percentage of longitudinal main reinforcement, calculated as A_s/bd , varying from 0.2191% to 1.2883%. The beam lengths, depths and thicknesses were kept constant while varying the tensile reinforcements and web reinforcement ratios. All the beams were loaded to failure.

3.2 Materials and Material Properties

3.2.1 Steel properties

Two different types of reinforcement are used in this study: normal-strength steel (NSS) and high-strength steel (HSS) (Figure 3.1). Except for 9 mm non-deformed NSS reinforcing steel, the other reinforcing bars used are HSS deformed bars with properties as stated in Table 3.1. The properties are determined by carrying out tests on samples taken from each batch. In Table 3.1, f_y and f_u are the yield and ultimate strength of the bars, respectively. The average yield strength, f_y , was obtained from the stress-strain curves of three tension coupon tests for each bar size. E_s was obtained from the slope of the linear part of the stress-strain curves of the reinforcing steel. The tension coupon samples were 500 mm long and were tested in a MTS 2000 machine under displacement control until failure. All bars of the same size and grade used were from the same batch of steel. A 50 mm gauge length extensometer was utilised for strain measurement in the sample tests. NSS reinforcement showed a well-defined yield plateau (Figure 3.2). But for HSS coupon tests, the 0.2% offset method was used to determine an effective f_y magnitude.

Table 3.1: Bar specification

bars (mm)	Area(mm ²)	f_y (MPa)	f_u (MPa)
Φ_9	63.585	353.0	446.0
Φ_{10}	78.500	614.4	666.0
Φ_{12}	113.04	621.6	678.4
Φ_{16}	200.96	566.3	656.0

Figures 3.1 shows deformed and non-deformed steel bar. ASTM E8 Standard Test Methods is used for Tension Testing of Metallic Materials.

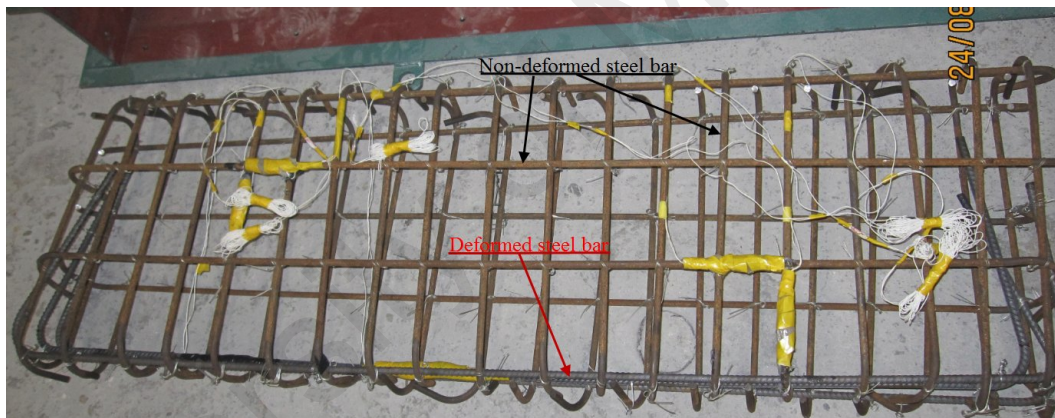


Figure 3.1: Deformed and non-deformed steel bar in beam B2

Figure 3.2 shows Stress-strain curves of NSS specimens.

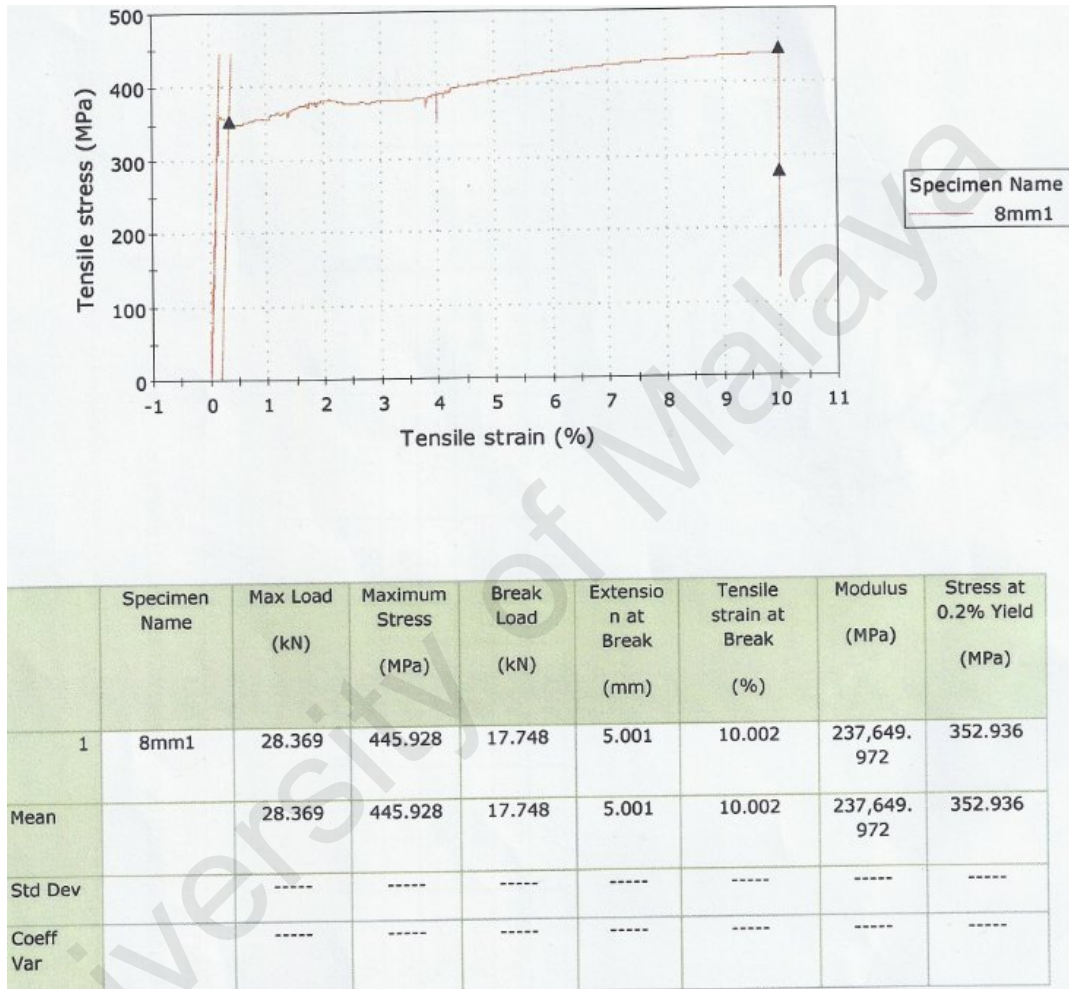


Figure 3.2: Stress strain curve for NSS reinforcing bar ($\varnothing 9$ mm)

Figure 3.3 shows Difference in the stress-strain curves of HSS and NSS reinforcing steels.

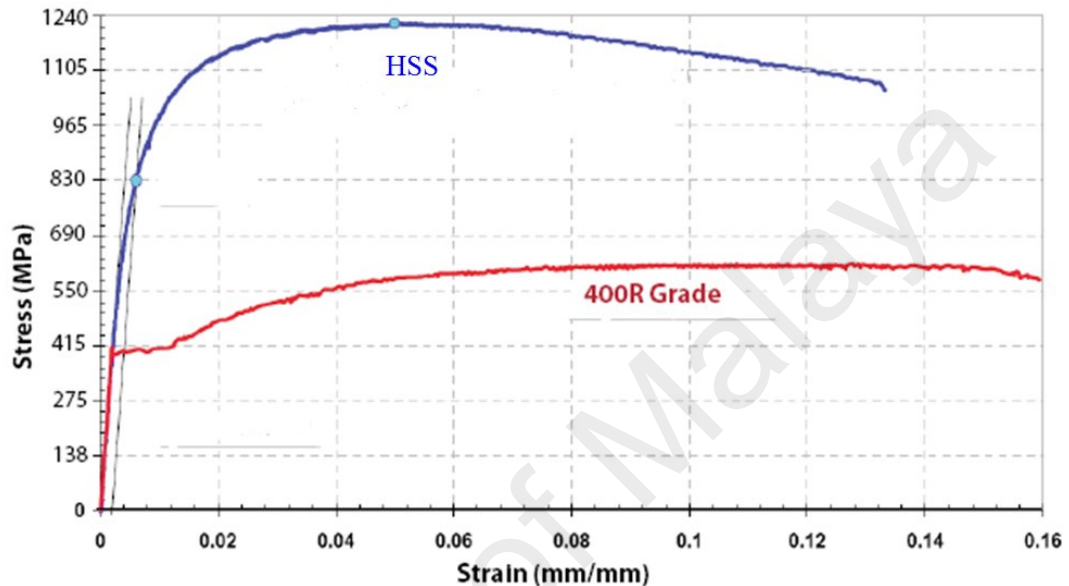


Figure 3.3: Comparison of typical stress-strain curves for HSS and NSS reinforcing steel (El-Hacha & Rizkalla, 2002)

3.2.2 High-Strength Self-Compacting Concrete

All the concrete used in this research was produced in the laboratory. The material used for the present experimental study is high-strength-self-compacting-concrete (HSSCC). Self-compacting concrete is a highly flowable, non-segregating concrete that can spread into a mould and fill the formwork and encapsulate the reinforcement without any need for consolidation. Due to the density of reinforcing bars in deep beams, the vibration of concrete is not an easy task. Therefore, the use of self-compacting concrete is highly desirable. Moreover it eliminates vibration and labour costs. Initial mix design of the concrete's strength was with a nominal compressive strength of 75 MPa. The mix design or the proportions of ingredients and other relevant data for a typical batch of

HSSCC is given in Table 3.2. In the mix design aggregate of a maximum 20 mm diameter, ordinary Portland cement, natural river sand, micro silica and super plasticiser are used. The aggregates were obtained locally and the moisture content of the aggregate tended to dry.

Table 3.2: HSSCC mix design

Characteristic cube strength	75 MPa
Aggregate type	Crushed granite and natural sand
Cement type	Ordinary Portland cement
Slump of concrete	More than 650 mm
Coarse aggregate content	553 kg/m ³
Fine aggregate content	887 kg/m ³
Water/binder	0.25
Silica fume/cement	0.1

All the ingredients were batched by weight and mixed in a vertical axis drum mixer with super plasticiser added until the desired workability was reached. The desired workability of HSSCC was achieved avoiding segregation and bleeding. Figure 3.4 shows the workability with a slump value of 580 mm.



Figure 3.4: Workability slump value

To prevent segregation, the workability was in the range of 550 to 740 mm. For each beam, nine cubes (100 mm × 100 mm × 100 mm) and three cylinders (150 mm diameter, 300 mm height) were cast as control specimens. Cubes are tested for measuring strength at 7 days, 28 days, and at the age of loading. One of the cylinders was tested for splitting tensile strength at 28 days, and others were tested to determine the modulus of elasticity. Figure 3.5 shows two halves of a cylinder sample after a splitting test.

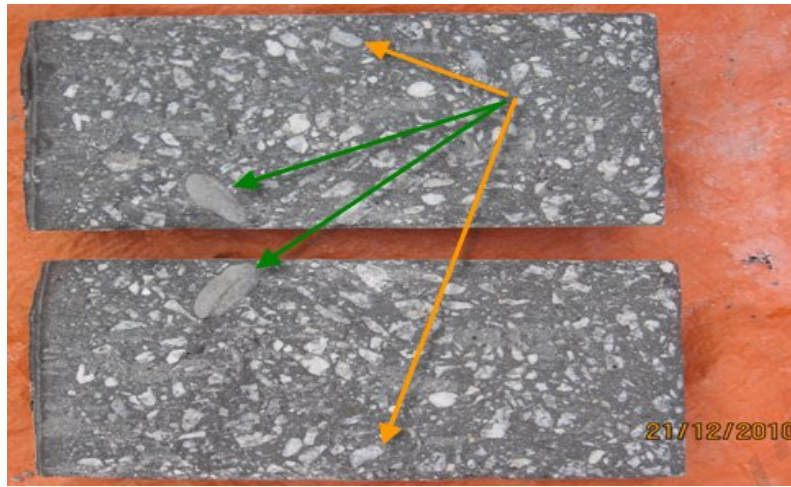


Figure 3.5: Splitting test of HSSCC cylindrical sample used

This figure shows sandy aggregate (as indicated by arrows) perfectly split and its original shape maintained. This proves the quality of the binder used.

Cylinders and cube samples used for strength control were demoulded after 24 hours and cured in humid conditions.

All deep beam samples were cast in the concrete laboratory of the Civil Engineering Department at the University of Malaya. The concrete was placed in the mould immediately after mixing. An adjustable steel mould was constructed to simultaneously cast two samples. The steel mould was levelled and oiled prior each cast. Figure 3.6 shows the mould of a deep beam with reinforcement and strain gauges. The beams were cast in horizontal positions. The test samples are covered with canvas and plastic after 3 days of casting. The canvas is watered twice a day for 11 days.



Figure 3.6: Casting arrangement of deep beam

The properties of hardened cementitious materials for deep beams are listed in Table 3.3. The concrete strength mentioned is an average strength of 3 cube samples at the age of loading for each beam.

Table 3.3: Specification of deep beams tested

Beam	f_{cu} (MPa)	f_t (MPa)	Age(day)
B1	91.50	4.444	86
B2	91.50	4.920	89
B3	91.10	4.901	87
B4	93.72	4.823	106
B5	79.10	4.052	72
B6	87.50	4.861	115
B7	82.24	4.234	93
B8	97.20	4.932	89

In this table, f_{cu} and f_t are the concrete compressive strength of cube samples at loading age, and the tensile strength of splitting test of cylinder samples for each deep beam, respectively.

3.3 Deep Beam Details

All eight beams were made at full-scale and designed according to the general requirements of the ACI 318-05 code. Beam design took into consideration the main tension steel ratio, minimum web reinforcement requirements, typical concrete covers and bar spacing.

The variables that needed testing were the tensile reinforcement ratio, steel strength, and the web bar percentage. For this purpose the HSSCC deep beams were cast based on three combinations of steel bar strength:

- a) NSS for tensile bar, horizontal web bar and vertical web bars (e.g. B1)
- b) NSS for horizontal web bar and vertical web bars only; HSS for tensile bars (e.g. B2–B4)
- c) HSS for tensile bar, horizontal web bar and vertical web bars (e.g. B5–B8)

The geometrical parameters of deep beams are shown in Figure 3.7.

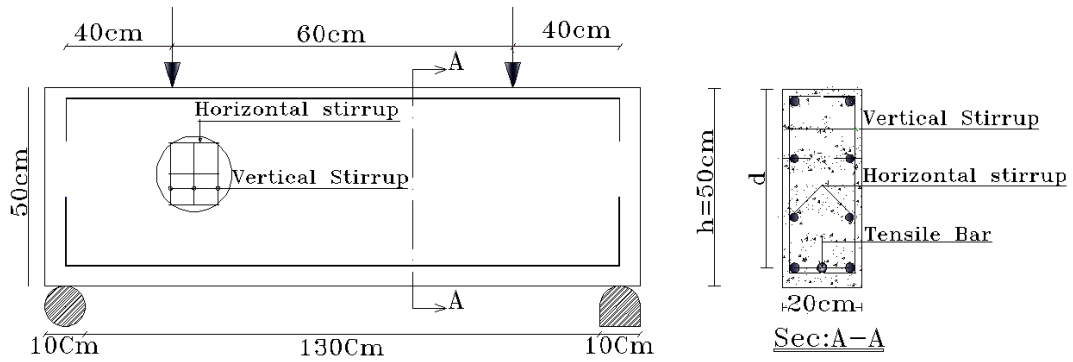


Figure 3.7: General geometrical specifications of deep beams

As shown in Figure 3.7, the anchorage of the main tension reinforcements is enhanced by providing 90-degree hooks at the bar ends for preventing bond failure.

All deep beams had a section of 500 mm depth, 200 mm width and 1500 mm length.

Table 3.4 shows the deep beam reinforcement details.

Table 3.4: Bar schedule specification of deep beams

Beam No.	Tensile bar	Vertical web stirrup	Horizontal web stirrup	d (mm)	a/d
B1	3Ø9	Ø9@100mm c/c	Ø9@150mm c/c	435.5	0.920
B2	3Ø10	Ø9@100mm c/c	Ø9@150mm c/c	438.5	0.910
B3	2Ø10+2Ø12	Ø9@100mm c/c	Ø9@150mm c/c	469.0	0.850
B4	2Ø10+2Ø16	Ø9@100mm c/c	Ø9@150mm c/c	462.0	0.860
B5	2Ø10+3Ø16	Ø10@100mm c/c	Ø10@80mm c/c	470.0	0.850
B6	1Ø9+4Ø16	Ø10@100mm c/c	Ø10@80mm c/c	455.0	0.880
B7	2Ø10+4Ø16	Ø10@100mm c/c	Ø10@80mm c/c	460.0	0.760
B8	2Ø10+5Ø16	Ø10@100mm c/c	Ø10@80mm c/c	451.0	0.778

3.3.1 Individual beam testing details

3.3.1.1 Detail of specimen B1

Beam B1 had a length of 1500 mm with a rectangular cross-section of 200 mm width and 500 mm height. The bar used as tensile reinforcement consisted of 3 \varnothing 9 NSS with an effective yield strength of 353 MPa that was distributed in one layer. This arrangement of longitudinal steel provided a reinforcement ratio of 0.2191%.

Vertical web reinforcement consisted of \varnothing 9 mm NSS bar with a f_y of 353 MPa and spaced at 100 mm. Horizontal web reinforcement consisted of (6 \varnothing 9) NSS. The shear span was 350 mm, giving a shear span/depth ratio of 0.920. Dimensions and reinforcement details of beam B1 are shown in Figure 3.8.

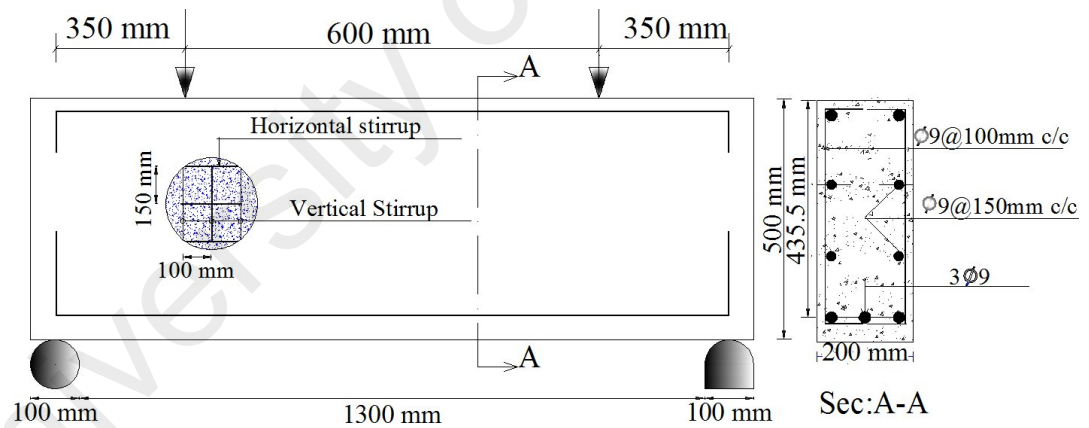


Figure 3.8: Details of beam tested B1

3.3.1.2 Detail of specimen B2

Beam B2 had a length of 1500 mm with a rectangular cross-section of 200 mm width and 500 mm height. Bar used as tensile reinforcement consisted of 3 ϕ 10 HSS with an effective yield strength of 614.4 MPa, that was distributed in one layer. This arrangement of longitudinal steel gave a reinforcement ratio of 0.2687%.

Vertical web reinforcement consisted of ϕ 9 mm NSS bar with f_y of 353 MPa and was spaced at 100 mm. Horizontal web reinforcement consisted of 6 ϕ 9 NSS. The shear span was 350 mm, giving a shear span/depth ratio of 0.910. Dimensions and reinforcement details of beam B2 are shown in Figure 3.9.

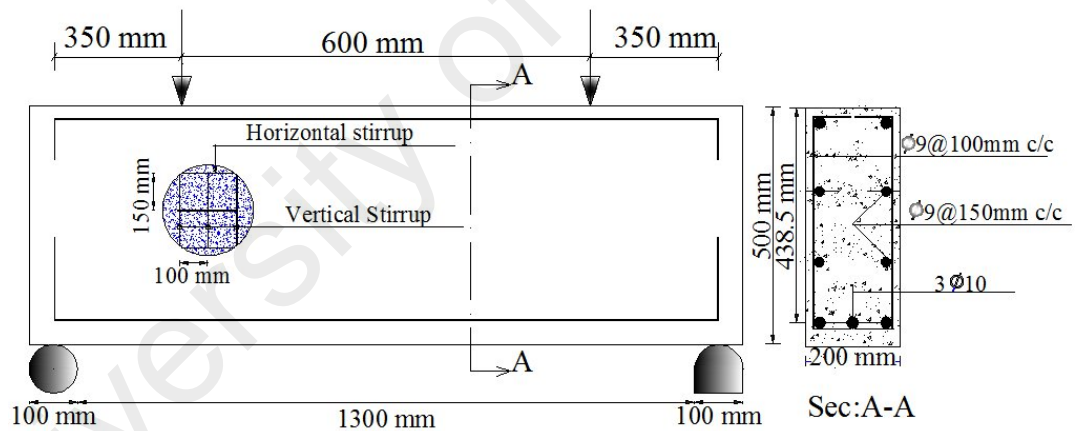


Figure 3.9: Details of beam tested B2

3.3.1.3 Detail of specimen B3

Beam B3 had a length of 1500 mm with a rectangular cross-section of 200 mm width and 500 mm height. Bar used as tensile reinforcement consisted of 2 ϕ 10+2 ϕ 12 HSS with an effective yield strength of 618.0 MPa that was distributed in one layer. This arrangement of longitudinal steel gave a reinforcement ratio of 0.4086%.

Vertical web reinforcement consisted of ϕ 9 mm NSS bar with a f_y of 353 MPa and was spaced at 100 mm. Horizontal web reinforcement consisted of 6 ϕ 9 NSS. The shear span was 350 mm giving a shear span/depth ratio of 0.850. The dimensions and reinforcement details of beam B3 are shown in Figure 3.10.

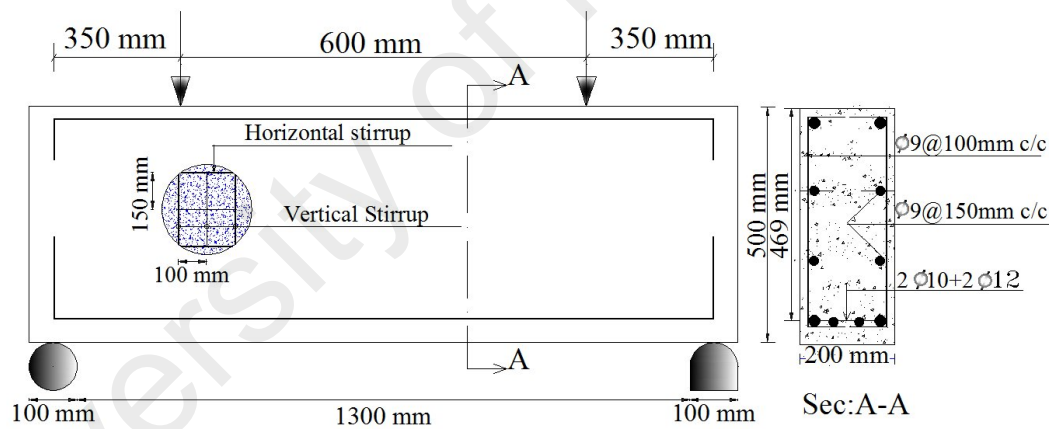
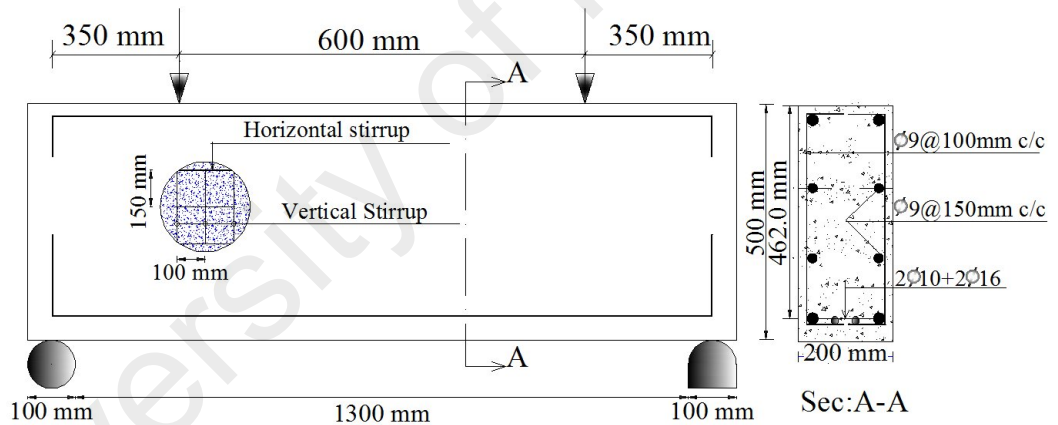


Figure 3.10: Details of beam tested B3

3.3.1.4 Detail of specimen B4

Beam B4 had length of 1500 mm with a rectangular cross-section of 200 mm width and 500 mm height. Bar used as tensile reinforcement consisted of 2 ϕ 10+2 ϕ 16 HSS with an effective yield strength of 590.35 MPa that was distributed in one layer. This arrangement of longitudinal steel gave a reinforcement ratio of 0.6052%.

Vertical web reinforcement consisted of ϕ 9 mm NSS bar with a f_y of 353 MPa and was spaced at 100 mm. Horizontal web reinforcement consisted of 6 ϕ 9 NSS. The shear span was 350 mm, giving a shear span/depth ratio of 0.860. Dimensions and reinforcement details of beam B4 are shown in Figure 3.11.



3.3.1.5 Detail of specimen B5

Beam B5 had a length of 1500 mm with a rectangular cross-section of 200 mm width and 500 mm height. Bar used as tensile reinforcement consisted of 2 ϕ 10+3 ϕ 16 HSS with an effective yield strength of 585.54 MPa that was distributed in one layer. This arrangement of longitudinal steel gave a reinforcement ratio of 0.8019%.

Vertical web reinforcement consisted of ϕ 10 mm HSS bar with a f_y of 614.4 MPa and was spaced at 100 mm. Horizontal web reinforcement consisted of 8 ϕ 10 HSS. The shear span was 400 mm giving a shear span/depth ratio of 0.850. Dimensions and reinforcement details of beam B5 are shown in Figure 3.12.

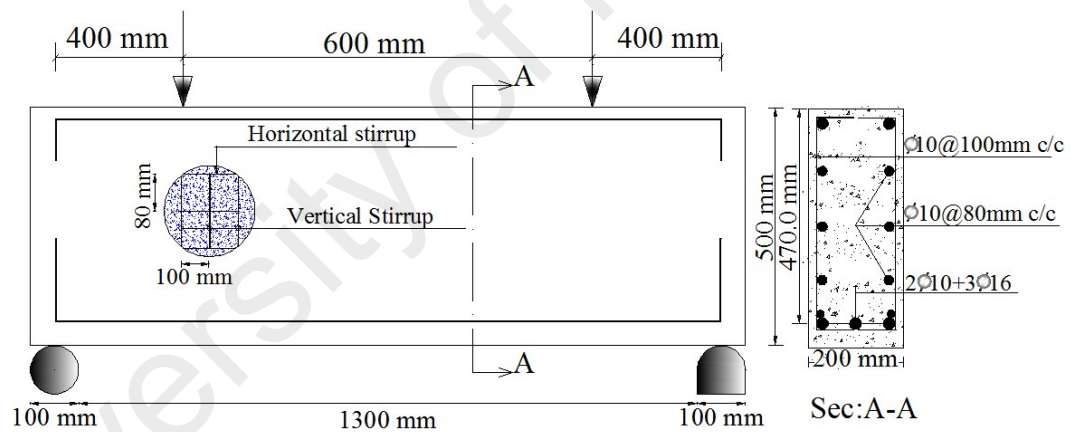


Figure 3.12: Details of beam tested B5

3.3.1.6 Detail of specimen B6

Beam B6 had a length of 1500 mm with a rectangular cross-section of 200 mm width and 500 mm height. Bar used as tensile reinforcement consisted of 1Ø9+4Ø16 HSS with an effective yield strength of 523.64 MPa that was distributed in two layers. This arrangement of longitudinal steel gave a reinforcement ratio of 0.9534%.

Vertical web reinforcement consisted of Ø10 mm HSS bar with a f_y of 614.4 MPa and was spaced at 100 mm. Horizontal web reinforcement consisted of 8Ø10 HSS. The shear span was 400 mm, giving a shear span/depth ratio of 0.880. Dimensions and reinforcement details of beam B6 are shown in Figure 3.13.

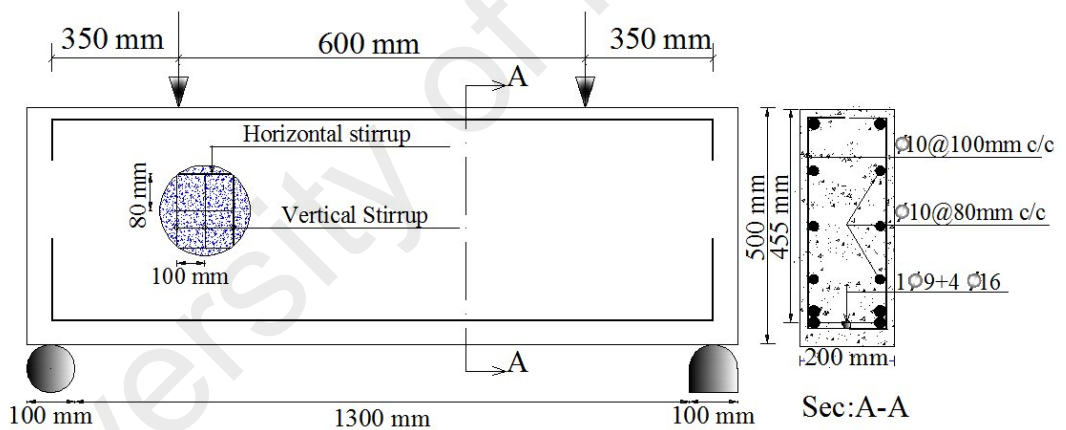


Figure 3.13: Details of beam tested B6

3.3.1.7 Detail of specimen B7

Beam B7 had a length of 1500 mm with a rectangular cross-section of 200 mm width and 500 mm height. Bar used as tensile reinforcement consisted of 2 ϕ 10+4 ϕ 16 HSS with an effective yield strength of 582.33 MPa that was distributed in two layers. This arrangement of longitudinal steel gave a reinforcement ratio of 1.0447%.

Vertical web reinforcement consisted of ϕ 10 mm HSS bar with a f_y of 614.4 MPa and was spaced at 100 mm. Horizontal web reinforcement consisted of 8 ϕ 10 HSS. The shear span was 400 mm giving a shear span/depth ratio of 0.760. Dimensions and reinforcement details of beam B7 are shown in Figure 3.14.

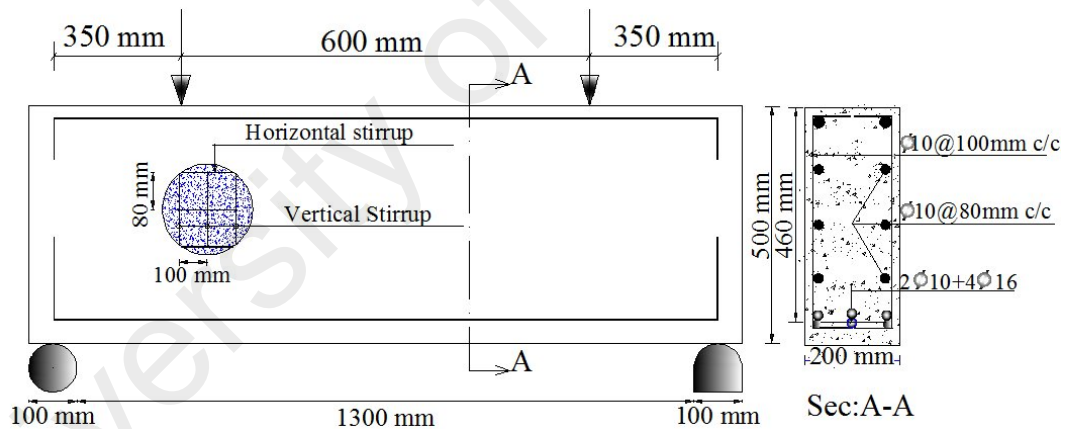


Figure 3.14: Details of beam tested B7

3.3.1.8 Detail of specimen B8

Beam B7 had a length of 1500 mm with a rectangular cross-section of 200 mm width and 500 mm height. Bar used as tensile reinforcement consisted of 2 ϕ 10+5 ϕ 16 HSS with an effective yield strength of 580.04 MPa that was distributed in two layers. This arrangement of longitudinal steel gave a reinforcement ratio of 1.2883%.

Vertical web reinforcement consisted of ϕ 10 mm HSS bar with a f_y of 614.4 MPa and was spaced at 100 mm. Horizontal web reinforcement consisted of 8 ϕ 10 HSS. The shear span was 400 mm giving a shear span/depth ratio of 0.778. Dimensions and reinforcement details of beam B8 are shown in Figure 3.15.

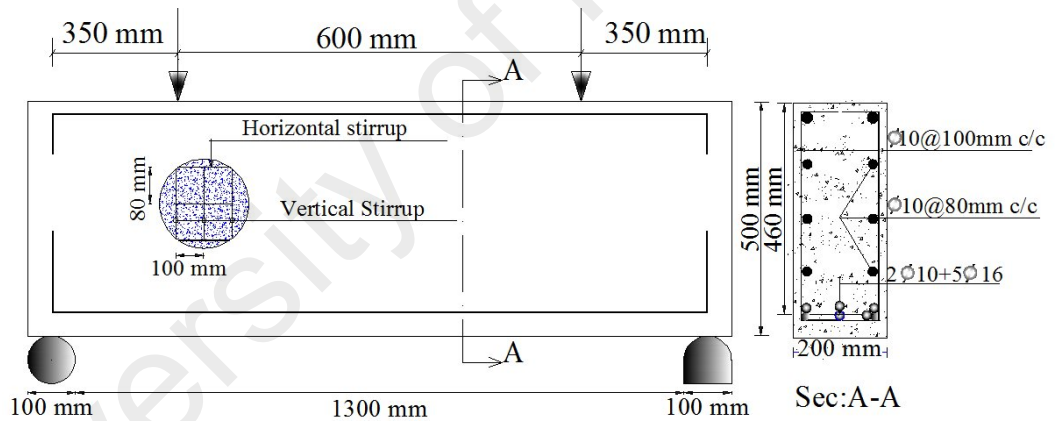


Figure 3.15: Details of beam tested B8

3.4 Test Setup and Loading Process

All simply supported deep beams are subjected to two static point loads as shown in Figure 3.16. The loads are applied using a hydraulic jack, until failure. Figure 3.16 also shows the details of the experimental setup adopted for the present study.

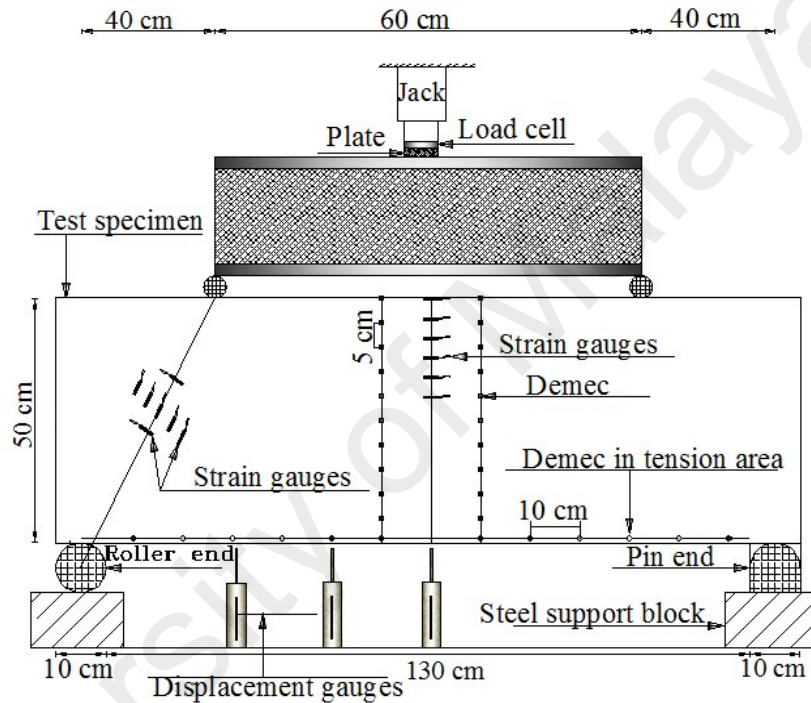


Figure 3.16: Experimental setup for HSSCC deep beams

The beams are supported on two steel cylinders of 10 cm diameter. Two different cylinders were used, allowing the free rotation and elongation of the beam. One of the roller assemblies at the loading points was fixed to provide translation stability during the loading process. A stiff steel spreader beam was used to distribute the load from the hydraulic 2000 kN jack to the two loading points. The spacing between centres of the loading point was 600 mm. After the beam is centred and levelled the steel beam is

placed on the test specimen and the load is applied at midpoint with 20 kN intervals until the first flexural crack occurred. The load at which the first flexural/vertical crack occurred is recorded. Periodically during the test loading is paused to observe cracks. The loads at which cracks occurred are determined by visual inspection. After the appearance of the first flexural crack the loading interval is changed to 50 kN until complete failure is noted. Strains and deflections are recorded at each step of loading using strain gauges and transducers.

In the loading process, the specimens are vertically aligned to reduce failure due to irregularity of supports. To avoid errors in data collection, the data acquisition system is electronically zeroed prior to testing. The observations are marked on the deep beam surface using markers.

3.5 Instrumentation

3.5.1 Overview

An experimental program was conducted to study the behaviour and to predict the strain in the tie section and serviceability of the deep beams under two-point loading containing high-strength steel and HSSCC. The beams were heavily instrumented to obtain as much information as possible about the behaviour of the beams at each stage of loading.

All loads were determined with a load cell. For analysing the behaviour of the deep beams mentioned, instrumentation was used on the surface of the concrete at mid-span, on the tensile bar, on the horizontal bar, on the vertical bar, on the surface of concrete along the compression strut trajectory and perpendicular to it. Also deflection at two points along the beam length and the crack width were measured during the

experimental programme. In this regards, strain gauges, Demec gauges, linear variable displacement transformers (LVDTs) and crack width comparator gauges were used. The strains of the web and tensile bars were measured using strain gauges. Strain gauges on the web bar were used for determining the contribution of web bars within the load capacity of the beams. The concrete strains on the upper half of the beam is measured using strain gauges, while the lower half is measured with Demec gauges due to the initial cracks that appear on the bottom surface of the lower half. Displacements were measured with standard LVDT's. All data was monitored and recorded by data loggers.

3.5.2 Strain gauges

All the strain gauges used were TML (Type PFL-30-11) and regular 120 Ω gauges. First the surface of the reinforcing bars was smoothed with using sand paper and a grinder. Strain gauges were placed on the prepared surface area using glue. Then all strain gauges were covered with a waterproof coating and a layer of silicon to prevent damage during the casting and curing of the concrete. Figures 3.17 to 3.24 show the strain gauge location for all specimens.

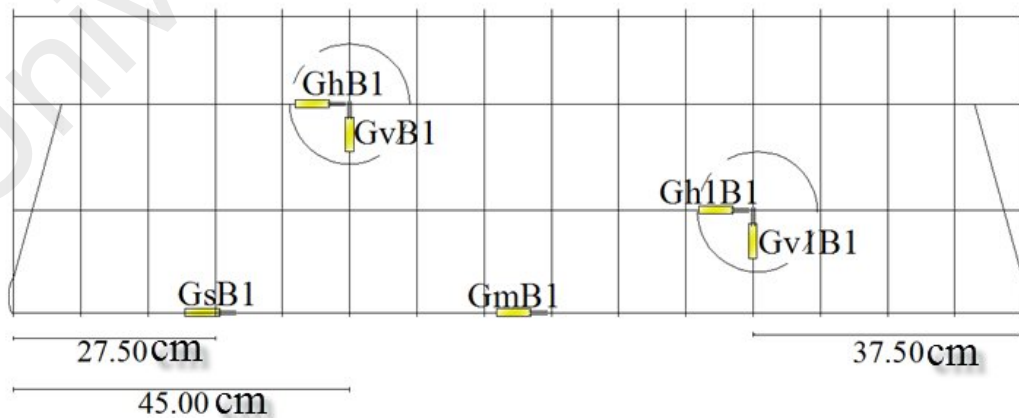


Figure 3.17: Strain gauge locations on beam B1

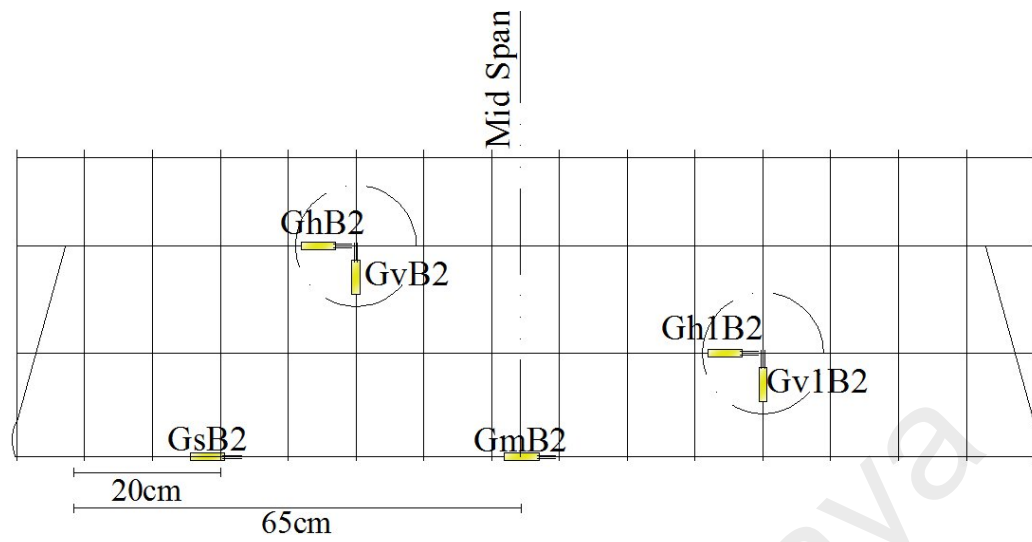


Figure 3.18: Strain gauge locations on beam B2

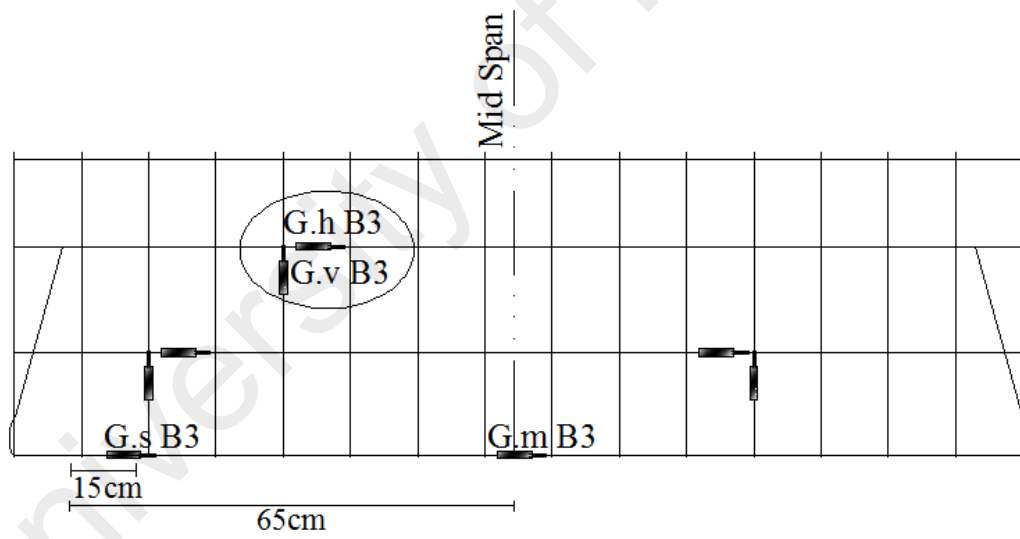


Figure 3.19: Strain gauge locations on beam B3

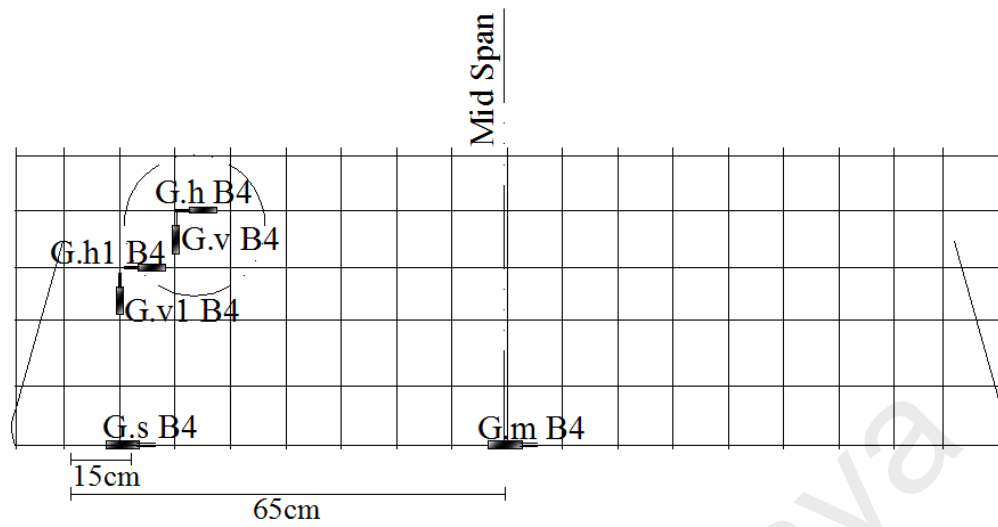


Figure 3.20: Strain gauge locations on beam B4

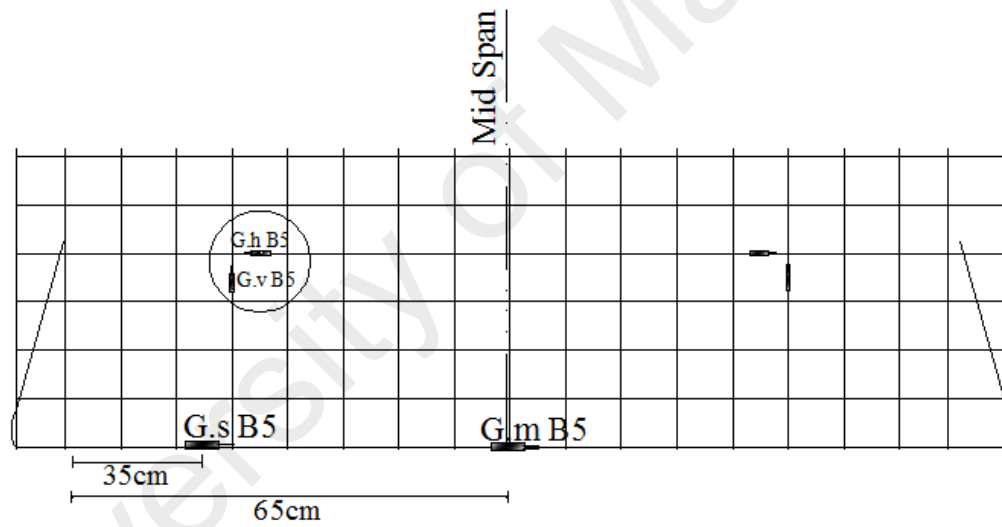


Figure 3.21: Strain gauge locations on beam B5

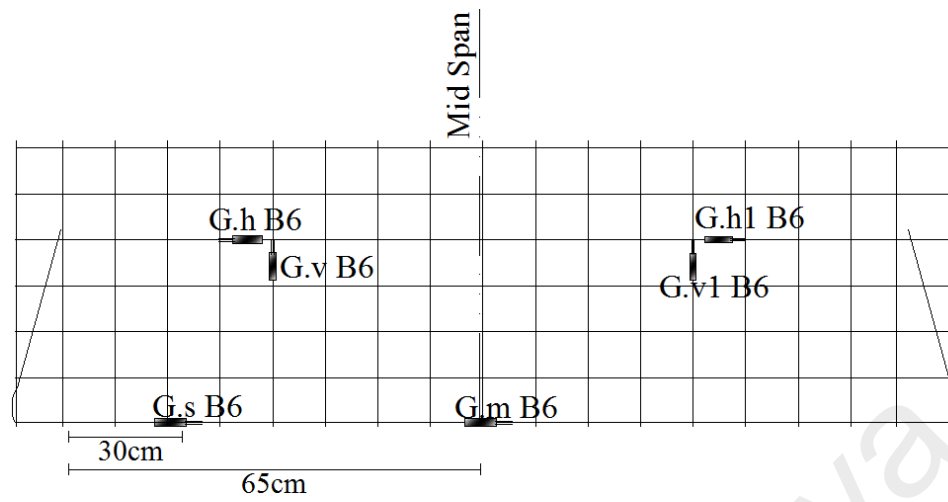


Figure 3.22: Strain gauge locations on beam B6

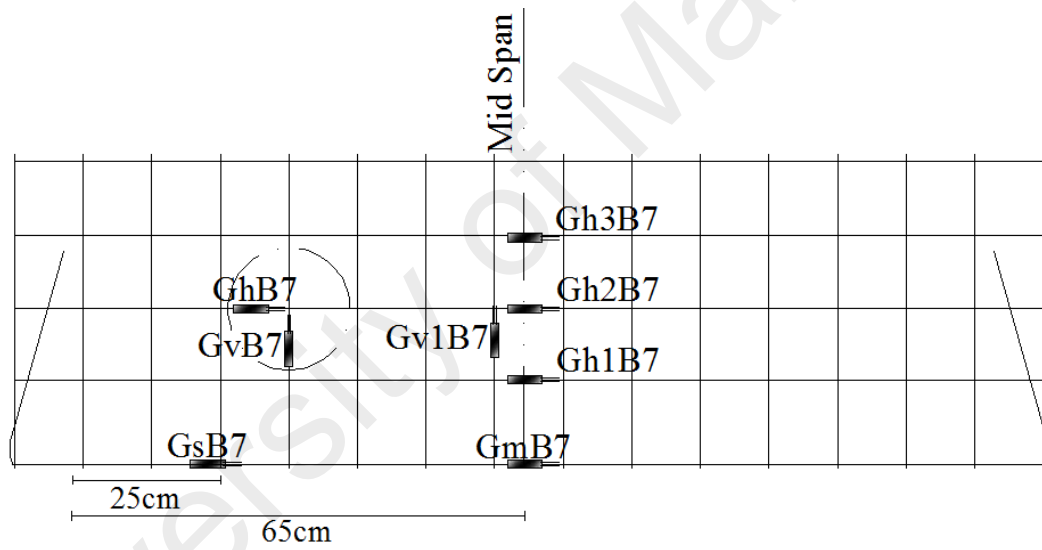


Figure 3.23: Strain gauge locations on beam B7

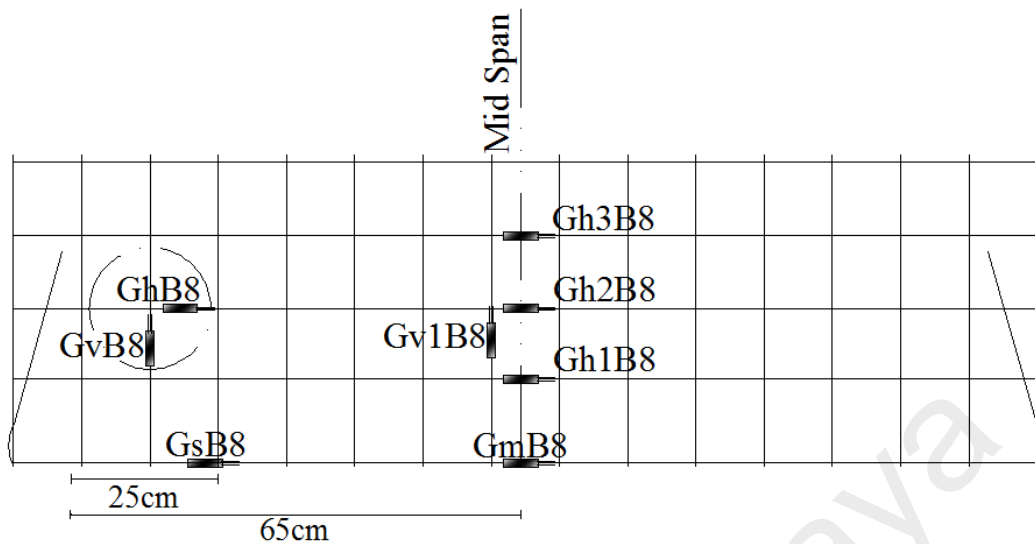


Figure 3.24: Strain gauge locations on beam B8

The strain gauges on the concrete surface were used in different locations for different purposes, which are considered in Figure 3.16.

3.5.3 Data acquisition system

A data logger was used to store all instrumentation readings during each test. 30 channels were monitored. All data were zeroed prior to the start of the tests. The data were recorded every 5 seconds.

3.6 Methodology of Numerical Study

3.6.1 Adaptive network-based fuzzy inference system (ANFIS)

Given the complexities in deep beam behaviour and the difficulties in the accurate evaluation of its deflection as a serviceability index and prediction of strain and stress in

tie section of STM, the current study has employed the Adaptive Network-based Fuzzy Inference System (ANFIS) as one of the modelling tools to predict deflection and strain and stress in tie sections of STM for HSSCC deep beams. Effective input data and the corresponding deflection and strain of tie sections as output data were recorded at all loading stages up to the failure load for all deep beams tested.

3.6.1.1 Data availability

An extensive data set was gathered from eight HSSCC deep beams. The data used in this study are based on the parameters presented in Table 3.5. The available data set covers 3668 data points (instances) collected from the tested concrete deep beams for deflection predictions, and 3773 data for strain in tie section prediction.

Each instance is represented by a 10-dimensional real-valued vector, and is the input parameter shown in Table 3.5 or Table 3.6 with its corresponding deflection or strain in tie section as the output.

Table 3.5: Different parameters of the eight HSSCC deep beams for deflection prediction

Input Parameters										Output
P	f_{cu}	a/d	l_0/d	f_{yv}	f_{yh}	$A_v/b.s_v$	$A_h/b.s_h$	ρ	f_y	Δ

For tie strain prediction, each instance is represented by a 10-dimensional real-valued vector and is the input parameter shown in Table 3.6 with its corresponding strain in tie section as the output.

Table 3.6: Different parameters of the eight HSSCC deep beams for tie strain prediction

Input Parameters										Output
P	f_{cu}	a/d	l_0/d	f_{yv}	f_{yh}	$A_v/b.s_v$	$A_h/b.s_h$	ρ	f_y	ε

The input parameters consist of applied load (P), concrete cube strength (f_{cu}), ratio of shear span to effective depth of beam (a/d), ratio of effective span to effective depth of beams (l_0/d), yield strength of vertical web reinforcement (f_{yv}), yield strength of horizontal reinforcement (f_{yh}), area of vertical bar to distance of vertical bars ($A_v/b.s_v$), area of horizontal bar to the distance of horizontal bars ($A_h/b.s_h$), tensile reinforcement ratio (ρ) and strength of tensile bar at yielding condition (f_y), while (Δ) is used as the output or deflection amount at the mid-span of the HSSCC deep beams in Table 3.5 and (ε) as the strain in tie section in Table 3.6.

3.6.1.2 System modelling

System modelling alters the parameters of an adaptive intelligent system (like ANN and ANFIS) to suit an unknown actual/engineering system transfer function. A schematic of the system modelling problem utilising the adaptive intelligent system is shown in Figure 3.25. As shown in this figure, the parameters of the estimated intelligent system are tuned using proper learning methods to ensure the accurate estimation of the actual system. In other words, performance function, typically the mean squared error (MSE) between the intelligent system's output and actual response, is minimised.

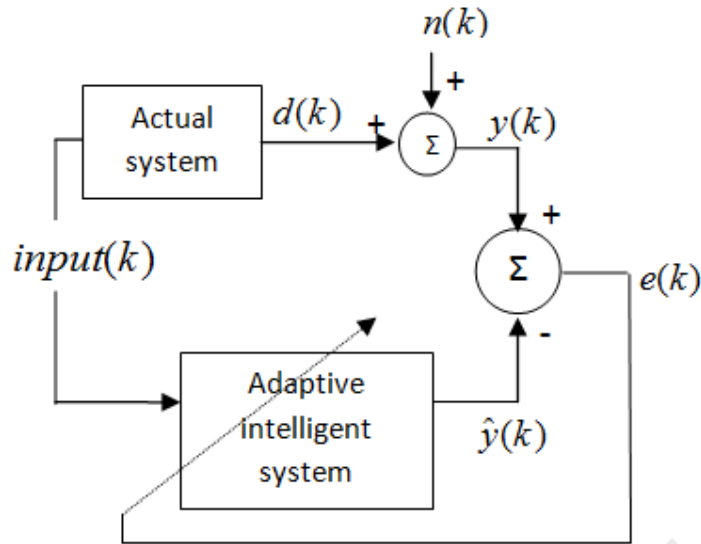


Figure 3.25: System modelling using an adaptive intelligent system

The objective function in system modelling problems is expressed as follows:

$$MSE = \frac{1}{L} \sum_{k=1}^L (\hat{y}(k) - y(k))^2 \quad (\text{Eq. 3.1})$$

where $y(k)$ is the noisy output of the actual system (measured or observed output), $\hat{y}(k)$ is the adaptive intelligent system output and L is the number of instances. Some cases are noise free where $y(k)$ is equal to $d(k)$ which is the desired output. When noise is present, $\hat{y}(k)$ is the estimation of the desired output or semi desired output. ANFIS is used in this study as an adaptive intelligence system tool to model the deflection of deep beams.

3.6.1.3 Fuzzy expert system

Human reasoning is able to process uncertainties and vague concepts appropriately. It, however, cannot express it precisely. Fuzzy logic allows the modelling of uncertainties

and the human brain's thinking, reasoning and perception (Jang et al, 1997). Based on Boolean logic, we apply two concepts only, either 'True' or 'False', represented by 1 and 0 respectively. Therefore a proposition can only be true or false. Fuzzy logic, an extension of Boolean logic, allows intermediate values between these two values where the classical theory of binary membership in a set is extended to incorporate memberships between 0 and 1. This allows each proposition to be either True or False to a certain degree between them. With X as the space of objects and x as an element of X , a classical set $A, A \subseteq X$, is defined as a collection of elements $x \in X$, such that x can either belong or not belong to set A . In other words, set A is described in Equation (3.2)

$$A = \{x | x \in X\} \quad (\text{Eq. 3.2})$$

whereas, a fuzzy set A in X is defined by Equation (3.3)

$$A = \{(x, \mu_A(x)) | x \in X\} \quad (\text{Eq. 3.3})$$

where $\mu_A(x)$ is the membership function for the fuzzy set A . Here, A is a linguistic term (label) that is determined by the fuzzy set. The membership function maps each element of x to a membership grade between zero and one; ($\mu_A(x) \in [0,1]$). For example, this set can present x as 'medium', which is a linguistic term that can be described by a fuzzy set with soft boundaries. Figure 3.26 shows two sets, one based on Boolean logic and the other on fuzzy logic.

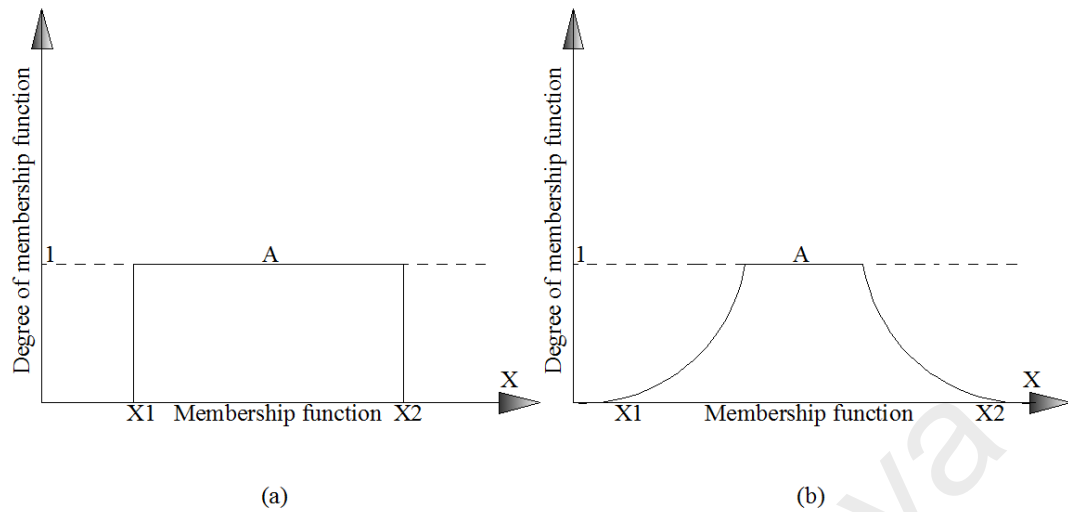


Figure 3.26: An example of (a) a classical Boolean set, and (b) a Fuzzy Logic set

3.6.1.4 Fuzzy inference system (FIS)

Fuzzy systems provide a means of representing the expert knowledge of the human about the process in terms of fuzzy (IF–THEN) rules which is the basic unit for capturing knowledge in a fuzzy system. Similar to a conventional rule in artificial intelligence, a fuzzy rule has two components: an ‘IF’ part and a ‘THEN’ part which are also referred to as antecedent and consequent, respectively. The main structure of the fuzzy rule is shown in Equation (3.4):

$$IF \text{ <antecedent> } THEN \text{ <consequent>} \quad (Eq. 3.4)$$

The antecedent of a fuzzy rule can conditionally be satisfied to a degree. Similarly to conventional rules, the antecedent of a fuzzy rule may combine multiple simple conditions into a complex string using AND, OR and NOT logic operators. The consequence of a fuzzy rule can be classified into two main categories:

- a) Fuzzy consequent (Equation 3.5) where C is a fuzzy set.

b) Functional consequent (Equation 3.6) where p, q and r are constant.

$$\text{IF } x \text{ is } A \text{ and } y \text{ is } B \text{ THEN } f \text{ is } C \quad (\text{Eq. 3.5})$$

$$\text{IF } x \text{ is } A \text{ and } y \text{ is } B \text{ THEN } f = px + qy + r \quad (\text{Eq. 3.6})$$

Basically, fuzzy inference systems incorporates an expert's experience into the system design and are composed of 4 blocks (Figure 3.27). A FIS comprises a 'fuzzifier' that transforms the 'crisp' inputs into fuzzy inputs by membership functions that represent fuzzy sets of input vectors. It also contains a knowledge-base that includes the information given by the expert in the form of linguistic fuzzy rules. An inference-system (engine) uses them together by a method of reasoning and a 'defuzzifier' that transforms the fuzzy results of the inference into a crisp output using a 'defuzzification' method (Haykin, 1998).

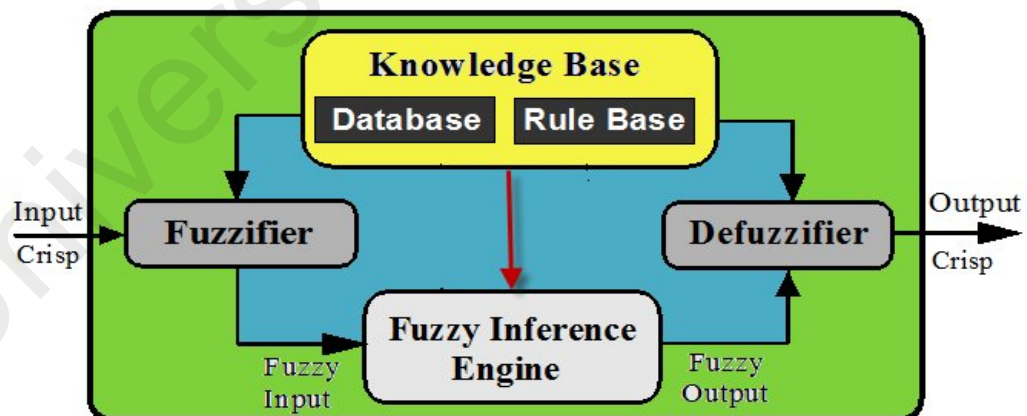


Figure 3.27: A flow diagram of a fuzzy inference system (FIS)

The knowledge-base comprises two components: a data-base, which is the membership functions of the fuzzy sets used in the fuzzy rules, and a rule-base which comprises a collection of linguistic rules that are combined by a specific operator. The generic structure of a FIS is shown in Figure 3.27. The two common types of FIS vary according to differences between the specifications of the consequent part of fuzzy rules (Equations 3.5 and 3.6). The first fuzzy system uses the inference method proposed by Mamdani in which the rule consequent is defined by fuzzy sets and has the structure of Equation 3.5 (Mamdani & Assilian, 1975).

The second fuzzy system proposed by Takagi, Sugeno and Kang (TSK) contains an inference engine where the conclusion of a fuzzy rule is made up of a weighted linear combination of the crisp inputs rather than a fuzzy set (Takagi & Sugeno, 1985). The TSK system has the structure shown in Equation 3.6. TSK models are suitable for approximating large nonlinear systems.

The knowledge-base containing the database and rule-base of a FIS can be constructed from an expert's knowledge. For this, the expert selects the membership functions and rules. In this way, fuzzy models can help in extracting expert knowledge at an appropriate level. Fuzzy systems can also be constructed from data and this alleviates the problem of knowledge acquisition. Various techniques have been used to analyse data with the best possible accuracy. There are two common approaches for constructing a FIS using available data. The first approach is where the rules of the fuzzy system are often designated a priori and the parameters of the membership functions are adapted during the learning process from input to output data using an evolutionary algorithm (e.g. genetic algorithm). In the second approach, the fuzzy system can be generated using hybrid neural nets. The neural net defines the shape of the membership functions of the premises; this architecture and learning procedure is called an adaptive network-based fuzzy inference system (Jang, 1993).

3.6.1.5 Adaptive network-based fuzzy inference system (ANFIS)

ANFIS is a multilayer feed-forward network in which each node performs a particular function on incoming signals as well as a set of parameters pertaining to this node (Jang, 1993). Similarly to ANN, ANFIS is capable of mapping unseen inputs to their outputs by learning the rules from the previously seen data. A simple structure of this type of network having just two inputs of x and y and one output of f is shown in Figure 3.28.

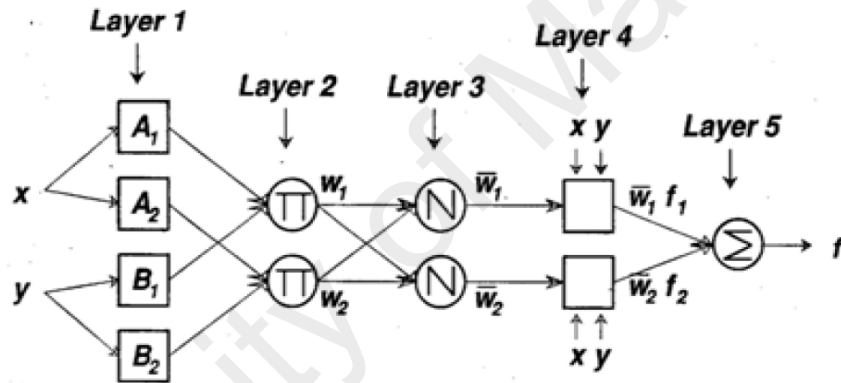


Figure 3.28: ANFIS architecture (Jang, 1993)

As can be seen from the figure above, ANFIS contains five layers in its architecture, including the fuzzify layer, product layer, normalised layer, defuzzify layer, and total output layer. It is highlighted here that by assuming just two membership functions for each of the input data x and y , the general form of a first-order TSK type of fuzzy if-then rule has been given by Equation 3.7. Here, we re-write the rule i of the ANFIS as:

$$\text{Rule } i: \text{ IF } x \text{ is } A_i \text{ and } y \text{ is } B_i \text{ THEN } f_i = p_i x + q_i y + r_i, \quad i = 1, 2, \dots, n \quad (\text{Eq. 3.7})$$

where n is the number of rules and p_i , q_i and r_i are the parameters determined during the training process. In the first stage of the learning process, the membership function (μ) of each of the linguistic labels A_i and B_i are calculated as follows:

$$O_i^1 = \mu_{A_i}(x), \quad i=1,2,\dots,n \quad (\text{Eq. 3.8})$$

$$O_i^1 = \mu_{B_i}(y), \quad i=1,2,\dots,n \quad (\text{Eq. 3.9})$$

In the second layer, which is the product layer, the previously calculated membership degrees of linguistic variables are multiplied as shown in Equation 3.10:

$$O_i^2 = w_i = \mu_{A_i}(x) \mu_{B_i}(y) \quad i=1,2,\dots,n \quad (\text{Eq. 3.10})$$

The third layer, the normalised layer, is where the ratio of each weight to the total weights is calculated:

$$O_i^3 = \bar{w}_i = \frac{w_i}{\sum_{i=1}^n w_i} \quad i=1,2,\dots,n \quad (\text{Eq. 3.11})$$

The fourth layer is the defuzzification layer with adaptive nodes, where their outputs depend on the parameter(s) pertaining to these nodes and the learning rule specifies how these parameters are altered to minimise the measure of the prescribed error (Jang, 1993). The relationship for these nodes is as follows:

$$O_i^4 = \bar{w}_i = f_i = \square w_i(p_i x + q_i y + r_i) \quad i=1,2,\dots,n \quad (\text{Eq. 3.12})$$

Finally in the fifth layer, the summation of all the incoming signals is performed where the output of the system is the final result:

$$O_i^5 = \sum_{i=1}^n \bar{w}_i f_i \quad i=1,2,\dots,n \quad (\text{Eq. 3.13})$$

3.7 ANN Structure and Definition

ANNs are modelling tools that work in a similar manner to the human brain; ANNs were, in fact, extracted from a biological neural network. ANN is an intelligent information processing system and consists of three main aspects, including transmission, processing and storage of information.

The matching parts of an ANN are:

- (a): The input layer which consists of number of nodes which receive input data of an independent variable. Therefore, the total number of nodes in the input layer is equal to the total number of the input variables of the problem.
- (b): The one or more hidden layers which receive information from the input layer, using the applied weights and pre-specified activation functions.
- (c): The output layer which receives the processed information from the hidden layer and sends the results to an external recreant.

The number of nodes in the output layer is equal to the number of output variables. The number of hidden layers and the number of nodes in each hidden layer are important factors in the design of the network, and there are no generally applicable rules to exactly determine these numbers (Flood & Kartam, 1994).

The data collected for the problem is divided into training and testing data sets. Depending on the available data, about 80% of the total data is utilised as the training set. The number and distribution of training patterns affect the generalisation ability of the ANN (Flood & Kartam, 1994). The training pattern must cover all possible ranges of the study.

Once the topology of the ANN is determined, the training process is started by assigning values to the training parameters and specifying the activation function and learning algorithm. Different learning algorithms can be applied; amongst which is the back-propagation algorithm that is predominantly used in civil engineering applications (Adeli, 2001). This algorithm looks for the minimum error function in weight space using the method of gradient descent.

3.7.1 Evaluation

To evaluate the comparative methods, the MSE and Correlation Coefficient/Pearson Coefficient (R) values are used in this study. MSE is a risk function which corresponds to the expected value of the squared error loss or quadratic loss. R is the degree of success in reducing the standard deviation (SD). It is widely used in the sciences as a measure of the strength of linear dependence between two variables. Equation 3.14 presents the MSE and R is calculated as follows:

$$R^2 = 1 - \frac{\sum_{k=1}^L (y(k) - \hat{y}(k))^2}{\sum_{k=1}^L (y(k) - y_{ave})^2} \quad (\text{Eq. 3.14})$$

where $\hat{y}(k)$ is the output predicted by ANN, $y(k)$ is the actual (observed) output, y_{ave} is the averaged actual output and L is the total number of training/testing instances.

3.7.2 Training and testing of neural networks

Training means to present the network with the experimental data and have it learn, or modify, its weights, so that it correctly predicts the mid-span deflection of HSSCC deep

beams. However, training the network successfully requires many choices and training experiences.

The master unit of the network is a complex network of neurons that act in parallel and work as a numerical processing unit. The effect of the connection between neurons is referred to as the weight of the internal connection. In the generation process, the network gets a random amount of the weight to find the optimum relationship between the experimental data. ANN learns to solve the problems based on the relationship between the experimental data. The mathematical neuron model is shown in Figure 3.29.

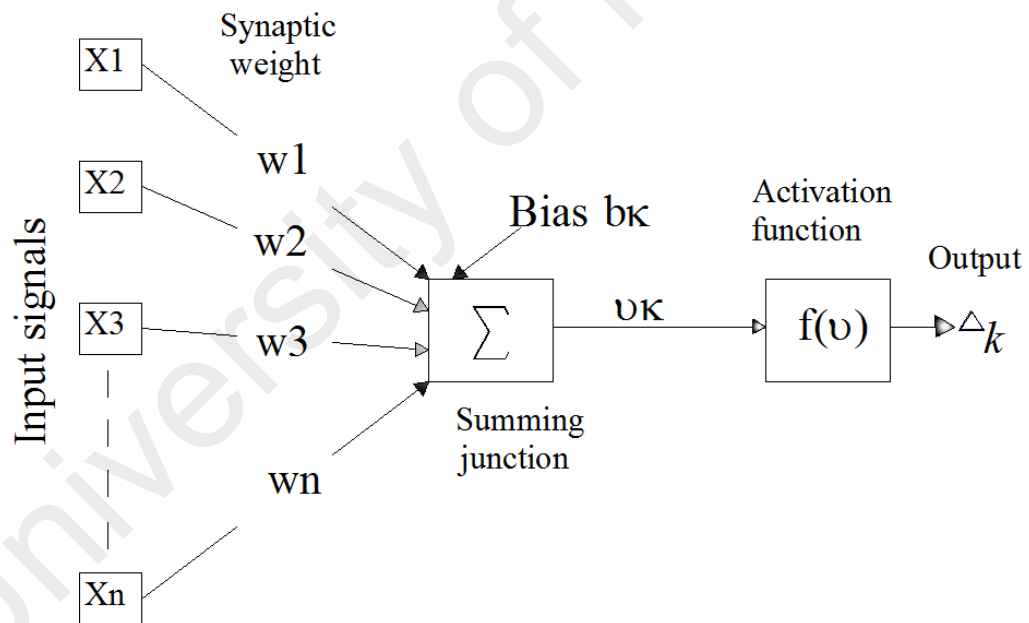


Figure 3.29: Neuron model with n-element in the input model

The effect of input vector (X) on output (Δ) is defined by the weight (W). The other input is the constant value of 1 that is multiplied by bias (b_k), and then added with WX .

In general, ANN can be structured in either a single layer or a multilayer networks. The structure of single and a multilayer ANNs are shown in Figure 3.30. A typical multi-layer ANN (MLNN) includes an input layer, output layer and at least one hidden layer of neurons. MLNNs are sometimes known as layered networks.

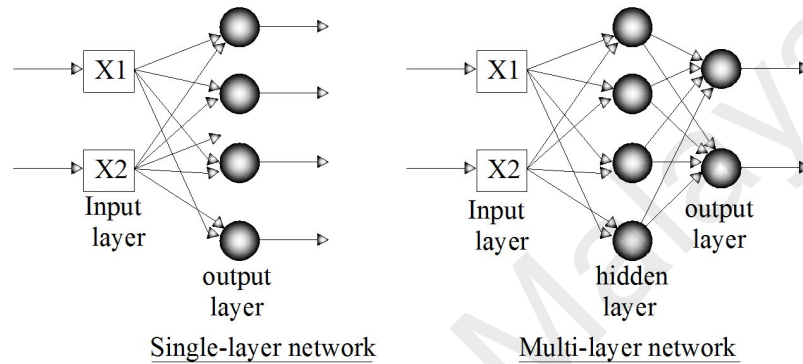


Figure 3.30: Single-layer and multi-layer networks

MLNNs supply an improvement in computational ability over a single-layer neural network unless there is a nonlinear relationship between layers. Many of neural network abilities, such as learning, nonlinear functional approximation, generalisation, etc. are in fact completed because of the nonlinear activation function of neurons.

Twenty percent of data is applied for network testing, and the other outputs are used for verifying and training. Regarding Tables 3.5 and 3.6, a multi-layered feed-forward neural network (MLFFNN) equipped with back-propagation (BP) learning is constructed.

3.7.3 Variants of back-propagation learning algorithms

To train the MLFFNN, five variants of BPs are examined. More precisely, the Levenberg-Marquardt BP (Trainlm), Gradient descent with momentum (Traingdm) and (Traingda), Basic gradient descent (Traingd) and Adaptive learning rate (Traingdx) were used for network training at the end of the analysis. Descriptions of training algorithms are presented in Table 3.7.

Table 3.7: BPs learning functions used in this study

Function	Description
Trainlm	Trainlm Levenberg-Marquardt BP algorithm. Fastest training algorithm for networks of moderate size with a memory reduction feature for use when the training set is large
Traingdm	Gradient descent with momentum. Is generally is faster than Traingd and can be used in incremental mode training.
Traingda	Updates weight and bias values according to gradient descent with an adaptive learning rate, can train any network as long as its weight, net input, and transfer functions have derivative functions. Gradient descent with adaptive lr back-propagation.
Traingd	Basic gradient descent. Slow response, can be used in incremental mode training.
Traingdx	Adaptive learning rate. Faster training than Traingd, but can only be used in batch mode training.

4. RESULTS AND DISCUSSION

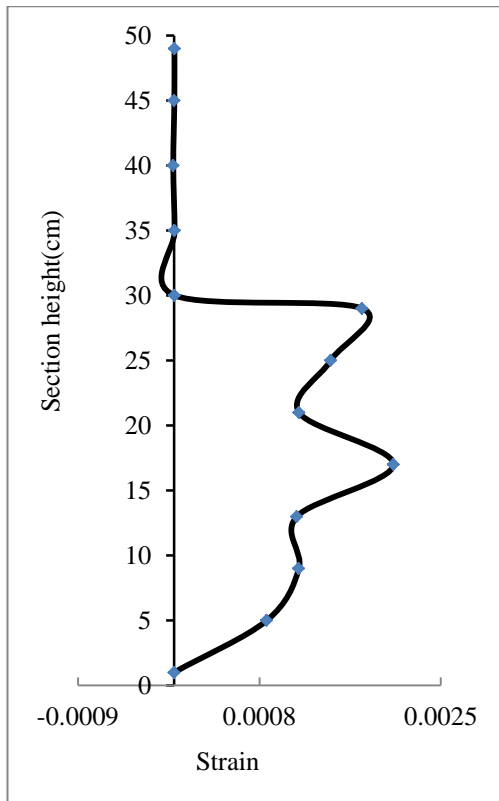
This chapter discusses and compares the experimental and numerical results of the beams tested. In this project, the design, prediction of serviceability and strain are considered which are effected of reinforcing steel type, tensile reinforcement ratio and the presence of web reinforcement. The influence of these parameters on the behaviour of the beams is analysed and the results are compared. Deflection prediction as a serviceability index and strain in tie section are studied with ANN, ANFIS and LR. The results are compared for performance assessment.

For the study of the results, three subchapters are presented regarding the experimental study, numerical investigation and finite element modelling.

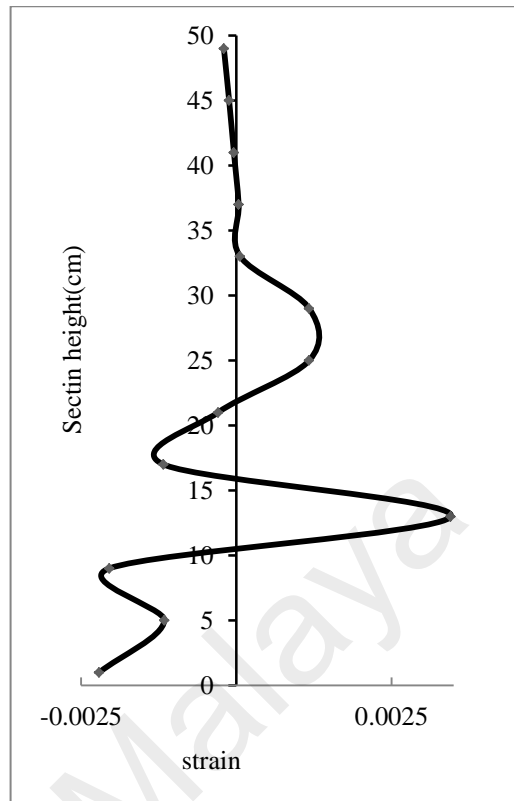
4.1 Experimental Study and Discussion

4.1.1 Horizontal strain distribution at the height of mid-span in HSSCC deep beams

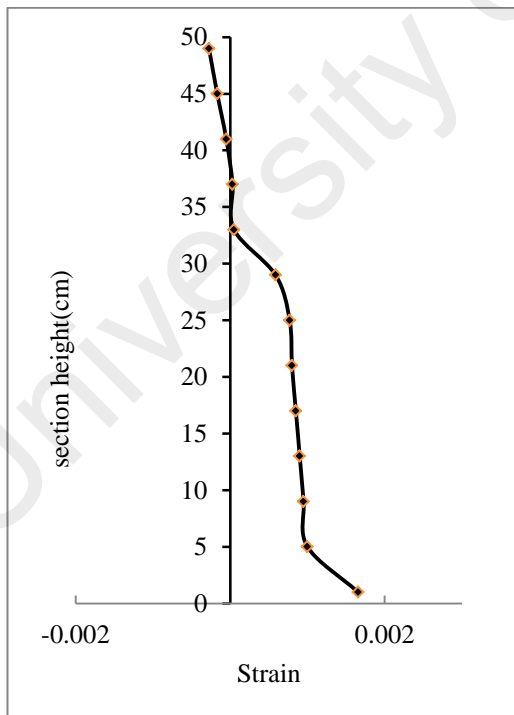
The basic assumption for shallow beams that the plane section remains plane after deformation does not apply to deep beams. The strain distribution throughout the height of the beam section in the first stage of loading, at the appearance of the first crack, at the initiation of yielding of the main tensile reinforcement and at the ultimate loading stage were recorded. The results of beams tested are presented in Figures 4.1 to 4.6.



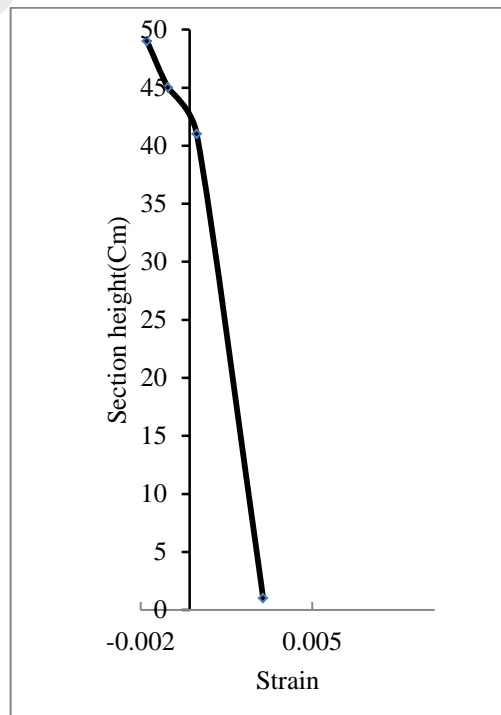
(a) First load



(b) First crack

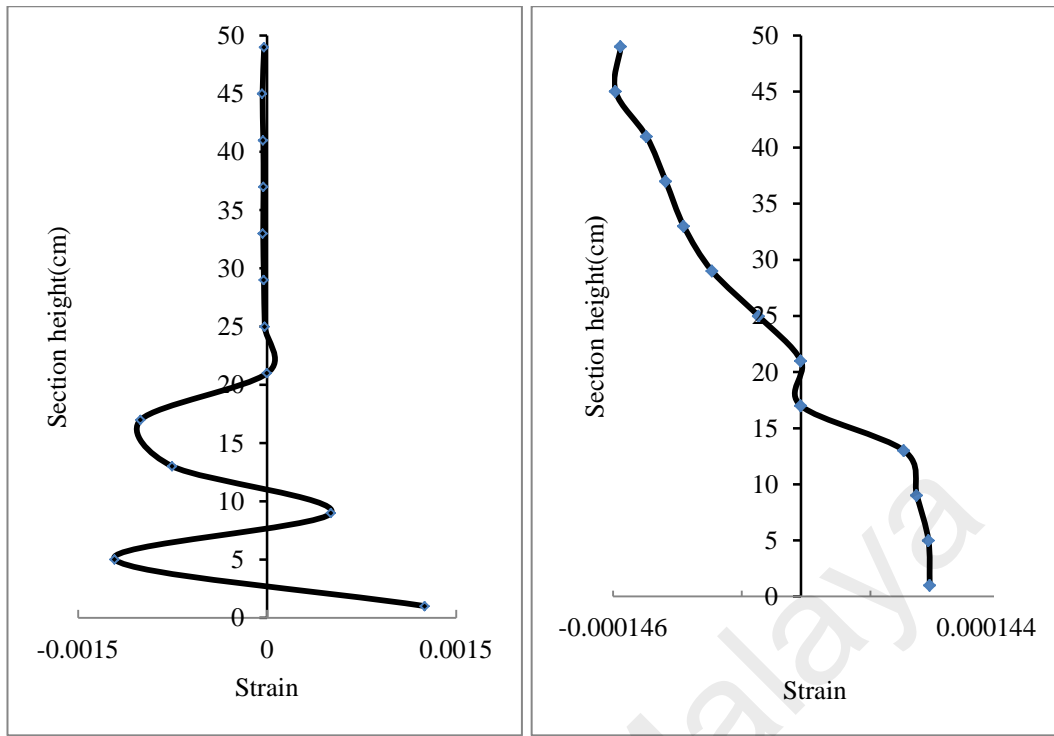


(c) Yielding state



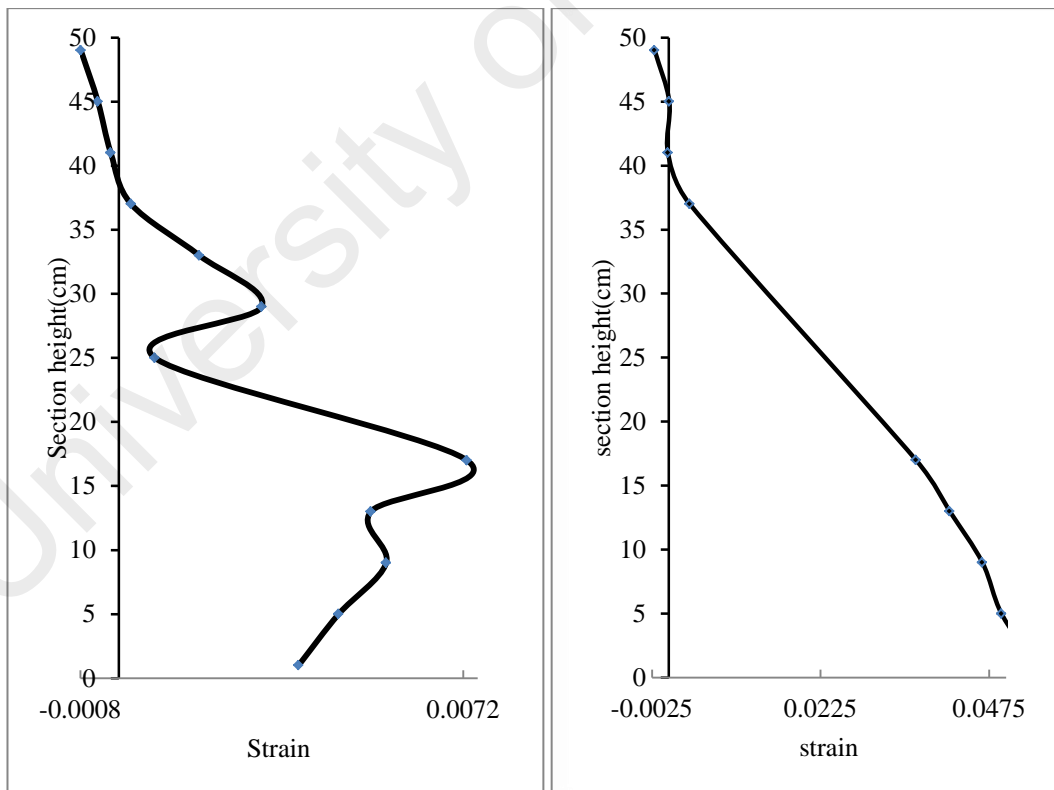
(d) Ultimate state

Figure 4.1: NAD variations at mid-span at different loading stages for B1



(a) First load

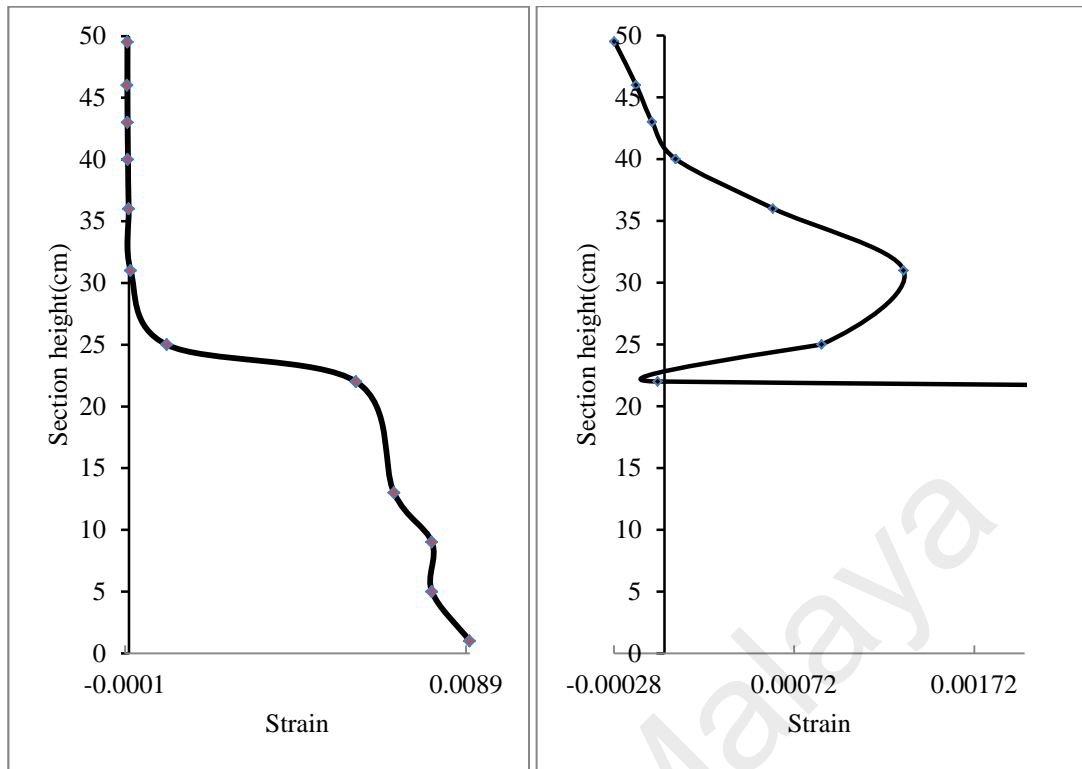
(b) First crack



(c) Yielding state

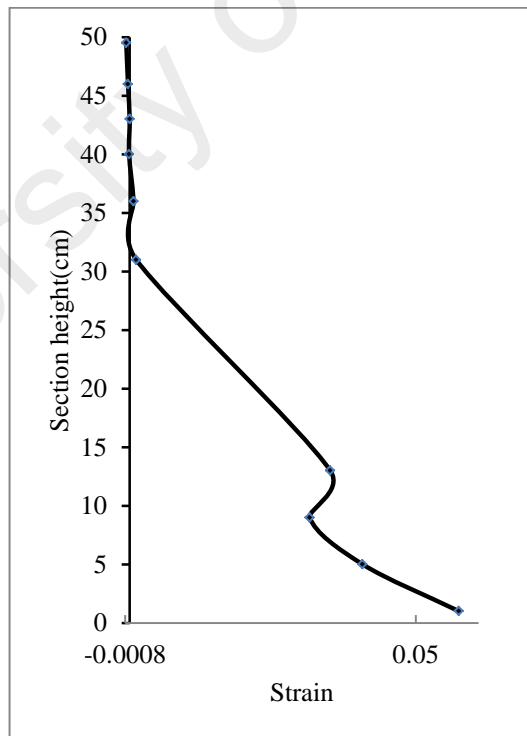
(d) Ultimate load

Figure 4.2: NAD variations at mid-span at different loading stages for B2



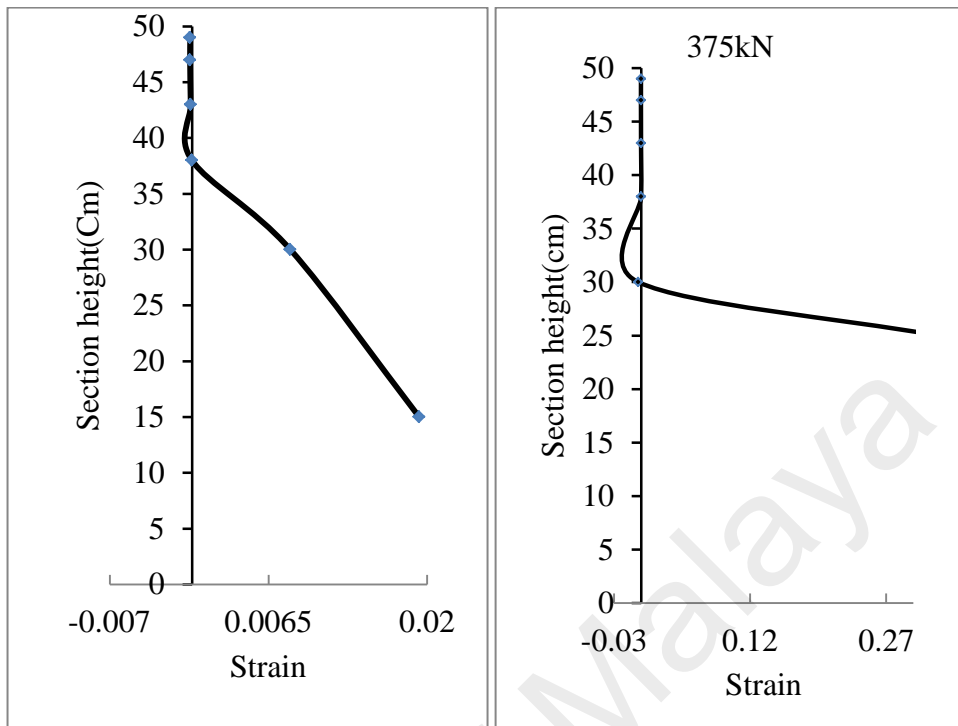
(a) First crack

(b) Occurrence of inclined crack



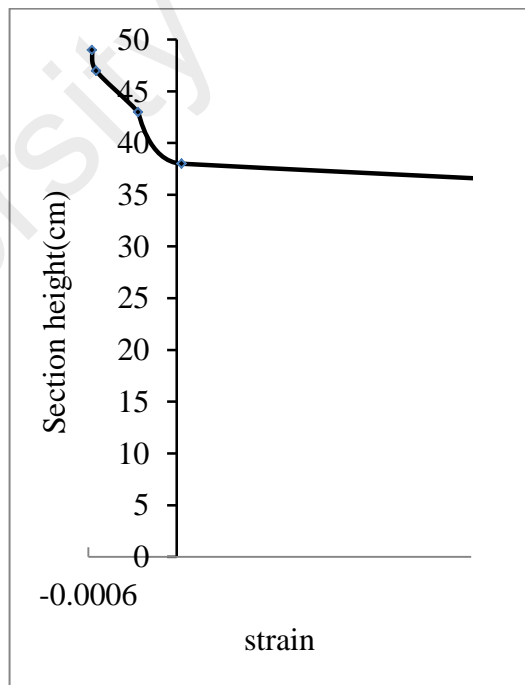
(c) Ultimate load

Figure 4.3: NAD variations at mid-span at different loading stages for B3



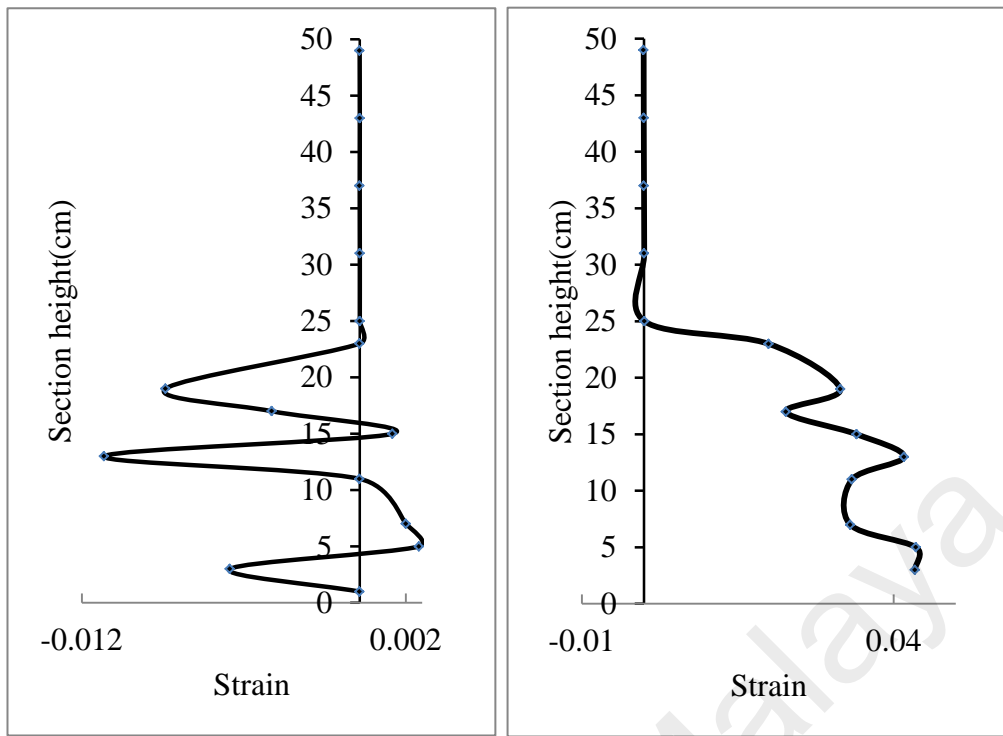
(a) First crack

(b) Specified load



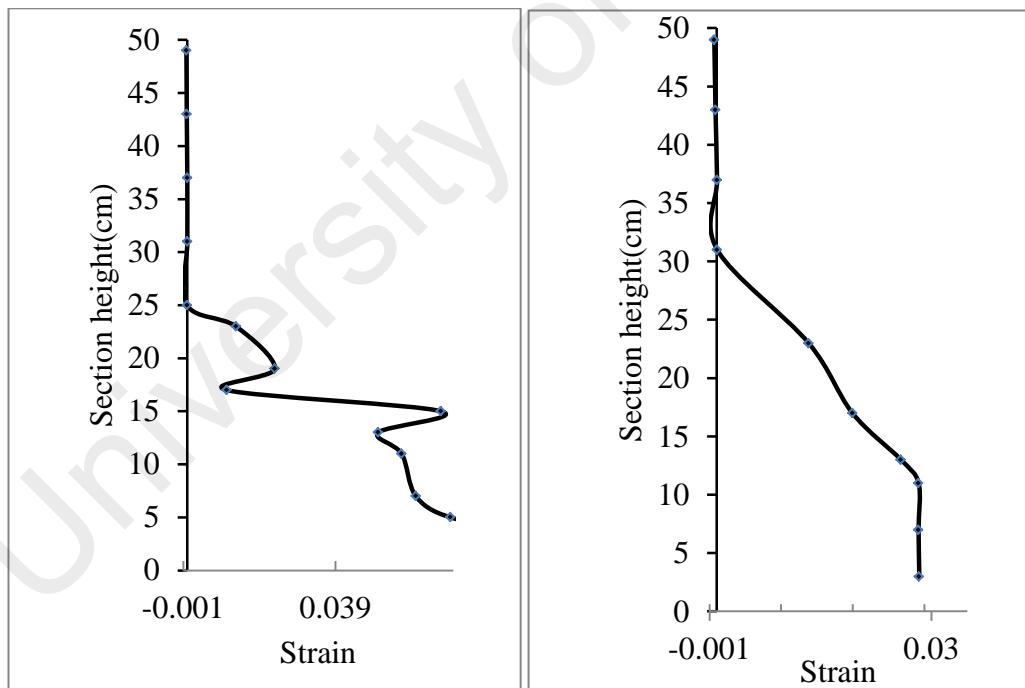
(c) Ultimate load

Figure 4.4: NAD variations at mid-span at different loading stages for B4



(a) First load

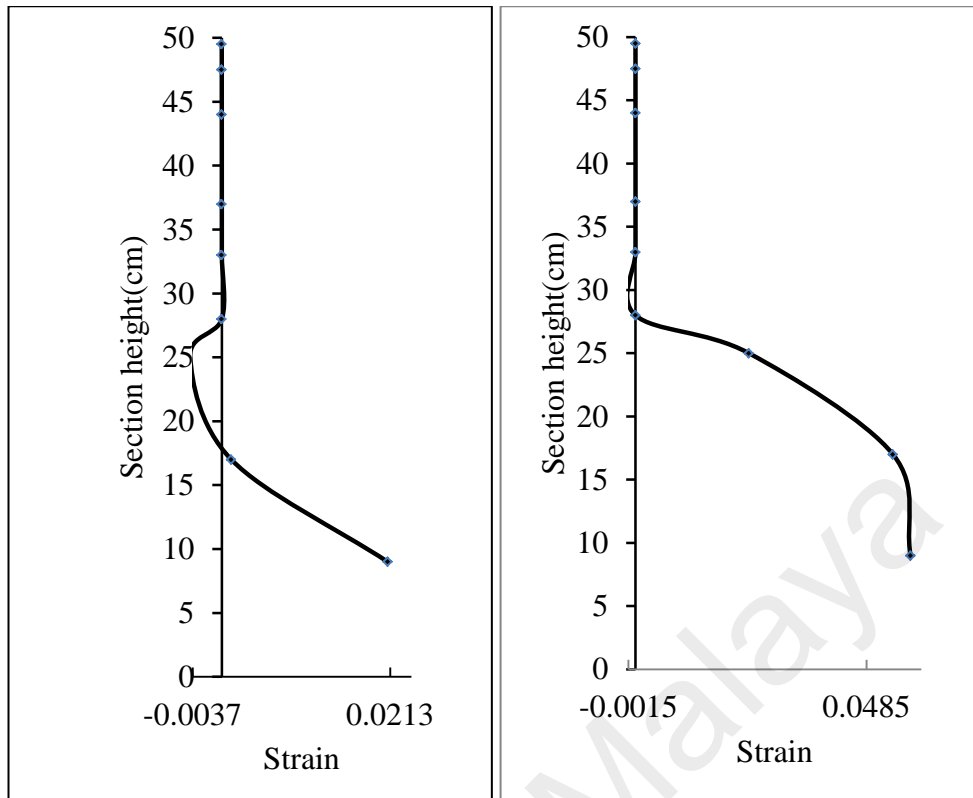
(b) First crack



(c) Specified load

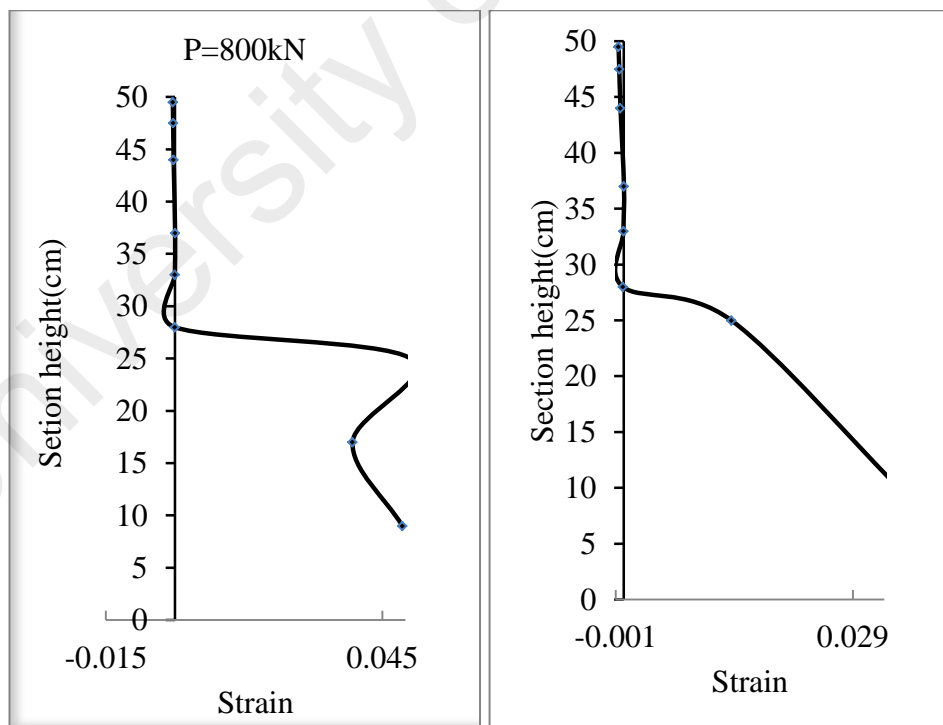
(d) Ultimate load

Figure 4.5: NAD variations at mid-span at different loading stages for B5



(a) First load

(b) First crack



(c) Specified load

(d) Ultimate load

Figure 4.6: NAD variation at mid-span at different loading stages for B6

Figures 4.1 to 4.6 show that the strain distribution in deep beams is nonlinear. The number of neutral axis (N.A.) at ultimate load is one, while there are more than one neutral axes before ultimate failure. The figures show that 40 to 80% of the section height at mid-span is under tension. The area under tension decreases as the tensile reinforcement ratio increases.

The compression strain in the top fibre of the mid-span section increases as the load increases, but in the tension area the strain readings were disturbed by the cracks and the flexibility in this area. As shown in the aforementioned figures, at the ultimate load state, the compressive strain distribution in the concrete is nonlinear as it no longer follows the parabolic shape or intensity linearity of NBs. This condition is due to the predominant effect of the horizontal bar post-cracking, the reduction in the concrete's compression area and the shear deformation that is prevalent in deep beams. CSA design code provision states that the maximum compression strain for deep beam design is 0.002, which is lower than for a NB. However it has no provision for HSSCC deep beams. The aforementioned figures show compression strains much lower than those of NBs. This observation should be taken into consideration when designing a deep beam, since the maximum strain at the extreme compression fibre is comparatively small. Figures 4.1 to 4.6 show that strain distribution is no longer linear, even before the tensile reinforcement yields. Therefore, shear deformations that are not observed in NBs become significant in deep beams in terms of bending deformation. The cracking in the tension zone affects the stiffness and redistribution of the internal load by increasing the deflection.

Furthermore, since deep beams have more than one NAD before the ultimate load, the section design equation for NBs is not valid for deep beams.

4.1.2 Modulus of rupture

The concept of the modulus of rupture is based on elastic beam theory. The modulus of rupture is defined as the maximum normal stress in the beam calculated from ultimate bending moment under the assumption that the beam behaves elastically.

Before the crack occurs in the tension zone, concrete behaves elastically and the tensile bar strain is nil. With the appearance of the first crack there is a sudden significant change in tensile bar strain, with nonlinear behaviour of concrete in the tension zone. Definition of stress corresponding to the appearance of first crack is important in recognising the change in the concrete from a linear elastic condition to nonlinear plastic condition.

The first crack is detrimental to the stability and serviceability of high risk structures, e.g. nuclear power plants, dams and reservoirs. The first crack exposes the steel reinforcement to the environment and possible corrosion. The prevention of cracking is usually achieved by reducing the stress in the extreme tension fibre of the concrete section.

As the beam load exceeds the load corresponding to cracking moment P_{cr} , a hairline crack will appear near the bottom mid-span. By increasing the load, the crack will propagate towards the neutral axis. Additional cracks are observed at the mid-span of the beam towards the supports. At mid-span, the stresses in the beam are primarily flexural tension and compression. These stresses are horizontal and result in vertical cracks. The increase in shear stress towards the support causes the cracks to be more inclined towards the load point; these inclined cracks are known as 'diagonal tension' cracks associated with shear.

The stress and strain distributions are different along the beam's length, based on geometry and load variation. Thus the definition of the B-region (Beam or Bernoulli) and D-region (Disturbed or Discontinuity) is necessary to recognise the internal force distributions. ACI code defines B and D regions in deep beams based on the Saint-Venant strain distribution.

The Saint-Venant's principle states that a localised disturbance such as a concentrated load will dissipate within one beam height from the load point. This principle is illustrated in Figure 4.7.

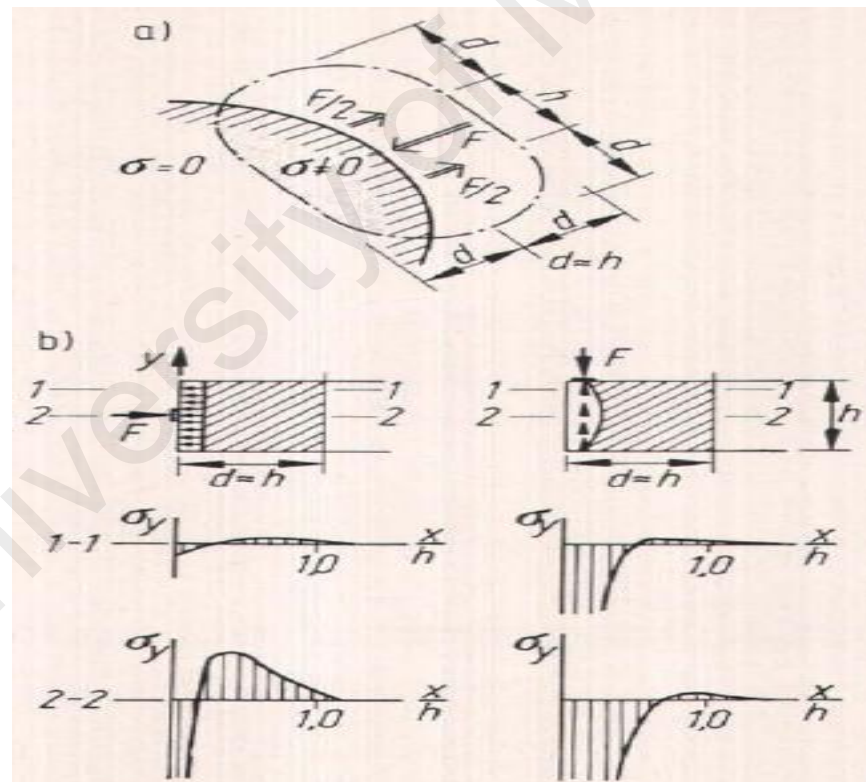


Figure 4.7: The principle of Saint-Venant: (a) zone of a body affected by self-equilibrating forces at the surface; (b) application to a prismatic bar (beam) loaded on one face (Schlaich & Schäfer, 1991; Schlaich et al., 1987)

It is useful to classify portions of the structure as either B-regions or D-regions as shown in Figure 4.8. The discussion of these regions is vital in understanding the internal distribution of forces in a reinforced concrete structure.

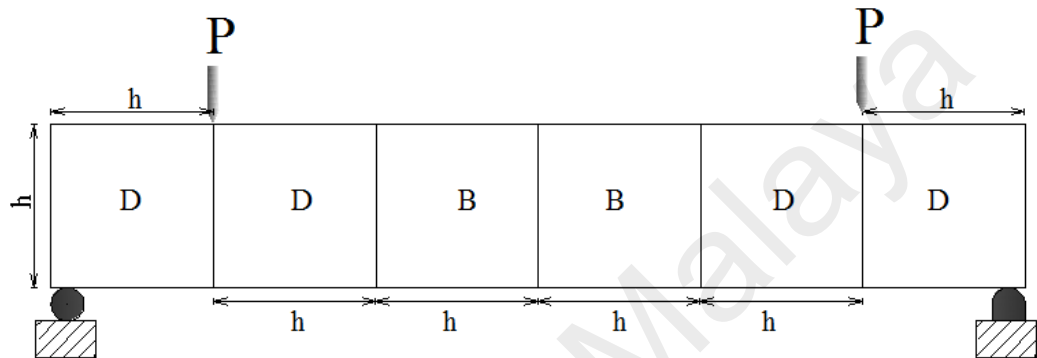


Figure 4.8: B-regions and D-regions

The B-regions of a member have internal states of stress distribution that are simply obtained from the sectional forces in bending, shear, etc. In these regions, the strain in reinforcement and concrete is directly proportional to the distance from the neutral axis, and the beam behaves elastically. In the B regions (Bernoulli Beam theory) internal stresses are obtained from the direct integration equation as follows:

$$V = EI \frac{d^3 y}{dx^3}, M = EI \frac{d^2 y}{dx^2} \quad (\text{Eq. 4.1})$$

where V is the shear force, M is the moment, EI is the bending stiffness and y is the deflection curve of the beam. In these B regions, the strain in the reinforcement and concrete is directly proportional to the distance from the neutral axis depth.

Schlaich and Schäfer (1991) and Schlaich et al. (1987) stated that a concrete element will crack under elastic stresses, and if the element is reinforced cracking will be minimised. They defined the horizontal strut in a deep beam as a B region. Figure 4.9 shows the location of the horizontal strut and the load transfer mechanism in deep beams.

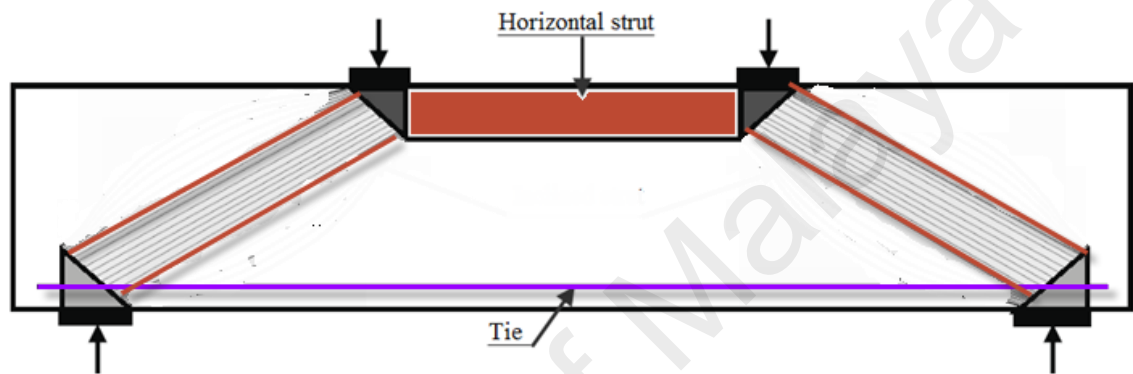


Figure 4.9: Load transfer mechanism in deep beams

In deep beams, a large part of the load is transferred to the supports directly through the compression struts formed between the load and the support point. This kind of load transfer mechanism commonly leads to shear failure in the form of splitting.

The D-regions are regions adjacent to the concentrated load points that are affected by abrupt change in the load and reactions points, or adjacent to abrupt changes in geometry, such as internal holes or changes in cross-section. In D-regions, the strain distributions are nonlinear. For structural members where plane sections are non-planar after bending, the strain distribution is nonlinear and therefore the linear approach does not apply. The elastic stress distribution in a D-region is difficult to determine and it changes as cracks progress. Schlaich et al. (1987) introduced a design method on

plasticity theory using a STM. The model could be used for both the ultimate and serviceability check. In this model, the internal forces can be calculated using STMs. These models have three components, the strut, the tie, and the node(s). They described three strut configurations that should adequately cover all cases of compression stress fields:

- prismatic stress fields (Figure 4.10(a))
- bottle shaped stress fields which develop considerable transverse stresses (Figure 4.10(b))
- fan shaped stress fields which do not develop transverse stresses (Figure 4.10(c)).

University of Malaya

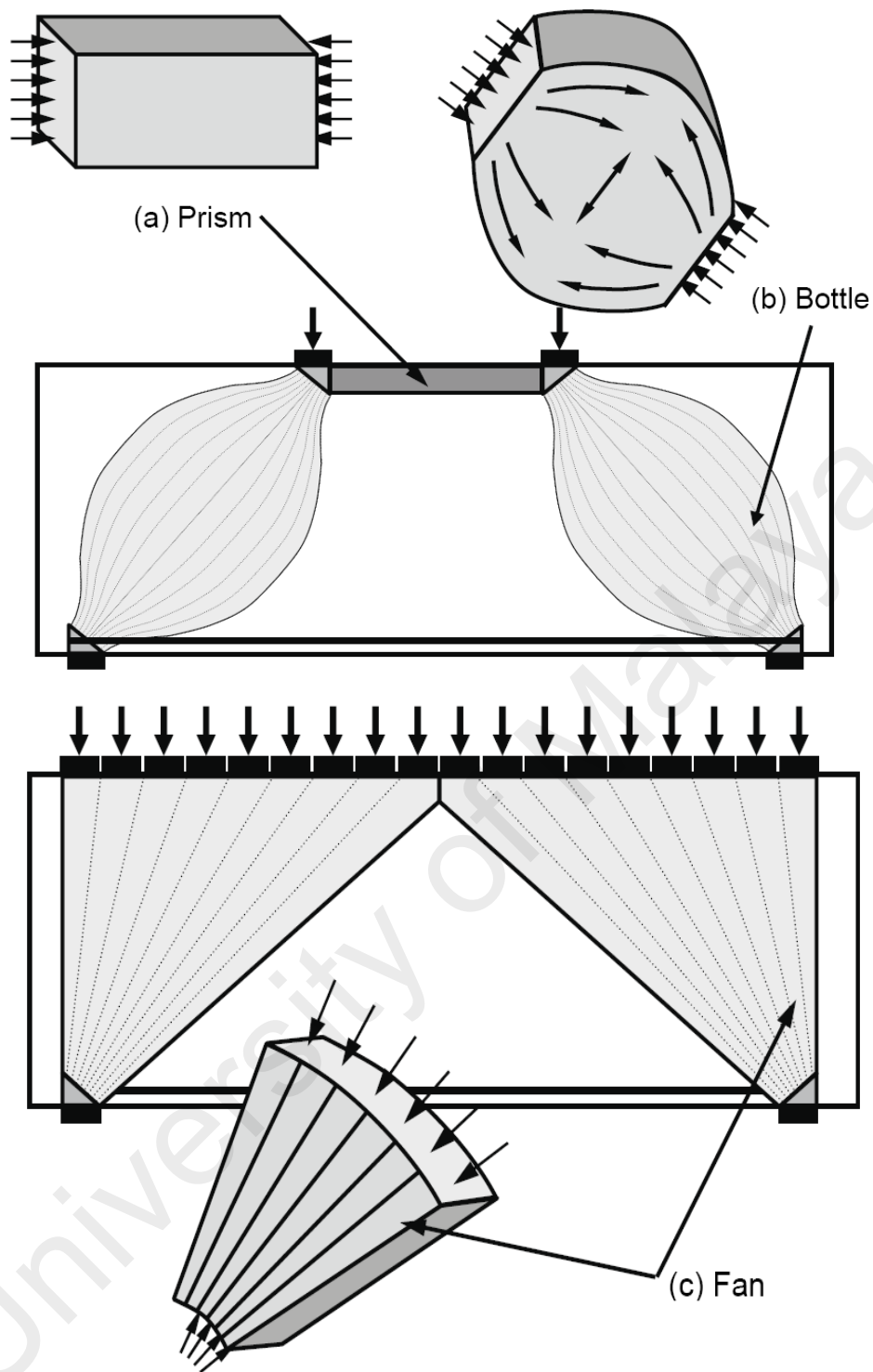


Figure 4.10: Common types of strut (a) Prism (b) Bottle (c) Fan

Based on their method, the fan and bottle shaped stress fields are normally found in D-regions while the prismatic stress field is found in B-regions. The theory of linear elastic

behaviour is applicable in B-regions and it is not applicable in D-regions. Based on the Schlaich and Schafer (1991) method, the mid-span area between the two point loads undergoes linear prismatic stress and therefore it is a B-region. Figures 4.11 to 4.16 show evidence of vertical cracks due to only horizontal strain distribution in a pure flexure zone.



Figure 4.11: Crack progression in B1

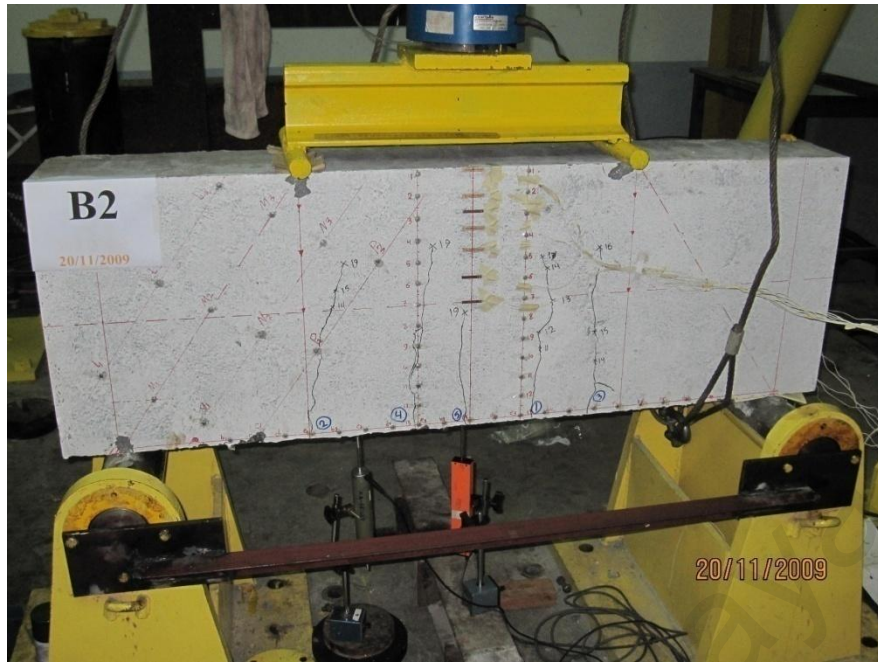


Figure 4.12: Crack progression in B2

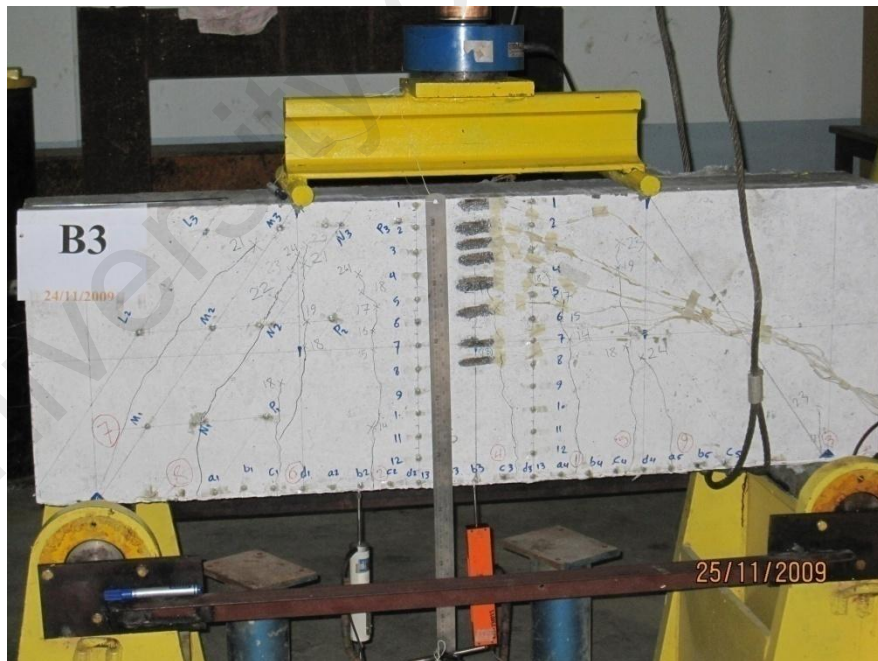


Figure 4.13: Crack progression in B3

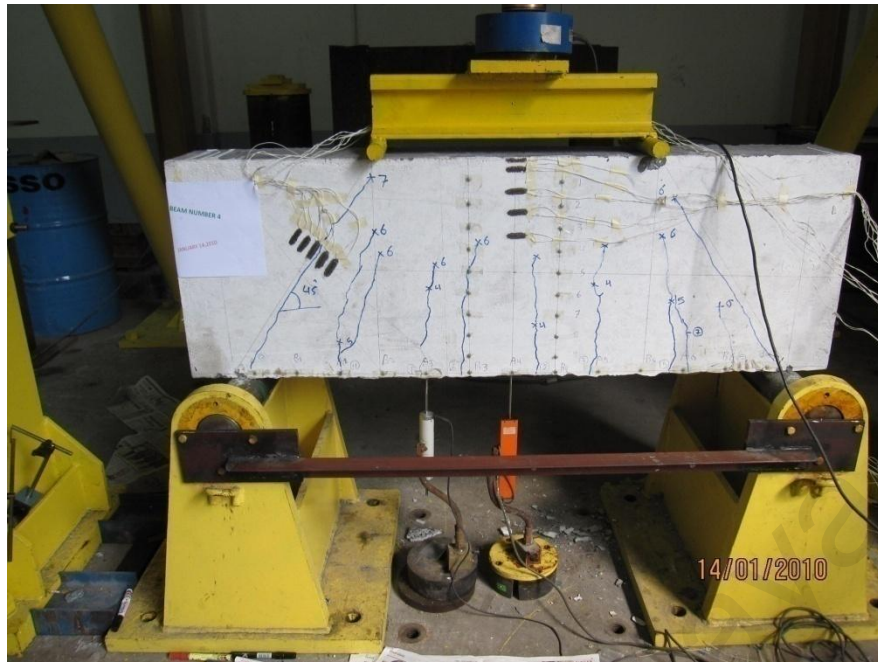


Figure 4.14: Crack progression in B4

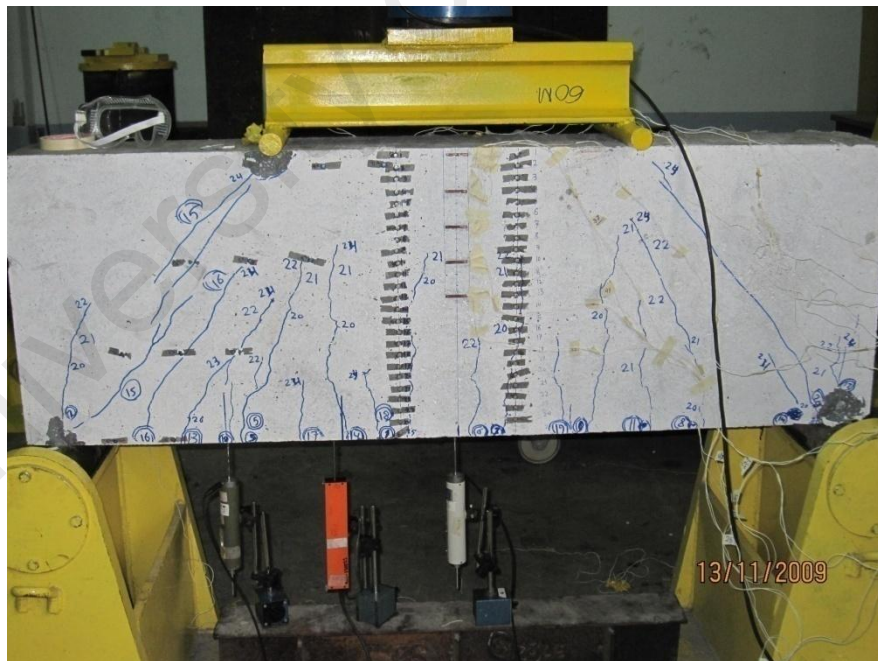


Figure 4.15: Crack progression in B5



Figure 4.16: Crack progression in B6

Before cracking, the concrete is nearly elastic in tension and largely unaffected by the presence of reinforcement. The experimental cracking moments $M_{cr,exp}$ is computed with the corresponding moments based on Equation 4.2:

$$M_{cr} = \frac{f_r I_g}{y_t} \quad (\text{Eq. 4.2})$$

where

f_r = the modulus of rupture

I_g = the moment of inertia of gross concrete section.

y_t = the distance of extreme tension fibre from the neutral axis.

Figure 4.17 shows a general shear force and bending moment diagram of all the deep beams tested.

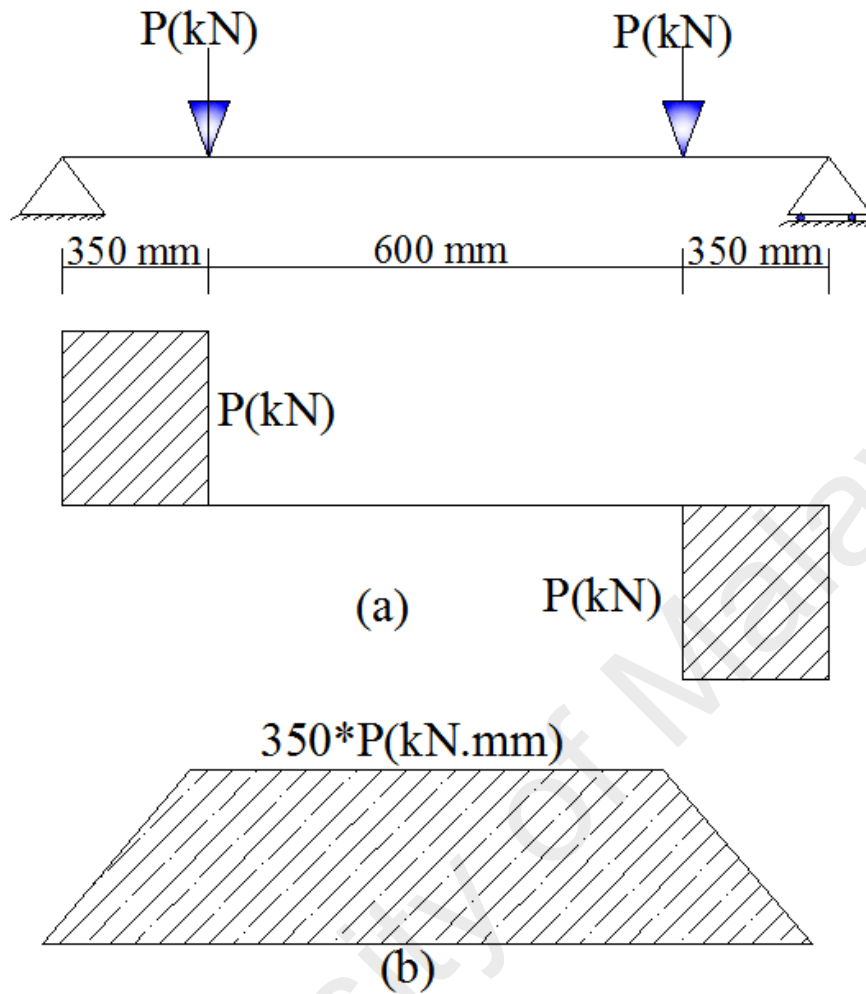


Figure 4.17: The (a) shear diagram and (b) moment diagram of deep beams tested

The maximum bending moment obtained is $350 \cdot P$ (kN.mm). Based on Equation 4.2, the location of the first neutral axis depth is important for determining the value of y_t .

Regarding Figures 4.1(b), 4.2(b), 4.3(b), 4.4(a), 4.1(b), 4.5(b) and 4.6(b) the corresponding loads of the first bending crack and the neutral axis depth is presented in Table 4.1. It shows that the cracking loads in the deep beams tested range from 13–42% of the failure loads. The comparison of this index from this study and that by Rigoti

(2002) confirms that the ratio of the first bending crack load to the ultimate load is greater than 13%.

Table 4.1: Corresponding load to first flexural crack

Beams	$P_{cr}(kN)$	P_{cr}/P_u	$y_t(mm)$
B1	215.8	0.42	330
B2	187.3	0.25	180
B3	242.0	0.30	280
B4	285.0	0.42	360
B5	239.0	0.36	250
B6	307.0	0.25	270
B7	198.0	0.13	250
B8	325.0	0.17	190

where y_t is the distance of the extreme tension fibre from the neutral axis and P_u is the ultimate load.

For a better comparison of the modulus of rupture with code provisions an α coefficient is added to the concrete strength as shown in Equation 4.3:

$$f_r = \alpha \sqrt{f'_c} \quad (\text{Eq. 4.3})$$

Experimental cracking moment corresponding to the first crack and the modulus of rupture are shown in Table 4.2. Furthermore, the value of α calculated from the respective concrete strengths (refer to Table 3.3) using Equation 4.3 are presented in Table 4.2.

Table 4.2: Corresponding experimental moment and the modulus of rupture of deep beams

Deep beam No.	M_{cr} (exp) (N.mm)	$f_{r(exp)}$ (MPa)	α
B1	37765000	5.98	0.625366
B2	32777500	2.83	0.296060
B3	42350000	5.69	0.596339
B4	49875000	8.62	0.890247
B5	47800000	5.74	0.644942
B6	53725000	6.96	0.744350
B7	34650000	4.16	0.458504
B8	56875000	5.19	0.526118

From Table 4.2, $\alpha_{mean} = 0.6$ is calculated. The modulus of rupture for the deep beams studied with an a/d ratio of 0.8 is shown in Equation 4.4:

$$f_r = 0.6 \sqrt{f'_c} \text{ MPa} \quad (\text{Eq. 4.4})$$

Table 4.3 shows the comparison between the modulus of rupture in HSSCC deep beams with code provisions, as well as those by Ahmad and Shah (1985) and the proposed equation from this study.

Table 4.3: Comparison of the various modulus of rupture

Reference and authors	f_r MPa	$f_{r(f'_c=70)}$ MPa
ACI 318-95[1995]	$0.62 \sqrt{f'_c}$	5.18
ACI 363 [1984]	$0.97 \sqrt{f'_c}$	8.12
CSA94[1994]	$0.30 \sqrt{f'_c}$	2.51
Ahmad and Shah[1985]	$0.42 (f'_{c,150})^{0.68}$	7.58
Proposed equation	$0.60 \sqrt{f'_c}$	5.02

Based on Table 11, the modulus of rupture from ACI 318-95 (1995) is the value nearest to that obtained from the proposed modulus of rupture in this study. Thus based on this study, the ACI 318-95 code provision is an acceptable conservative prediction for the modulus of rupture in HSSCC deep beams.

During the loading process, the load exceeds the P_{cr} , hairline cracks usually appears near the mid-span area and the bottom of the beam. As the load increases post-cracking, the neutral axes will move to a higher region of the beam. Also, the initial crack will propagate towards these neutral axes. Additional cracks are also observed between the load points and the support points. At the mid-span of the beam, the strain and stress are primarily flexural tension in the lower part and compression in the upper part of the beam. These horizontal stresses result in vertical cracks. (Figures 4.11 to 4.16).

At the supports, the shear stresses are inclined. The cracks are also inclined and are referred to as ‘diagonal tension’ cracks associated with shear. The general form of crack propagation is shown in Figure 4.18.

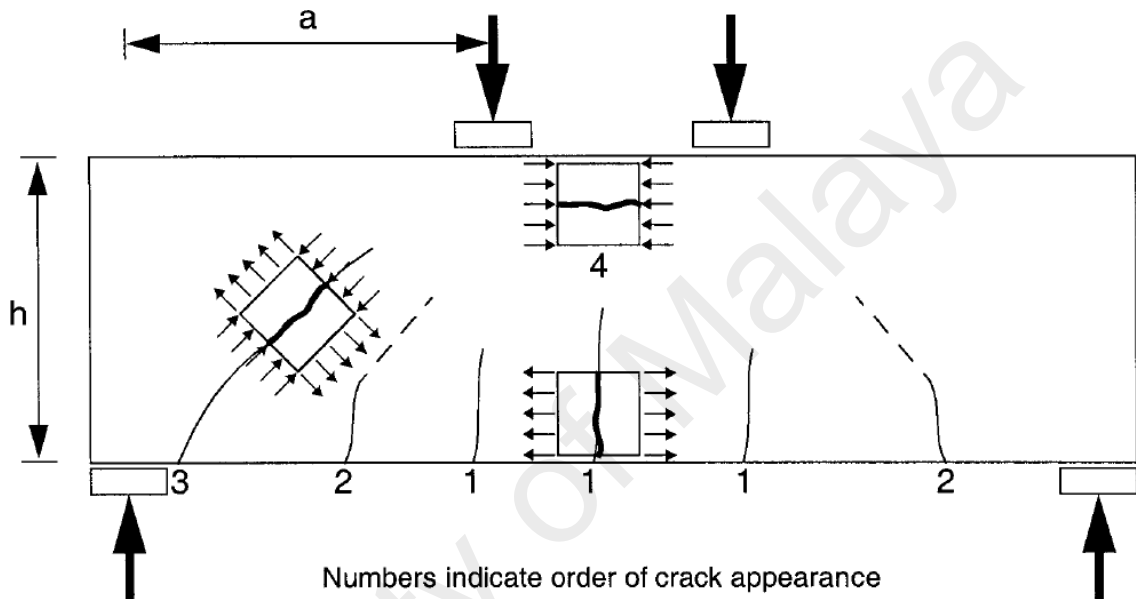


Figure 4.18: General crack progress in deep beams tested (Rigoti, 2002)

4.1.3 Failure modes and serviceability of HSSCC deep beams

Based on structural behaviour, the failure modes of deep beams can be classified into two regions, B and D. The B region follows the Bernoulli theory in which the strain distribution is linear. In the D region, or Discontinuity region, the strain distribution is nonlinear. D-Regions include the area where concentrated load is applied, or abrupt changes in geometry occur. According to the Saint-Venant's principle the D-Region is equal to one section depth on either side of the discontinuity. Figure 4.8 shows B and D regions of deep beams. Figure 4.19 shows the failure pattern of the deep beams under study.

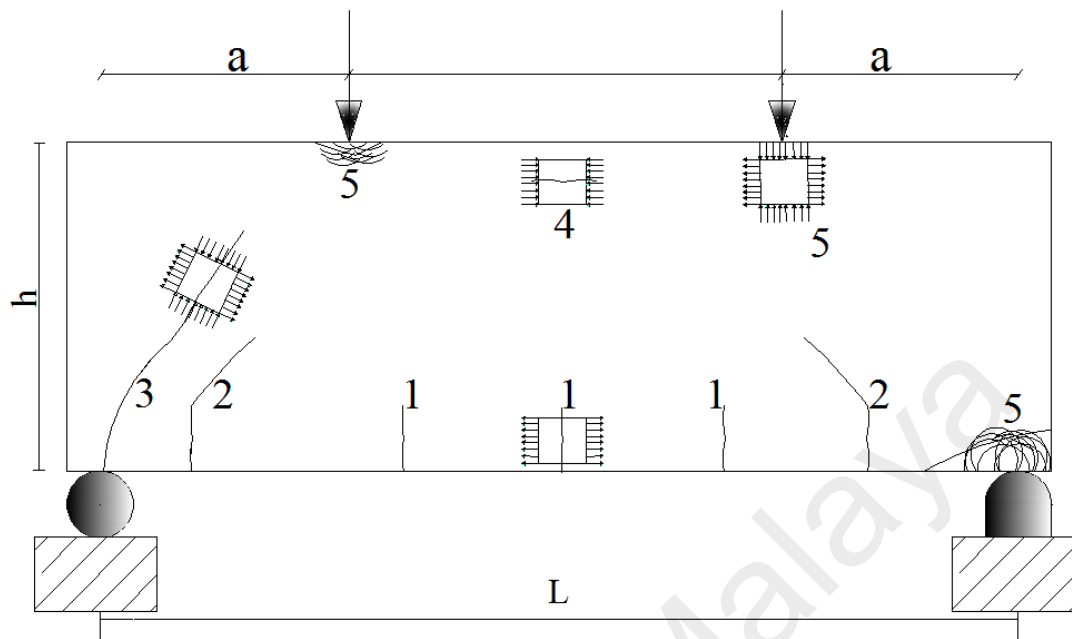


Figure 4.19: Typical crack pattern of deep beams with two-point loading

As per the Saint-Venant's principle, the whole beam is under a D region. The D region experiences local failure at the support and load point areas. Flexural failure is observed in the pure bending zone. In the compression strut trajectory, the failure is pure shear by diagonal cracking. The area between the compression strut and mid-span contains combined flexural and shear failure. Failure due to compression is observed in the extreme compression fibres of the mid-span.

4.1.3.1 Flexural failure in deep beams

Figure 4.19 shows cracks at mid-span. These are pure flexural cracks and are labelled crack type 1. These cracks appear when the tension stress exceeds the tensile strength of the concrete. The cracks are vertical due to the effect of horizontal tension stress in the pure bending zone. The appearance of these cracks is due to an inherent shortage of

concrete in tension. The crack type 1 is not critical except in the case where the tensile reinforcement ratio is less than the minimum percentage suggested by the codes. As shown in Table 3.4, in the case of beam B1 the tensile reinforcement ratio used is less than the ACI building code 318-83 (1986). The code states that the main steel percentage ρ shall be no less than $\rho_{\min} = \frac{200}{f_y}$. Thus, beam B1 failed by a widening of flexural cracks as shown in Figure 4.11. The failure type of this beam is flexural failure due to vertical cracks at the bottom, crushing at the top and also formation of diagonal tension cracks at the end of the flexural cracks. More than 50% of the cracks formed are flexural/vertical cracks.

Table 4.1 shows the ratio of the first flexural to ultimate load. These ratios represent the range of load at which the cracks appear.

Flexural cracks in the mid-span region were always vertical and within the range of 13–42% of the failure load. The heights of flexural cracks were in the range 0.24 and 0.6 of the section height. It was found that when the shear span in the beam is very narrow, the crack propagates in the cross-section plane rather than in an inclined direction.

4.1.3.2 Shear failure in deep beams

In deep beams, a significant part of the load is transferred to the support directly through the compression struts formed between the load and support points. This mechanism of transferring load leads to the type of failure that is most common in deep beams. Deep beams fail by a widening of diagonal shear cracks and crushing of the concrete. These cracks are shown schematically in Figure 4.19 as type 3. As shown in Figure 4.20, the failure of beams B2 is initiated by diagonal cracks which appear along the compression strut trajectories from the support to load points.

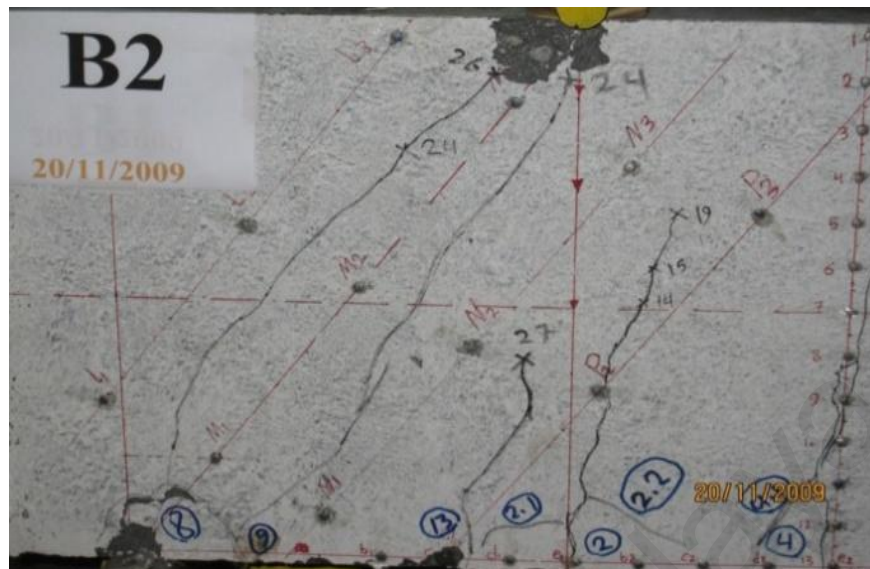


Figure 4.20: Crack pattern for beam B2

Table 4.4 shows that the shear and diagonal cracks appear between 46 to 92% of failure load.

Table 4.4: Ratio of first inclined crack load to ultimate load

Beams	$P_{cr}(kN)$	$P_{diagonal\ cr}$ (KN)	$\frac{P_{cr}}{P_{diagonal\ cr}}$
B1	510.8	-	-
B2	743.7	550.0	0.74
B3	806.9	504.0	0.62
B4	677.6	540.0	0.79
B5	661.6	610.7	0.92
B6	1206.1	560.0	0.46

These types of crack only appear between the load and support points. They have an angle of $\theta = \tan^{-1}(d/a)$, where d is the effective depth and a is the shear span. In all cases of beams tested, the load corresponding to the inclined cracks is in close proximity. Appearance of these cracks is independent of tensile reinforcement ratio or web bar percentages. It is dependent on the concrete compressive strength.

4.1.3.3 Combined flexural and shear failure in deep beams

Type 2 cracks are combined flexural and shear cracks. It can be observed from Figure 4.19 that upon increasing the load, inclined cracks appear at the end of the vertical cracks. These cracks are directed towards the load points. These cracks seldom appear as failure cracks at ultimate load. The failure of beam B5 is shown in Figure 4.21. It shows that diagonal crack appears perpendicularly to the strut compression trajectory, which causes a failure of the support.

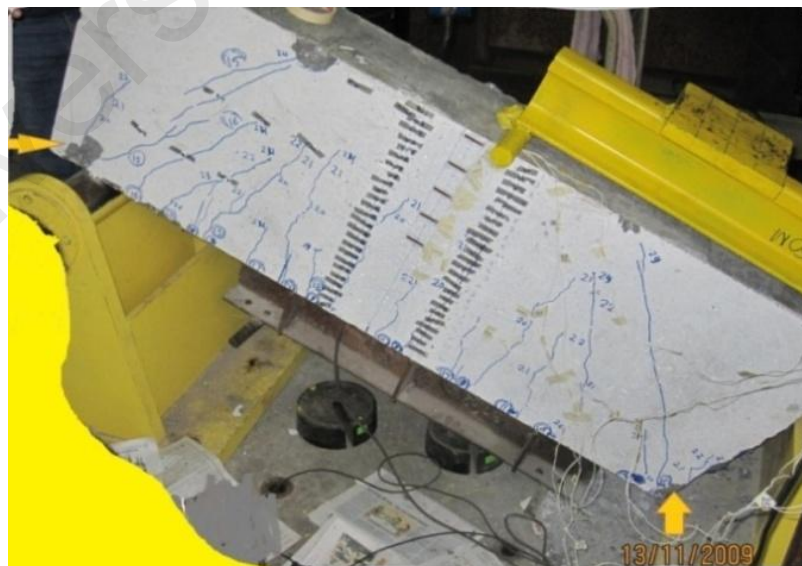


Figure 4.21: Crack pattern for beam B5

Diagonal cracks rarely develop within the exterior shear span, only beam B5 shows two diagonal cracks in this region. After the emergence of these cracks at the support, the beam abruptly fails in shear. Combined shear and flexural cracks appear within 25% of the pure bending zone from load point to the centre of the beam.

4.1.3.4 Local failure of deep beams

Figure 4.19 also shows a local failure at the support and load points. This failure is denoted as type 5. It is due to high compressive stress occurring in the area around the load and support. Failure of beam B6 occurred at 1206.1 kN by a widening of two diagonal cracks and crushing of the concrete at the support point as shown in Figure 4.16.

This type of failure is also observed in beams B3 and B4. To overcome this failure mode the high compressive stress should be distributed over an area using bearing plates at the support and load points. This failure is recognised as premature failure, which is not desirable. It occurs when the stress exceeds the allowable compression stress of the concrete. The crushing of concrete by the settling of the support or load points causes a high redistribution of internal forces. Table 4.4 shows that the ratio of first crack load to ultimate load is least for beams B6, B7 and B8, even though these beams experience the maximum applied load in all first eight deep beams tested. This is due to the effect of the support and load point width. In the case of beam B6 the width is $L/26$, whereas that of the other beams is $L/52$. The narrow support and load point width causes an increase in the bearing pressure and consequently tensile and compression stresses leading to premature failure. The failure in the D-region is typically due to the crushing of concrete in the nodal zone.

4.1.3.5 Compression failure of deep beams

The other possible failure mode in deep beams is the explosion of concrete in the compression zone. It occurs when the strain in the compression zone exceeds the ultimate strain. This type of failure is labelled type 5 in Figure 4.19. This failure pattern is rare because concrete in compression may not reach the ultimate strain due to the beam height and the different load transferring mechanism. In all HSSCC deep beams tested, the highest strain in the extreme compression fibre recorded was 0.002.

Occurrence of this phenomenon is in accordance with the plasticity theory which assumes the yielding of all steel reinforcement before compression failure. In this case the failure capacity of tensile reinforcement is higher compared with the compression area.

4.1.4 Serviceability of deep beam

In the present work, only deflections are studied for the serviceability of deep beams. In general, deflections of deep beams are small compared with shallow beams. As beam section height increases the stiffness of the beam increases leading to brittle failure. Figure 4.22 shows the load deflection variation in the deep beams studied.

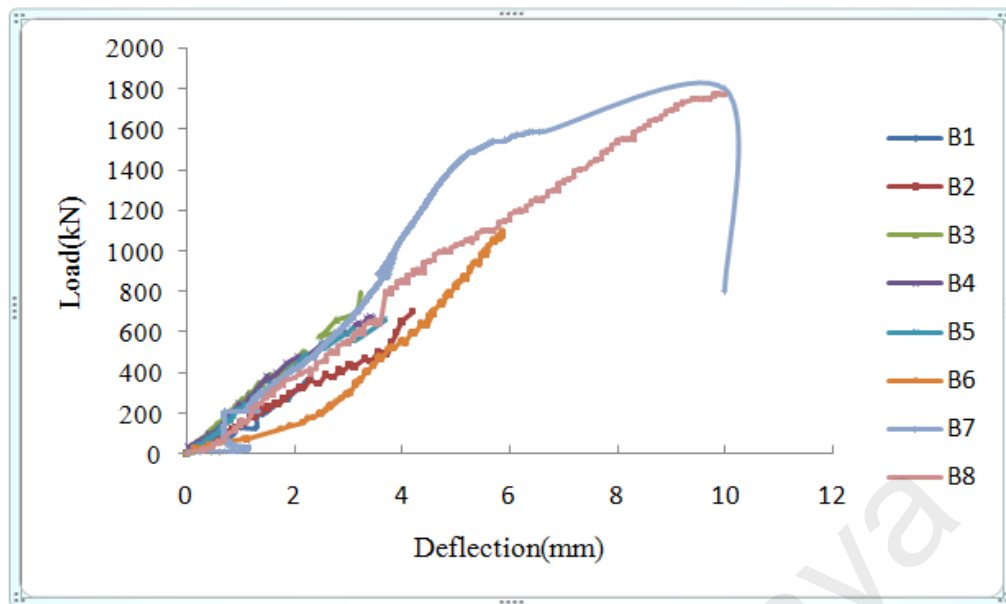


Figure 4.22: Load-deflection curve of deep beams tested

In all beams the load deflection curve is almost linear until ultimate strength failure. This shows that shear deformation is the predominant behaviour leading to brittle failure. Brittle failure reduces the strength of the structural elements below the flexural capacity and considerably reduces the ductility of the elements. The area under the load deflection curve represents the energy absorbed by the structural elements during failure.

Comparison of the deflections of the HSSCC deep beams tested shows that only beam B1 has a large deformation at lower loads in contrast with the other beams. Beams B2–B6 exhibit nearly the same behaviour of deflection pattern. The stiffness or the slope of the load deflection curve varies slightly at the beginning of loading, and finally it remains constant. The behaviour of the deep beam is dominated by the strength of the tensile reinforcement. For tensile reinforcement complying with the ACI 318–05 (2005) provision, the load deflection behaviour is linear until yield point, and after that it remains constant as shown in Figure 4.22 for beam B1. At higher strengths of tensile bar the load deflection curve is linear until ultimate failure.

For over-reinforced beams with high-strength reinforcement the section may not reach its yield point, thus leading to local compressive failure in the concrete strut. In beam B1, only 5 cracks appeared until the failure point, but in beam B6 the number of cracks was more than 18; although the progress of the cracks towards the compression area was reduced by increasing the tensile reinforcement ratio. The increase in tensile reinforcement ratio also increases the number of cracks with lesser crack widths. It is noted that the diagonal cracks were significantly wider than the flexural cracks, which confirms that shear is a major parameter in the failure of deep beams. In the case of under-reinforced beams, such as beam B1, there were no diagonal cracks and the beam fails due to flexural cracks alone.

4.1.5 Behaviour and shear resistance of HSSCC deep beams reinforced with high-strength steel bars

The reinforcement concrete section is a combination of different materials, e.g. steel bars and concrete. The consistency in the behaviour of concrete section is dependent on the property and ductility of each material. Design codes limit the strength of concrete and steel bars to achieve the desired ductility. In order to study the behaviour of a concrete section, it is necessary to separately investigate the property of the steel and concrete used. As shown in Figure 4.23, the mechanical properties of steel bar alloys vary in three categories: low-strength, medium-strength and high-strength.

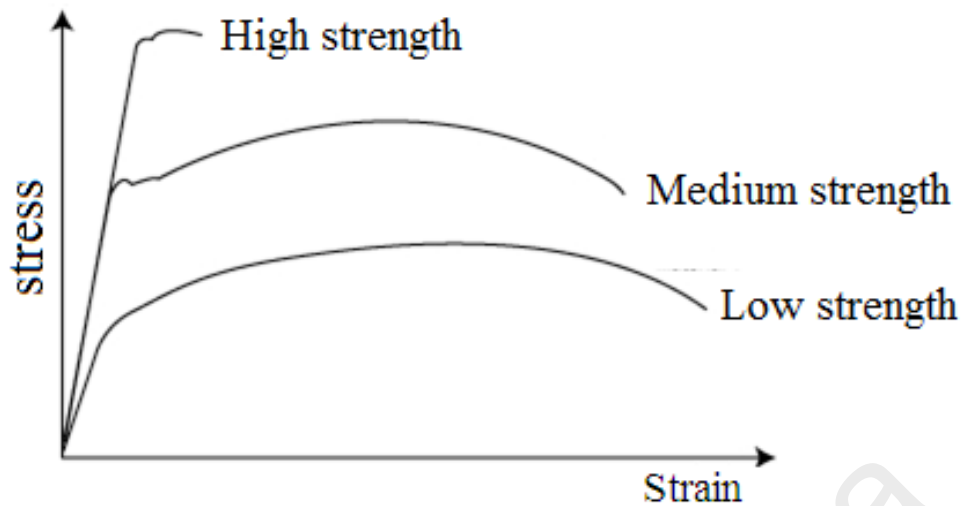


Figure 4.23: Comparison of steel bar behaviour by different strength

Figure 4.23 shows that all three categories of steel have the same gradient to the yield point. This means that the elongation created by a given load is the same for all the low-strength, medium-strength and HSS (high-strength) bars. The HSS material is able to tolerate larger loads and lower strains than the low-strength material. HSS bars display linear elastic behaviour in comparison to NSS. Figure 4.23 shows that the increase in strength results in a considerable decrease in strain. It is therefore important to know the stress at which plastic deformation (yielding) begins. For metals which experience gradual elastic-plastic transition, the yield stress may be taken as the point at which the stress-strain curve is no longer linear. A more precise way of determining the limit is to use the stress at a strain of 0.002; this value is known as the yield strength.

Material such as concrete that undergoes very little plastic deformation is brittle. Ductility is a measure of the degree of plastic deformation which has occurred prior to fracture. Comparison of ductile and brittle material is made in Figure 4.24.

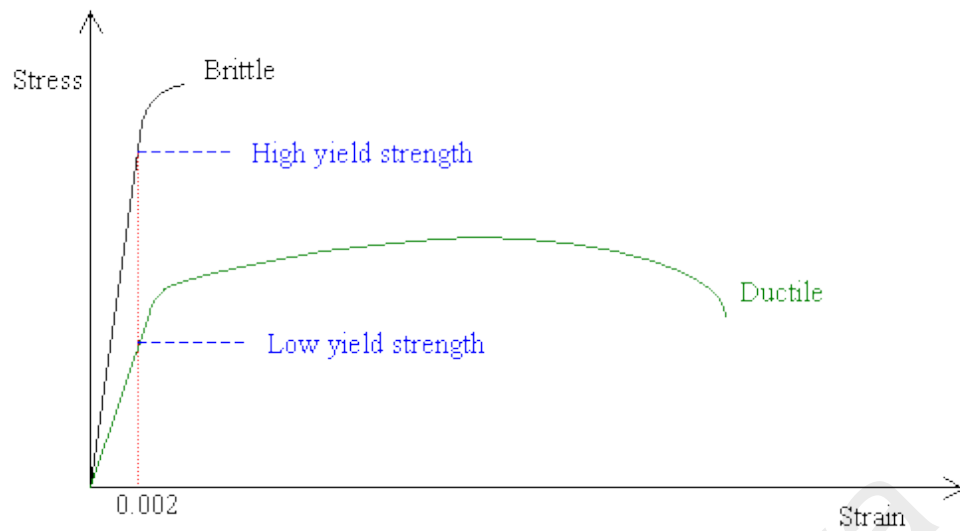


Figure 4.24: Comparison of stress and strain behaviour of ductile and brittle materials

The deformed specimen only returns to its original size if the stress does not pass beyond its elastic state, while a plastically deformed specimen will not return to its original size and shape when the load is removed. For many applications, plastic deformation is undesirable; it is used as a design limit where the serviceability in terms of deflection and crack width limits control the design. Plastic deformation is acceptable within a specified range of strength for structural elements, especially in seismically active areas.

The major property of HSC is its high modulus of elasticity. Though the increase in modulus of elasticity is less significant than the increase in compressive strength, its effect is very important in ductility design. Figure 4.25 shows that the behaviour of concrete is more linear with an increase in strength. This behaviour is observed in the modulus of elasticity where more than 85% of the ultimate stress behaves linearly (Mohammadhassani et al., 2011).

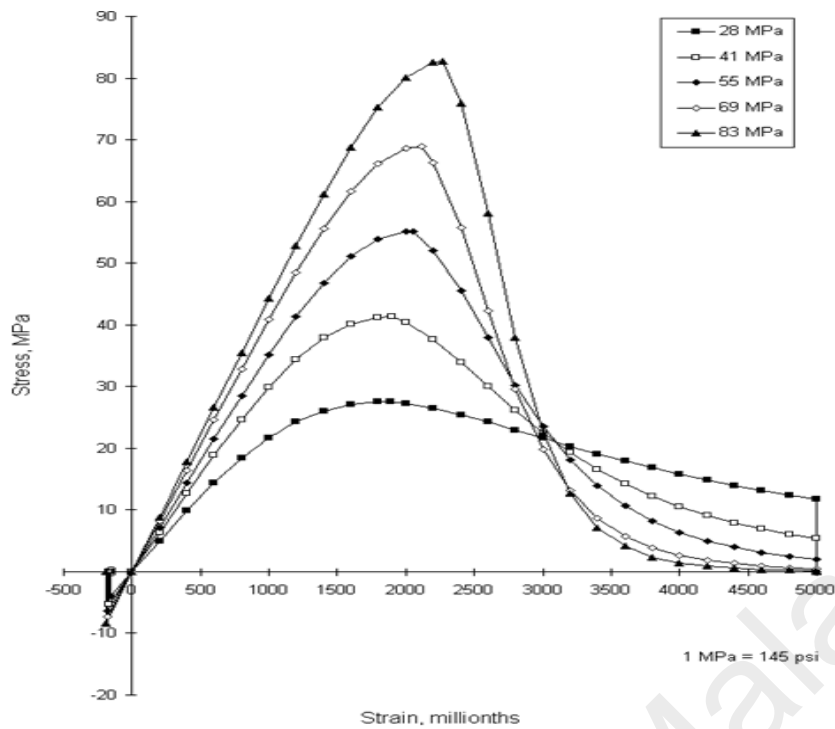


Figure 4.25: Stress–strain relationships of NSC and HSC (following Kani (1966))

When the compressive strength of concrete specimens is increased the stress-strain curves drop rapidly, and this is typical of brittle material. This brittleness in HSC results in a loss of ductility due to the sudden collapse mechanism. A material with a combination of HSC and HSS exhibits characteristics of a unique brittle material.

In addition, it is important to consider the nonlinear behaviour of deep beams in the strain and stress distribution. Deep beams do not conform to Bernoulli's assumptions for strain and stress distribution. Bernoulli's hypothesis facilitates the flexural design of reinforced concrete structures by allowing a linear strain distribution.

Figures 4.1 to 4.6 show that reinforced concrete deep beams are far from being linearly elastic when the ultimate load is reached. This nonlinearity of strain distribution is due to the shear deformations that are often less obvious in NBs, but that are significant in

deep beams. Thus the internal stresses and behaviour of deep beams cannot be determined using ordinary beam theory.

The desired behaviour of concrete sections in the design codes is based on failure that is initiated by the yielding of steel reinforcement. The design code also requires that the subsequent deformation occurs without significant loss in its load bearing capacity and without the crushing of concrete in ultimate failure. Table 4.5 presents the strain at the extreme compression fibre and along the tensile bar of the HSSCC deep beams tested (refer to Figures 4.1 to 4.6). The results show complete disagreement with the design code assumption. When the tensile bar yielded, the concrete compressive strain or stress was far from its ultimate range.

Table 4.5: Strain in the extreme compression fibre of concrete and along the tensile bar

Beam	$\varepsilon_{s_y} (\mu)$	$\varepsilon_{c_y} (\mu)$	$\varepsilon_{s_u} (\mu)$	$\varepsilon_{c_u} (\mu)$	$\frac{\varepsilon_{c_u}}{\varepsilon_{c_y}}$
B1	1885	283	3916	607	2.14
B2	2966	793	14053	2172	2.74
B3	-	-	2612	1074	-
B4	-	-	1924	575	-
B5	-	-	1421	406	-
B6	-	-	1916	696	-
B7	3000	1105	8013	2254	2.04
B8	2991	1885	3548	1963	1.05

where:

ε_y = strain in the tie section at the yield of tensile bar,

ε_{cy} = strain in extreme compression fibre when tensile bar reaches yield state,

ε_{su} = strain in tie section at ultimate yield state and

ε_{cu} = strain in extreme compression fibre in ultimate state.

Beams B3 to B6 failed before the yielding of the tensile bar. Table 4.5 indicates that the ultimate strain in the extreme compression fibre in the pure bending zone of the HSSCC deep beam is slightly over the design code limit of 0.002; this is due to the heavy reinforcement used in this experimental work. The values of strains in the extreme compression fibre are acceptable due to the different load transferring mechanism in deep beams. In deep beams, the applied load is transferred to the supports by the formation of struts from the load points towards the support points, while in NBs the applied load is transferred through a fairly uniform diagonal compression. By the definition of load transferring mechanism, the ultimate strain of the concrete in the extreme compression fibre has significant effect on the reinforcement limits of the flexural members. To obtain the ultimate shear in deep beams, a higher ultimate strain has to be achieved in the struts. Another contributing factor towards the lower value of strain in HSSCC deep beams compared to NBs is the effect of the height of a section. The damage of localisation phenomenon (e.g. buckling) in a taller section prevents the beam from reaching its ultimate strain.

In addition, a shorter compressive stress block is needed in a HSC beam section against the tension zone forces in comparison to NSC. These reasons support the fact that HSC deep beams exhibit a lower ultimate strain in the extreme compression fibres. The value of ultimate strain is important in identifying the tension and compression internal forces.

ACI 318M-95 code provision, Section 10.3.2, suggests the balance reinforcement ratio

ρ_b as in the following Equation 4.5:

$$\rho_b = \frac{0.85 \beta_1 f'_c}{f_y} \frac{600}{600 + f_y} \quad (\text{Eq. 4.5})$$

in which f'_c is the concrete nominal compressive strength, f_y is the reinforcement nominal yield strength in (Mpa) and β_1 is a function of f'_c (ACI Code(2008), Section 10.2.7.3). Although Equation 4.5 is often used for the design of NBs and not for deep beams, with the presence of variables f'_c and f_y in Equation 4.5 it is still able to explain the effect of HSS and concrete compressive strength in any beam section design. This equation shows the reciprocal effect of concrete and steel bar strength in the design of a concrete section; when the steel strength (f_y) increases, the balance reinforcement ratio (ρ_b) decreases and vice versa.

ACI 318M-95 requirements for the minimum flexural tension reinforcement ratio in a beam section is as presented in Equation 4.6:

$$\rho_{\min} = \frac{\sqrt{f'_c}}{4 f_y} \geq \frac{1.4}{f_y} \quad (\text{Eq. 4.6})$$

The tensile reinforcement ratios of the deep beams tested are presented in Table 3.4. Based on Equation 4.6, it appears that only beam B1 is under-reinforced using the non-deformed 3Ø9. It is important to consider this beam as a fully non-deformed NSS bar with HSC. Figure 4.11 shows how the flexural failure and wide flexural cracks in beam B1 differ from the rest of the beams.

3Ø10 were used as tensile bars in Beam B2. The total area where the tensile bars are located in beams B1 and B2 only vary by a small area of 40 mm². The main difference refers to the strength of the steel bars used; the tensile bars in beam B1 are NSS and

they are HSS in B2. Figure 4.20 shows that the failure of beam B2 was due to the widening of the diagonal strut cracks and premature local failure by the crushing of concrete in the load and at the support points. This mode of failure is very common in deep beams due to the formation of struts. Compared to beam B1, the crack width in B2 is very low and critical cracks are also inclined.

The ratio of tensile reinforcement and its strength are also important in the failure of deep beams. Web steel arrangement is the same for beams B1, B2 and B3; the tensile bars used in beam B3 are 2Ø10+2Ø12. The failure in beam B3 occurred due to support crushing with no yield in its tensile bars.

The specifications of the web bars used are important in the behaviour of deep beams. Without reinforcement, the formation of inclined cracks leads to sudden failure in concrete beams. The ACI code requires that a minimum area of shear reinforcement be provided in reinforced concrete members, except where V_u is less than $\phi V_c / 2$. This requirement is to provide ductile failure by the yielding of the tensile bar. Then a minimum area of shear reinforcement is required by the ACI code as shown in Equations 4.7 and 4.8:

$$A_v \geq 0.0015 b_w s_1 \quad (\text{Eq. 4.7})$$

$$A_{vh} \geq 0.0025 b_w s_2 \quad (\text{Eq. 4.8})$$

where :

A_v = the area of vertical shear reinforcement perpendicular to the span

A_{vh} = the area of horizontal shear reinforcements parallel to the span

b_w = width of the beam section

s_1 = spacing of the vertical shear reinforcement measured parallel to the longitudinal reinforcement

s_2 = spacing of horizontal shear reinforcement in a direction perpendicular to the longitudinal reinforcement.

As seen in Table 3.4, all deep beams tested had a web reinforcement ratio greater than the minimum suggested by the design code. The effect of the web reinforcement is noted in the improved reserve strength and in preventing the widening of the crack. Reserve strength is defined as the ratio of the difference in ultimate load and diagonal cracking load to the diagonal cracking load, expressed in percentages. This index has been calculated and is presented in Table 4.6.

Table 4.6: Reserve strength of HSSCC deep beams tested

Beam Number	p_u ultimate load (kN)	p_{cr} diagonal crack load (kN)	reserve strength
B1	510.8	-	-
B2	743.7	550.0	35.27
B3	806.9	504.0	60.11
B4	677.6	540.0	25.56
B5	661.6	610.7	8.35
B6	1206.1	560.0	115.35
B7	1633.0	609.0	430.20
B8	1950.7	496.0	381.13

As presented in Table 4.6, the reserve strength shows no specific pattern or correlation. Web reinforcement stabilises the inclined cracks and therefore substantially more shear force can be endured before failure; so theoretically it should show an improvement in

the reserve strength in the deep beams tested. However, an abnormality in the reserve strength was noted in Table 6, and this was due to the failure mode of the deep beams tested. By considering the significant reserve of strength in beams B6, B7 and B8, it is concluded that the prevention of premature failure is the most important factor for serviceability and the achievement of the ultimate capacity for deep beams reinforced by HSS. In the aforementioned beams, the width of the support and load point increased for decreasing bearing stress. Figures 4.26 and 4.27 show the failure of beams B7 and B8.



Figure 4.26: Failure of beam B7



Figure 4.27: Failure of beam B8

Structural behaviour is a result of the combined behaviour of the materials present in the beam, i.e. concrete and steel. It is this combined reaction of the materials against the external applied loads that are expressed through relationships between generalised forces and corresponding displacements.

Figure 4.22 clearly shows a linear load-deflection relationship for all of deep beams tested. Load deflection graphs show a linear relationship of up to 85 percent of the ultimate load in the deep beams tested. This consistency in the linear behaviour of load-deflection graphs prior to the ultimate load is achieved through the combined behaviour of the HSS bar and the HSC.

For a performance assessment of the deep beams, the absorbed energy was calculated from the areas of the load deflection graphs. The fundamental program is based on Equation 4.9 as follows:

$$A = \frac{(P_i + P_{i+1}) * (\Delta_{i+1} - \Delta_i)}{2} \quad (\text{Eq. 4.9})$$

where A symbolises the area under load-deflection graphs, P_i represents the applied load in each loading step, and Δ indicates the measured deflection at the mid-span of the beam length. Based on the results taken from MATLAB software, the absorbed energy in each deep beam is presented in Table 4.7.

Table 4.7: Absorbed energy of deep beams tested

Beam number	B1	B2	B3	B4	B5	B6	B7	B8
Absorbed energy(KN.mm)	388.115	1287.6	1521.9	1325.8	1349.4	2564.4	12299	9690

Table 4.7 shows an increase in absorbed energy with an increase in tensile reinforcement ratio in all beams, except B4, B5 and B8 which show no increase. It is hereby concluded that the use of more HSS bar significantly increases the absorbed energy.

4.1.6 Experimental assessment of shear capacity and comparison with ACI code approaches

ACI code designs are one of the most important standards used. However, a general design approach has not been developed for the calculation of shear in deep beams. The shear provisions of ACI Code 318–08 (revised 1986) apply to top-loaded simple or continuous beams with a (clear span)/(effective depth) ratio (l_0/d) of less than 5, which are loaded on one face and supported on the opposite face. Based on this code provision, in the case of simple deep beams, calculation was carried out for the critical

section as being halfway between the load and the face of the support. Design code provision is based on:

$$V_u \leq \phi V_n \quad (\text{Eq. 4.10})$$

$$V_n = V_c + V_s \quad (\text{Eq. 4.11})$$

where:

V_u is the design shear force at the critical section (lb)

V_n is the nominal shear strength (lb)

ϕ is the capacity reduction factor for shear, taken as 0.85

V_c is the shear strength provided by concrete (lb) and V_s is the shear strength provided by the steel (lb).

Equations 4.12 and 4.13 show the calculation of the nominal shear strength V_n :

$$V_n < 8\sqrt{f'_c} bd \quad \text{for } l_o/d < 2 \quad (\text{Eq. 4.12})$$

$$V_n < (2/3)(10 + l_o/d)\sqrt{f'_c} bd \quad \text{for } 2 \leq l_o/d < 5 \quad (\text{Eq. 4.13})$$

where f'_c is the concrete cylinder compressive strength (lb/in^2), b is the beam width (in), and d is the effective depth (in). For the consideration of the section height, the

ACI code provisions permit the usual value of concrete shear strength V_c , to be

increased by a multiplier that depends on $\frac{M}{V.d}$. The shear provided by the concrete in

deep beams was calculated using Equation 4.14:

$$V_c = (3.5 - 2.5M_u/V_u d)(1.9\sqrt{f'_c} + 2500 \rho V_u d/M_u)bd \quad (\text{Eq. 4.14})$$

The shear contribution of V_s is given by the following equation:

$$\frac{V_s}{f_y d} = \frac{A_v}{s_v} \left[\frac{1 + l_o/d}{12} \right] + \frac{A_h}{s_h} \left[\frac{11 - l_o/d}{12} \right] \quad (\text{Eq. 4.15})$$

where A_v is the area (in^2) of vertical web reinforcement are arranged in a spacing of s_v (in), A_h is the area (in^2) of horizontal web reinforcement within a spacing s_h (in), and f_y is the yield strength of web bar used.

Thus the ratio of shear forces by ACI code to the suffered loads is presented in Table 4.8.

Table 4.8: Comparison of experimental and theoretical shear strength of HSSCC deep beams tested

Beam	V_{test} (KN)	V_{ACI} (KN)	$\frac{V_{ACI}}{V_{test}}$
B1	255.39	500.42	1.96
B2	371.83	509.06	1.37
B3	403.43	560.11	1.39
B4	338.78	631.13	1.86
B5	330.78	603.22	1.82
B6	603.02	608.44	1.01
B7	816.46	595.50	0.73
B8	991.45	635.9839	0.64

Based on Table 4.8, the tensile reinforcement ratio increases from B1 to B8 and the same is noted for the V_{ACI} . The comparison ratio between V_{ACI} and V_{test} shows a non-conservative decreasing trend. It can be concluded that the ACI code provisions are much higher than the experimental values for the low tensile reinforcement ratio beams

with NSS web reinforcement. Thus there is a need to revise existing ACI code provision for HSS and HSC in deep beam sections. The amount of V_c is the maximum permitted value by the ACI code for beams B6, B7 and B8. The ratio $\frac{V_{ACI}}{V_{test}}$ appears to be more conservative for the increase in load due to the increase in support widths in beams B6, B7 and B8. Thus by preparing the appropriate size for the load and support points, the ACI code provision exhibits shear strength in a conservative value for HSS sections. Figure 4.28, presents the contribution of concrete and steel bar in shear resistance for the deep beams tested and the comparison between V_{ACI} and V_{test} .

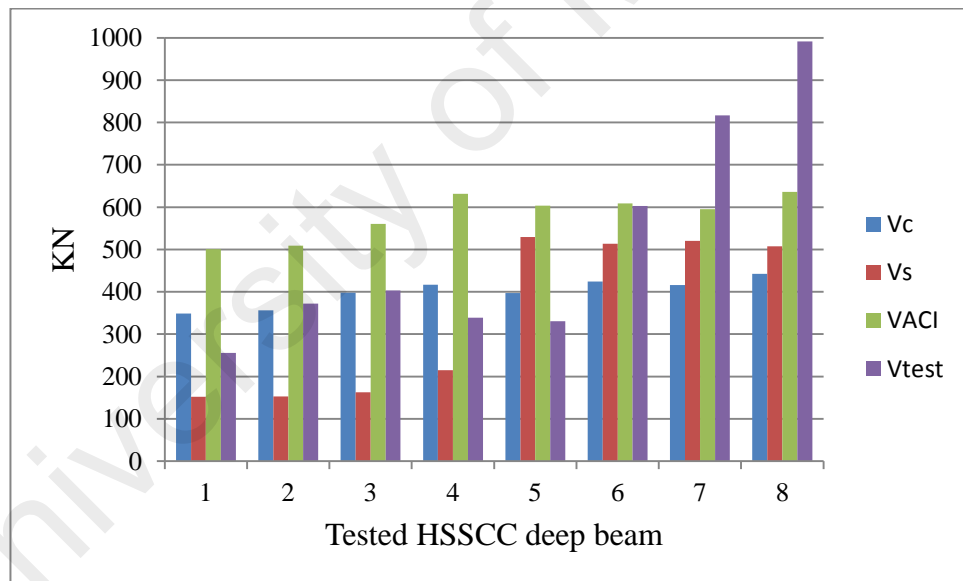


Figure 4.28: Comparison of shear strength component and ACI code provision

As noted, the contribution of V_c is more than twice the V_s for beams with NSS web reinforcement, e.g. B1, B2, B3 and B4. In these beams, V_{ACI} is much higher than V_{test} . In beams B5, B6, B7 and B8 the values of V_{ACI} and V_s are similar. While beams B1 and B2

failed at ultimate load, the ACI code provision provides a much higher shear strength value. Thus the use of HSC in deep beams with NSS web bar is justified as $V_{ACI} = V_S + V_C$.

From Figure 4.28, it is evident that the contribution of HSS steel bar is more than the concrete in beams B5, B6, B7 and B8, as the V_S are almost the same as their corresponding V_{ACI} . In addition, by choosing the appropriate dimension for load and support points, the improved shear strength from using HSS bar and HSC in the test specimens will exhibit design values greater than the ACI 318-02 (Appendix A).

Steel strength or tensile reinforcement ratio does not influence the occurrence of inclined cracks, but the existence of web reinforcement and steel strength is important in preventing the widening of crack widths. Table 4.9 shows that for beams B2–B6, the occurrence of the first inclined cracks from the load points to the support points corresponds to a similar load range, and the first inclined crack for beams B7–B8 appears in another load range. The evaluation of the HSSCC deep beams after loading revealed that in regions with large shear and small moments, diagonal cracks extend from the load points toward the support points at an average or nominal shear stress. This shear stress is approximated in Equation 4.16:

Table 4.9: Shear stress of tested HSSCC deep beam corresponding to the first inclined crack

Beam	V_{cr} (KN)	f'_c (MPa)	v_{cr} (MPa)
B1	-	91.50	0.000
B2	275.0	91.50	1.5680
B3	252.0	91.10	1.3435
B4	270.0	93.72	1.4610
B5	305.5	79.10	1.6250
B6	280.0	87.50	1.5385
B7	154.0	82.24	0.8360
B8	206.0	97.20	1.1445

$$v_{cr} = \frac{V_{cr}}{b_w d} = 0.14 \sqrt{f'_c} \text{ (Mpa)} \quad (\text{Eq. 4.16})$$

where V_{cr} is the shear force at which the formation of the diagonal cracks was observed from the support to the load points. This shear force is half the load applied using the hydraulic jack when the first inclined crack occurred (refer to Figure 3.16). It is evident that the shear at which diagonal tension cracks develop to failure depends on the ratio of shear force to the bending moment. The ACI Committee 326 determined that the shear capacity depends on three variables:

- (a) The dimensionless quantity $\frac{M}{V.d}$ involving bending moment M , shear force V , and effective depth d .
- (b) The longitudinal reinforcement ratio, ρ_w
- (c) The concrete compressive strength, f'_c

Apart from the aforementioned influence of $\frac{M}{V.d}$, increasing values of tensile reinforcing steel ratio have a beneficial effect in increasing the shear at which diagonal cracks develop. Following the expression in Equation 4.17 conservatively defines the trend of the test data based on the amount of V_{test} in Tables 4.8 and 4.9.

$$v_{cr} = \frac{V_{cr}}{bd} = 0.14 \sqrt{f'_c} + 0.0004 \frac{\rho_w V d}{M} \text{ (Mpa)} \quad (\text{Eq. 4.17})$$

where:

v_{cr} = the ultimate shear strength

$\rho_w = A_s/b_w d =$ tensile bar percentage

0.0004 = empirical constant at equilibrium.

4.1.7 Ductility and performance assessment in HSSCC deep beams: An experimental investigation

Notwithstanding decades of experimental and analytical research on deep beam design, shear failure is not fully understood in the design of deep beams. In the case of deep beams, shear deformation dominates and hence shear failure is the probable mode of failure. Shear failures are generally considered undesirable failures because such failures reduce the strength of the structural elements to below their flexural capacity and considerably reduce the ductility of the elements.

Ductility is a desirable structural property because it allows stress redistribution and provides an early warning prior to brittle failure. This is an important fact to consider, because a serviceability limitation is needed for special purposes in the lifetime of specified buildings. Figure 4.29 shows the calculation of ductility, which is the area below the load-deflection or moment-curvature graphs.

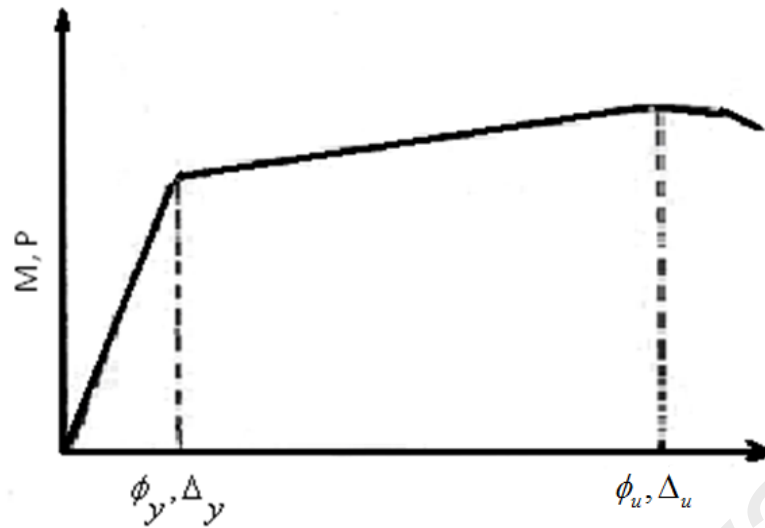


Figure 4.29: Definition of ductility

The meaning of ductility is failure that is initiated by the yielding of the steel reinforcement and the subsequent extensive deformation without any considerable loss of load bearing capacity. Depending on the type of structural element and the type of load applied, the measure of deformation for ductility may either be strain, curvature, displacement or rotation. Common methods of measuring ductility are curvature and displacement indexes.

4.1.7.1 Ductility measurement by the curvature method

In reinforced concrete beams, the curvature ductility measurement method is preferred.

This index can be expressed in the form (u_ϕ) as follows:

$$u_\phi = \mu = \frac{\phi_u}{\phi_y} \quad (\text{Eq. 4.18})$$

where φ_u is the ultimate curvature when the concrete compression strain reaches a specified limit, and φ_y is the curvature amount when the tension reinforcement first reaches its yield strength.

As stated in the literature review in the Introduction, deep beam design does not conform to the Bernoulli assumption. In the Bernoulli hypothesis it is assumed that a normal cross-sectional plane remains normal when the beam deforms. Bernoulli's hypothesis facilitates the flexural design of reinforced concrete structures by allowing a linear strain distribution for all loading stages. Figure 4.30 shows the overall template of strain distribution at the mid-span of a NB section based on the Bernoulli assumption.

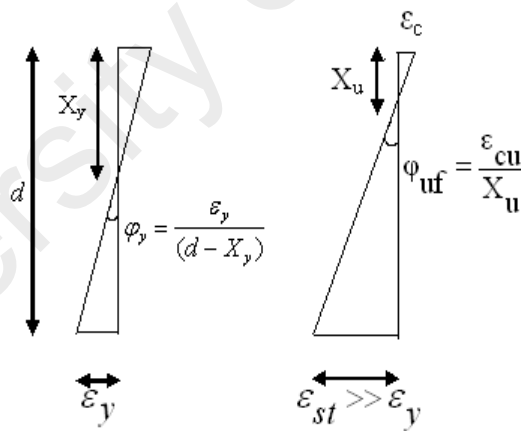


Figure 4.30: Yield curvature (φ_y) and ultimate destructive curvature (φ_{uf}) in a bending section

For the study of the curvature ductility index in the deep beams tested it is necessary to point out the strain distribution along the height of the bending zone at mid-span. Thus strain was measured at the mid-span on the vertical face along the beam length (refer to

Figure 3.16). This allowed the computation of the beam curvature in the constant moment regions. On the assumption that flexure cracks propagate from the base of the beam to the mid-height of the beam section, Demec gauges are used because they are resistant to cracks, Strain gauges are only used from mid-height to the extreme compression fibre.

As shown in Figures 4.1 to 4.6, the results of the strain distribution are nonlinear. As a result, the strain block in deep beams becomes nonlinear even in the elastic phase. This reiterates that deep beams do not conform to the common hypothesis for NBs that plane sections remain planar after bending. Figures 4.1 to 4.6 also show that the strain in tensile bars in the tension zone is more significant than the strain in the compression zone.

The yielding and ultimate strains in the compression and tension zones at the mid-span height of the beam length are presented in Table 4.10.

Table 4.10: Concrete strain at the mid-span height of the beam length at yield and ultimate loading states

Beam	ε_{cy}	ε_{cu}	φ_y	φ_u	$\mu = \frac{\varphi_u}{\varphi_y}$
B1	0.000283	0.000607	0.00498	0.0104	2.09
B2	0.000793	0.002172	0.00857	0.0182	2.12
B3	-	0.001074	-	-	-
B4	-	0.000575	-	-	-
B5	-	0.000406	-	-	-
B6	-	0.000696	-	-	-
B7	0.001105	0.002254	0.00891	0.022	2.47
B8	0.001885	0.001963	0.0108	0.012	1.11

In this table, ε_{cu} represents the experimental ultimate strains in HSSCC deep beams at the extreme compression fibre over the constant moment region. ε_{cy} is the experimental result of the concrete strain in the extreme compression fibre corresponding to the yielding of the tensile bar, μ represents the curvature ductility index, and ϕ_y and ϕ_u are yielding and ultimate curvatures calculated from geometrical proportions (refer to Figure 4.30). Equation 4.19 presents the ductility curvature:

$$\phi = \frac{\varepsilon_c + \varepsilon_s}{d} \text{ (rad/m)} \quad \text{(Eq. 4.19)}$$

There was no ultimate and yield strain data for B3, B4, B5 and B6 due to the localised concrete crushing at the load and support points prior to the yielding of the tensile bars.

The reason for the premature failure is due to high stress increase at the support and load points due to the high loads applied. Based on the PCA manual (Portland Cement Association, 1984), the stress curves at mid-span are optimised for support widths of 1/5, 1/10 or 1/20 of the span (centre to centre of the supports). Support widths are important because they affect the failure mode and the deflection amount (Mohammadhassani et al, 2011a). In the present study, the support and loading point widths were less than L/26 for beams B1 to B5. It was doubled to almost L/12 for B6 to B8 to increase their load bearing capacity in order to prevent localised concrete failure.

Table 4.10 indicates the ultimate strain in the extreme compression fibre in the pure bending zone of the HSSCC deep beam sections tested. All beams except B2 and B7 conform to the CSA94 provisions (Canadian Standard Association, 1994); B2 and B7 are slightly above the CSA94 limit of 0.002. This is probably due to the heavy reinforcement used in this experimental work. These strain measurements were taken in

the horizontal struts, similarly to the finding of Collins and Mitchell (1986) for strain measurements taken in the inclined struts.

The fundamentals of the CSA code for design of deep beams and corbels are based on the work by Collins and Mitchell (1986). Based on their findings, the cracked concrete behaves as a separate material and the compressive strength of concrete in deep beams is reduced due to strain-softening. The ultimate strain of concrete in the extreme compression fibre has a significant effect on the ductility index and the reinforcement limits of flexural members. ACI 441R-96 indicates that a strain limit of 0.003 is acceptable for both HSC and NSC NBs; however this is not applicable for HSC deep beams. For deep beams, design codes are only briefly described in the CSA design code. The difference in the maximum compression strain in the extreme compression fibre in normal and deep beams is due to reasons such as the size effect and the load transferring mechanism. Investigations by Van Mier (1986) on plain concrete prisms with heights of 51, 102, and 203 mm illustrated the scale effect and size dependency on the ultimate concrete strain. Based on this study, the size effect of the section height is explained by the localised damage phenomenon during the beam failure and this prevents the beam from reaching its ultimate load.

The other reason was the concrete strength. In a HSC beam section, a shallower compressive stress block is required to equilibrate the tension zone forces. Therefore the neutral axis in a HSC beam is closer to the extreme compression fibre compared to an NSC beam with the same reinforcement ratio. The lower neutral axis depth is expected to result in higher plastic strains in the tension reinforcement, leading to ductile behaviour. All these aforementioned reasons justify the fact that HSC deep beams exhibit a lower ultimate strain in the extreme compression fibre.

The need to study and identify the balance condition is highlighted to better understand the effect of ultimate strain in extreme compression fibres and the ductility of deep beam sections. This includes the study on tensile bar variation and its effect on the section behaviour. One of the important parameters that affect the ductility of bending sections is the tensile reinforcement ratio. Ductility is guaranteed in NBs by designing the tensile reinforcement ratio to be substantially below the ACI 318 the balanced ratio limit of at least 25%. Balanced ratio is the ratio at which steel yielding and concrete crushing occur simultaneously.

Based on ACI 318M-95 code provisions, Section 10.3.2, the balanced reinforcement ratio ρ_b is calculated for NB as Equation 4.20.

$$\rho_b = \frac{0.85 \beta_1 f'_c}{f_y} \frac{600}{600 + f_y} \quad (\text{Eq. 4.20})$$

where f'_c is the concrete nominal compressive strength, f_y is the reinforcement nominal yield strength in MPa, and β_1 is a function of f'_c (ACI Code(2008), Section 10.2.7.3).

The ultimate flexural strength of a member is reached when the strain at the extreme compression fibres reaches the ultimate strain of concrete at the time when the tension reinforcement reaches yield strain. But as noted in Table 4.10, the yielding of tensile bar corresponds to the strain in the extreme compression fibre (ϵ_{c_y}) at a range of 0.36 to 0.96 of the ultimate strain (ϵ_{c_u}). This variance in strain ratios complicates the classification of the balance condition in deep beams. Consequently, the theory of balance condition that is valid for NBs is not applicable in the design of deep beams. Thus, tensile bars in deep beam must meet the serviceability requirements.

ACI 318M-95 limits the minimum flexural tension reinforcement ratio in a beam section as shown in Equation 4.21:

$$\rho_{\min} = \frac{\sqrt{f'_c}}{4f_y} \geq \frac{1.4}{f_y} \quad (\text{Eq. 4.21})$$

Table 4.11 presents a comparison of the tensile reinforcement ratio of the code limit and the bars used.

These results are based on bar schedules and bar specifications that have been derived from Tables 3.4.

Table 4.11: Tensile reinforcement ratio of the code limit and bars used

Beam	ρ	Code limit
B1	0.0022	0.00390
B2	0.00269	0.00225
B3	0.00414	0.00224
B4	0.00605	0.00234
B5	0.00808	0.00236
B6	0.00938	0.00264
B7	0.0104	0.00261
B8	0.0125	0.00261

As seen in Table 4.11, only B1 has a tensile reinforcement ratio less than the code limit. Figure 4.11 shows that the failure of B1 exhibited flexural failure and wider flexural cracks. This was different from all the other beams (i.e. a tensile reinforcement ratio more than the code limit) which exhibited shear failure and premature failure (i.e. crushing of concrete).

Other effective parameters on the ductility of deep beam sections are both the horizontal and vertical web reinforcements. According to the ACI 318-99 code provisions, the formation of inclined cracks may lead to a sudden failure in concrete beams if there is no reinforcement. The ACI code requires that a minimum area of shear reinforcement has to be in reinforced concrete members, except where V_u (ultimate shear load) is less than $\phi V_c/2$ (V_c is the contribution of concrete in the ultimate shear load). This requirement is intended to guarantee a ductile failure. When $\phi V_c/2 \leq V_u \leq \phi V_c$, the minimum area of shear reinforcement is determined from Equations 4.22 and 4.23:

$$A_v \geq 0.0015b_w s_1 \quad (\text{Eq. 4.22})$$

$$A_{vh} \geq 0.0025b_w s_2 \quad (\text{Eq. 4.23})$$

where:

A_v = the area of vertical shear reinforcements perpendicular to the span

A_{vh} = the area of horizontal shear reinforcements parallel to the span

b_w = width of the beam section

s_1 = spacing of the vertical shear reinforcement parallel to the longitudinal reinforcement

s_2 = spacing of horizontal shear reinforcement perpendicular to the longitudinal reinforcement.

The above-mentioned code provisions were based on the findings of Rogowsky and Macgregor (Rogowsky & MacGregor, 1986). The web reinforcement ratios for the deep beams tested are presented in Table 4.12.

Table 4.12: Web reinforcement ratio for deep beams tested

Beam	$\frac{A_v}{b_w \cdot s_1}$	$\frac{A_{vh}}{b_w \cdot s_2}$
B1	0.0064	0.0042
B2	0.0064	0.0042
B3	0.0064	0.0042
B4	0.0064	0.0067
B5	0.0079	0.0098
B6	0.0079	0.0098
B7	0.0079	0.0098
B8	0.0079	0.0098

Table 4.12 shows that all the specimens were over-reinforcement at the web. Over-reinforcement of web also improves the shear response of deep beams. If the bearing stress is below the concrete strength limit, this over-web reinforcement can increase the shear strength and give a higher ductile response with stabilised the inclined cracks. Web bars help prevent the propagation of inclined cracks or the premature shear failure of deep beams.

4.1.7.2 Ductility index based on deflection measurements

Concrete deep beam elements are deformable structural elements. These elements respond to external loads, i.e. flexure and shear, as curvature and deflection, which are relatively lower than in NBs. The structural behaviour for deep beams is expressed through relationships between the generalised forces and corresponding displacements.

The other method in ductility assessment is the evaluation of displacement. The following discussion on the amount of experimental ductility index ($\mu_{\Delta(\text{exp})}$) is based on deflection amounts. $\mu_{\Delta(\text{exp})}$ is defined as the ratio of the maximum deflection to the yield deflection (Δ_y) as stated in Equation 4.24.

$$\mu_{\Delta(\text{exp})} = \frac{\Delta_u}{\Delta_y} \quad (\text{Eq. 4.24})$$

where Δ_y is the deflection corresponding to the initial of the tensile steel yielding and Δ_u represents the ultimate amounts of deflection when fracture occurred. For the ductility assessment of the deep beams tested, the load-deflection graphs at the mid-span of beam length are presented in Figure 4.22.

With reference to Equation 4.24 and Figure 4.22, the ductility of the deep beams tested is presented in Table 4.13.

Table 4.13: Ductility assessment of deep beams tested

Beams	Δ_u (mm)	Δ_y (mm)	$\mu = \frac{\Delta_u}{\Delta_y}$
B1	7.20	1.60	4.50
B2	4.22	3.71	1.14
B3	3.51	-	-
B4	3.55	-	-
B5	6.93	-	-
B6	5.86	-	-
B7	9.95	4.18	2.38
B8	10.2	8.40	1.21

Table 4.13 shows a significant difference in the ductility of deep beams tested, especially between B1 and the other beams. B1 fails by only flexure, in comparison to the other beams which fail due to a combination of a few failure modes. B2–B5 failed before the tensile bar yielded, and as such no data for the aforementioned parameters could be collected. B6–B8 reached the ultimate load and their load-bearing capacity is affected by the load and support point widths.

4.2 Numerical Study

In the last two decades, researchers explored the potential of ANNs and ANFIS as an analytical alternative to conventional methods, which are often limited by strict assumptions of normality, linearity, homogeneity, and variable independence.

An attempt is made to use the back-propagation neural network (BPNN) model, ANFIS and LR in predicting the mid-span deflection as a serviceability index and strain in the tie section for design purposes. The results obtained by the BPNN and ANFIS models are compared with LR.

4.2.1 Application of artificial neural networks (ANN) and linear regression (LR) in predicting the deflection of concrete deep beams

In relation to the failure mode of deep beams, the serviceability of a structure is determined by observing its deflection and cracking. In addition, it was observed that the stiffness of the beams increases with an increase in section height, and this leads to brittle failure.

As noted in Figure 4.22, all the beams demonstrated a nearly linear response up to about more than 85% of the ultimate load. In some cases, failure occurred closer to the peak of the applied loads. This is the result of the failure of the members where shear deformation is a predominant behaviour.

4.2.1.1 The best learning function and optimum architecture of MLFFNN

Fifty nets were examined in order to optimise the architecture of the network. A MLFFNN was first constructed, including two hidden layers where 20 and 15 neurons were considered for the first and second layers respectively. The tangent hyperbolic (tansig) and linear (purlin) transfer functions were used for the hidden layers and the output layer respectively.

This MLFFNN structure was independently trained 5 times to find the best type of BP. In the experiments, for each type of BP including “trainlm”, “traingd”, traingdm”, “traingda”, “traingdx”, “trainoss”, “traingcf” and “trainrp”, the network was trained in 25 runs with initial random weights. The results of the above-mentioned experiments are summarised in Tables 4.14 and 4.15. In these tables, for each trained network, the “MSE” and correlation coefficient “R” were computed for learn and test sets. The average of the MSE and R values over 25 independently initialised networks, the maximum and minimum values of MSE and R, and the average training time for each type of BP function are summarised and compared in Tables 4.14 and 4.15.

Table 4.14: Performance of different types of BP on the prediction of deflection

		Traingdm		Traingd		Traingdx		Trainlm	
		learn	test	learn	test	learn	test	learn	test
MSE	Max	47.347	46.46	7.751	6.952	174.86	172.94	0.0257	0.0123
	Min	0.8498	0.855	0.068	0.045	0.7970	0.7972	0.0181	0.0047
	Avg	14.762	15.42	0.895	0.838	35.526	35.598	0.0202	0.0064
Correlation(R)	Max	0.9283	0.913	0.993	0.995	0.9360	0.9312	0.9980	0.9995
	Min	0.4133	0.413	0.002	0.050	0.1510	0.1974	0.9972	0.9986
	Avg	0.1227	0.113	0.910	0.913	0.3601	0.3433	0.9978	0.9993
Time	3.7060			101.5654		4.8909		73.043	

Table 4.15: Performance of different types of BP on the prediction of deflection

		Trainrp		Traingda		Traincgf		Trainoss	
		Learn	test	Learn	test	learn	test	learn	test
MSE	Max	0.0548	0.0417	0.4621	0.4573	0.1369	0.1341	0.3247	0.3511
	Min	0.0229	0.0091	0.1223	0.132 4	0.0428	0.0237	0.0373	0.0267
	Avg	0.0326	0.0185	0.2161	0.216 1	0.0648	0.0441	0.0891	0.0829
Correlation(R)	Max	0.9975	0.9990	0.9875	0.9853	0.9951	0.9977	0.9959	0.9971
	Min	0.9939	0.9956	0.9501	0.947 4	0.9845	0.9868	0.9640	0.9618
	Avg	0.9964	0.9981	0.9774	0.975 6	0.9926	0.9957	0.9901	0.9910
Time	27.0868			21.7297		26.6724		23.2067	

The results are reported for 25 independently initialised weights. The best selection is based on the maximum average correlation coefficient value or the minimum average

MSE value. Therefore by this definition, the function “Trainlm” is selected as the best function for the training of MLFFNN for the remainder of the experiments.

The best architecture was found by testing the different number of hidden layers and neurons in each hidden layer. In this order, R and MSE measurements were used to determine the best architecture. First, we tested an MLFFNN with one hidden layer to determine the best number of neurons; various numbers of neurons between 1 and 30 are examined. Figures 4.31 and 4.32 summarise the results of MSE and R values for this step.

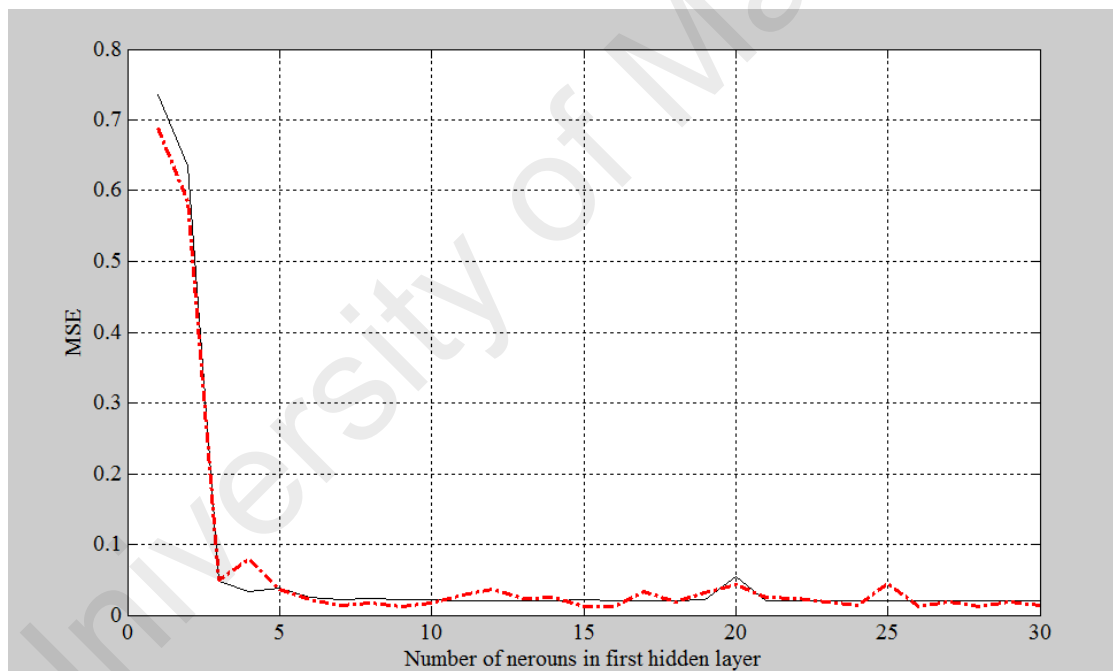


Figure 4.31: MSE value for different numbers of neuron in the first hidden layer

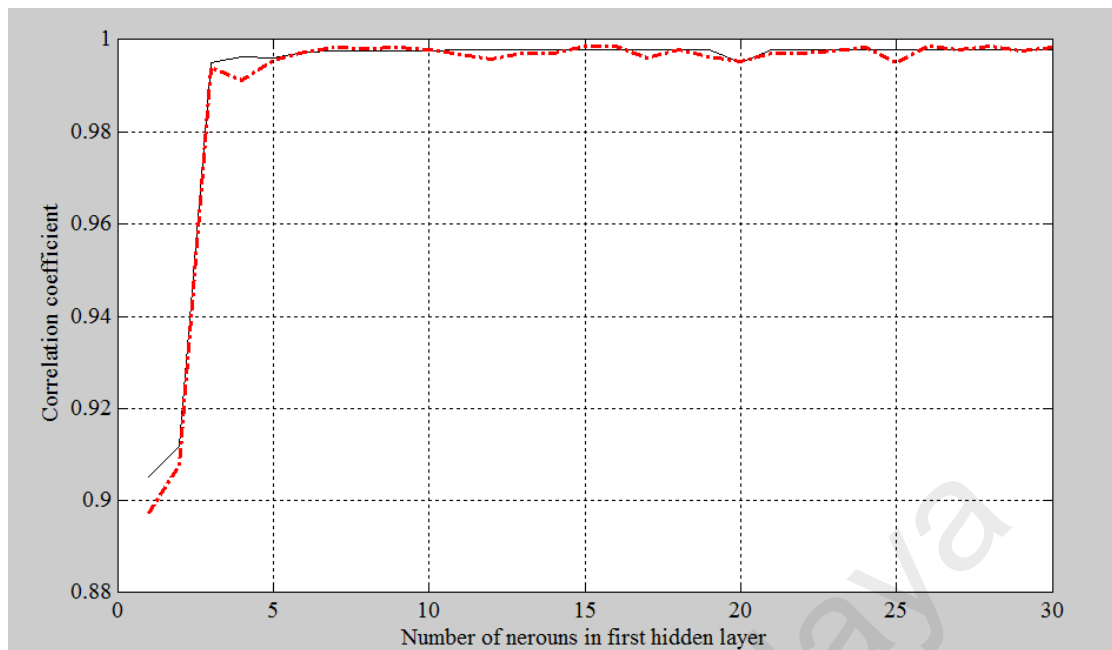


Figure 4.32: R value for different numbers of neuron in the first hidden layer

These figures show that having more than 5 neurons results in an acceptable model. However, among them the highest R and lowest MSE is obtained by 10 neurons in the first layer. It should be noted that increasing the number of neurons in the hidden layer through decreasing the MSE of the training set may lead to network over-fitting or over training. This means that the network losses its generalisation capability and cannot provide a good response to unseen data.

In the sequel, to determine the best number of neurons for the second layer, a MLFFNN was constructed with two hidden layers in which the number of neurons in the first hidden layer is fixed at 10 and the number of neurons in the second hidden layer varies from 1 to 15. Figures 4.33 and 4.34 summarise the MSE and R values for this step.

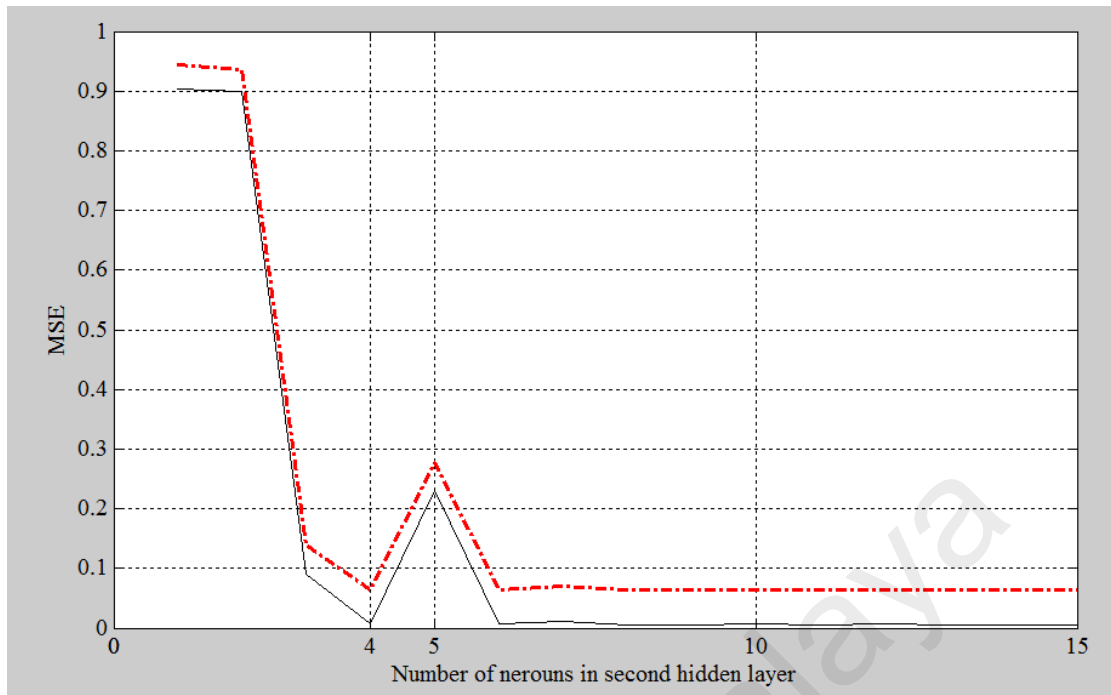


Figure 4.33: MSE values for different numbers of neuron in the second hidden layer

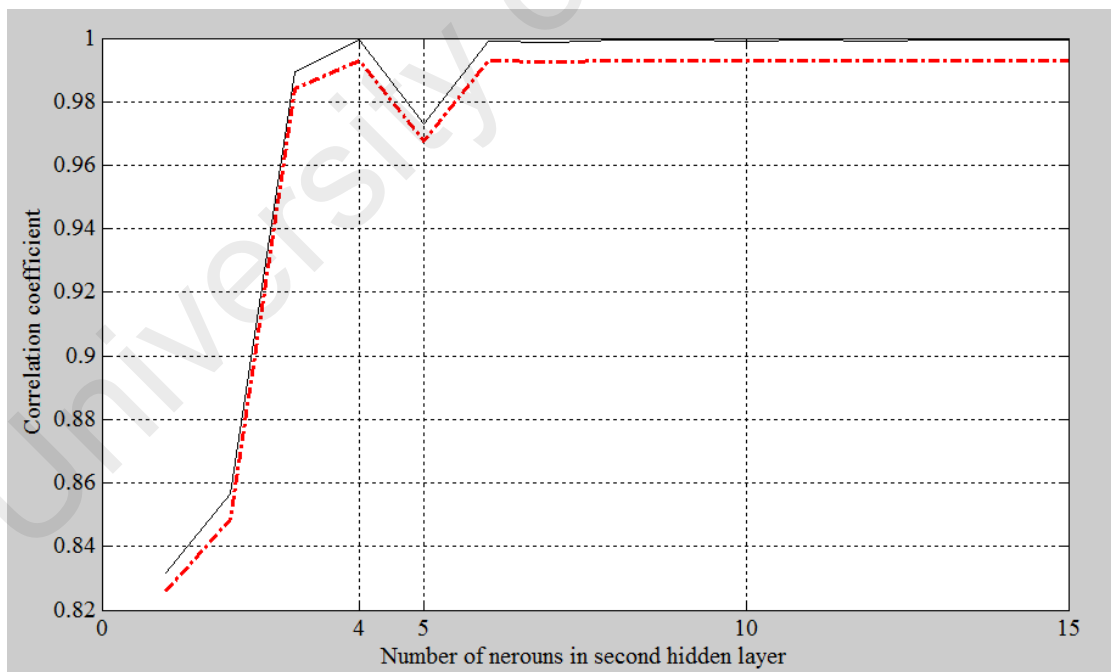


Figure 4.34: R values for different numbers of neuron in the second hidden layer

The dashed line represents the test data while the solid line is the learning data in Figures 4.33 to 4.34. These figures show that the results from the architecture including 4 neurons in the second hidden layer provides the best results. Therefore the optimum network is described in Table 4.16.

Table 4.16: Optimum network specification

Subject	Definition
Structure	10-10-4-1
Transfer function (hidden-layer)	Tangent hyperbolic (tansig)
Transfer function (output-layer)	Linear (purlin)
Learning function	trainlm

LR is an excellent, simple and yet effective scheme used for the prediction of domains with numeric attributes. The linear models function as building blocks for more complex learning tasks. LR analysis is carried out to establish a relationship between the output and input data for the proposed ANN modelling.

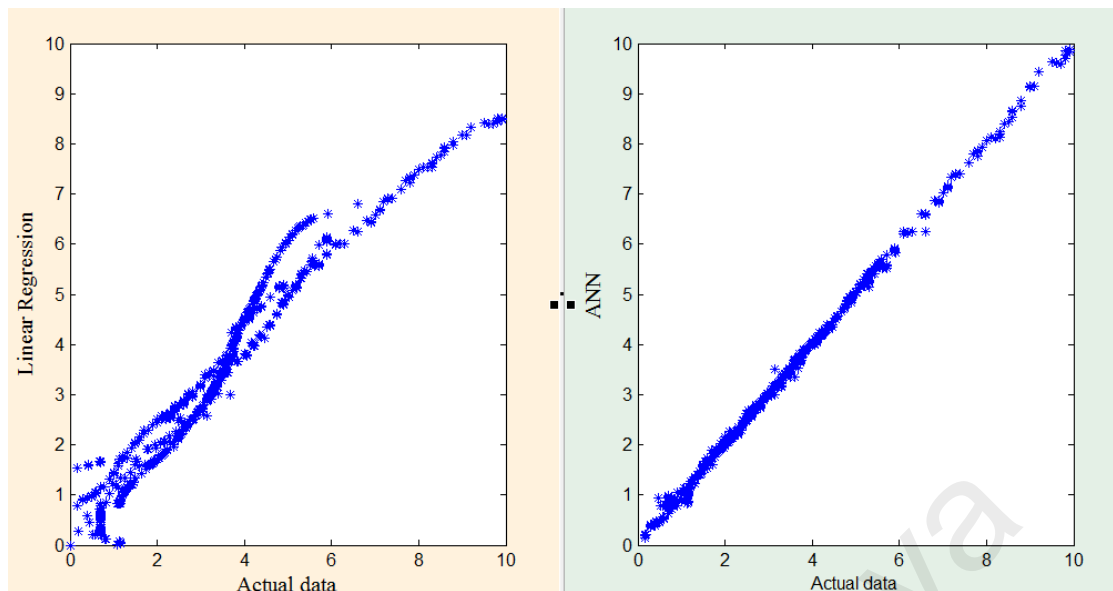
Table 4.17 summarises the MSE and R results obtained using the proposed method and the LR for training and testing data separately. The neural network was trained 25 times using independent initial weight values, and the average values of MSE and R are shown in Table 4.17.

Table 4.17: Comparison of MSE and R values from ANN and LR

Methods	Training Set			Testing set		
	Instances	MSE	R	Instances	MSE	R
Linear regression	2934	0.2275	0.9745	734	0.2148	0.9766
ANN	2934	0.0054	0.9999	734	0.0641	0.9931

As noted, the MSE values from ANN are approximately 40 times smaller than the values from classical LR. Furthermore, the R values from ANN for test data is 0.9931, which is an exciting value to a scientist because it is very close to the value 1 which is indicative of very high degree of confidence.

The results obtained by the experiments show that the difference between these two comparative methods is more obvious for the test set. Figure 4.35 shows the deflection prediction performance provided by LR and ANN for the test data. The horizontal and vertical axes present the actual and predicted data respectively.



(a)

(b)

Figure 4.35: Deflection prediction performance from a) LR b) ANN

Precise modelling should result in a direct linear relation between the actual and predicted data. Figure 4.35 reveals that the proposed ANN method is highly accurate and precise compared to the classical LR for the deflection prediction of HSSCC deep beams.

4.2.2 Application of adaptive network-based fuzzy inference system for the prediction of deflection in HSSCC deep beams

This section presents the use of ANFIS modelling to generalise empirical data and predict mid-span deflection amount of HSSCC deep beams.

4.2.2.1 Development of ANFIS model for the prediction of deflection of deep beam

Firstly, the data is normalised. To normalise the data, a Gaussian normalisation technique is used. Then 80% of the normalised data are randomly chosen as training data and the remaining 20% as testing data. The ANFIS models with different parameters (total of ten) as input are implemented. To implement ANFIS, the MATLAB programming language version R2010a is used.

Genfis2 function based on subtractive clustering method is used to generate the FIS structures. Finding the best structure with the appropriate membership function parameters involved two processes: learning and testing. Through the learning process, first the membership functions of the inputs are generated using subtractive clustering. Then the membership function parameters are tuned using a back-propagation algorithm in combination with a recursive least squares method, followed by the testing step where the generalisation capability of the generated model is checked. To decrease the Mean Square Error (MSE) obtained by this method, the number of membership functions was gradually increased by lowering the range of influence of cluster centres in a step by step and trial and error manner.

LR analysis is carried out to establish a relationship between the output and input data for the proposed ANFIS modelling.

To evaluate the comparative methods, the MSE and Correlation Coefficient/Pearson Coefficient (R) values are used in this study. MSE is a risk function which corresponds to the expected value of the squared error loss or quadratic loss. R is the degree of success in reducing the standard deviation (SD). It is widely used in the sciences as a measure of the strength of linear dependence between two variables.

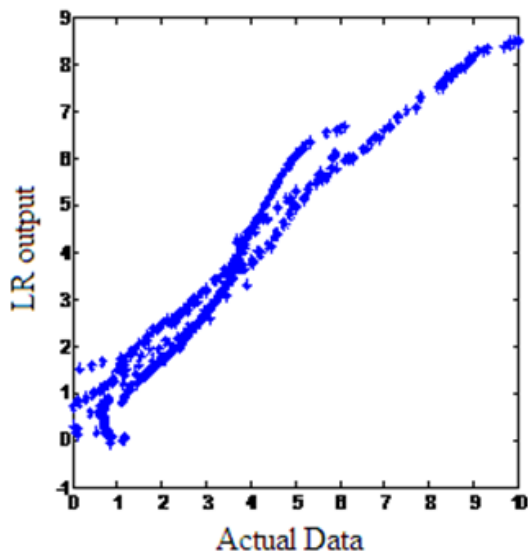
Table 4.18 summarises the MSE and R results obtained using the proposed method and the LR separately for training and testing data.

Table 4.18: Comparison of MSE and R values from ANFIS and LR

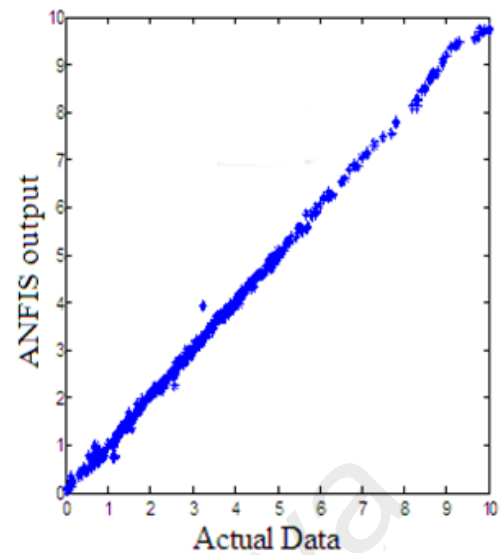
Methods	Training Set			Testing set		
	Instances	MSE	R	Instances	MSE	R
Linear regression	2934	0.2275	0.9745	734	0.2148	0.9766
ANFIS	2934	0.0217	0.9976	734	0.0087	0.9991

As noted, the MSE values from ANFIS are approximately 10 times smaller than the values from classical LR. Furthermore, the R value from ANFIS for the test data is 0.9991 which is an exciting value as it is close to 1. The results obtained by the experiments show that the difference between the two comparative methods is more obvious for the test set.

Figure 4.36 shows the deflection prediction performance provided by LR and ANFIS for the test data. The horizontal and vertical axes present the actual and predicted data, respectively. Precise modelling should result in a direct linear relation between the actual and predicted data. Figure 4.36 reveals that the proposed ANFIS method is highly accurate and precise compared with classical LR for the deflection prediction of HSSCC deep beams.



(a)



(b)

Figure 4.36: Deflection prediction performance from a) LR, b) ANFIS

The relation between the input variables and deflection output variable can be visualised with the modelled fuzzy surfaces shown in Figures 4.37 and 4.38. A Graphical User Interface (GUI) tool allows the examination of the output surface of a FIS model. GUI provides a visual impression of the possible combinations of the two input variables and the output in 3-D. This is a fast visual method to analyse the deflection amount in deep beams. The FIS gives mathematical solution to determine deflection based on data such as tensile reinforcement ratio vs. yield strength and tensile reinforcement ratio vs. load.

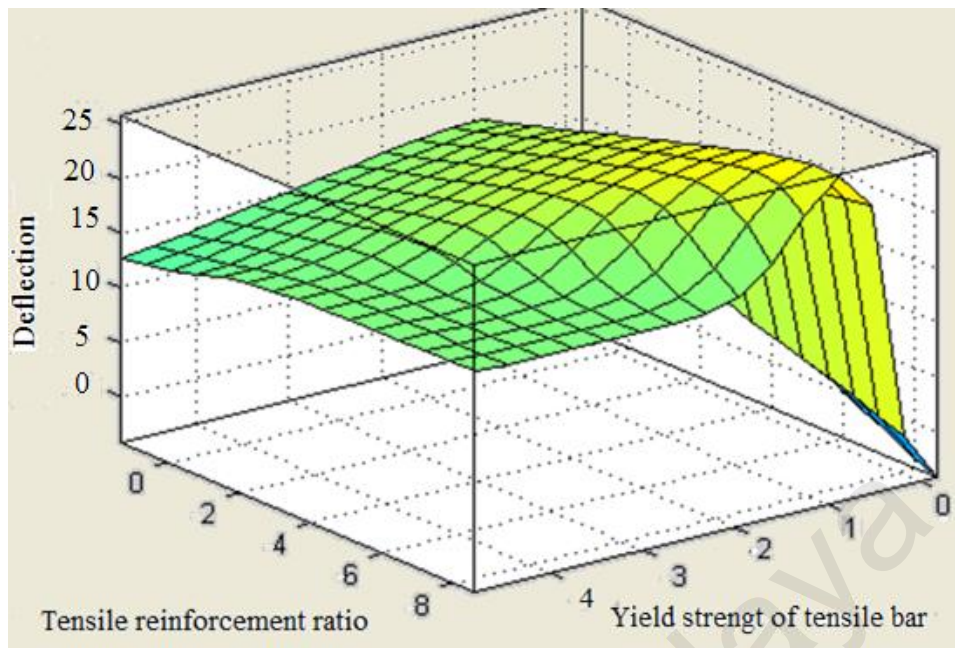


Figure 4.37: Fuzzy surface: Tensile reinforcement ratio and yield strength of tensile bar vs. deflection prediction

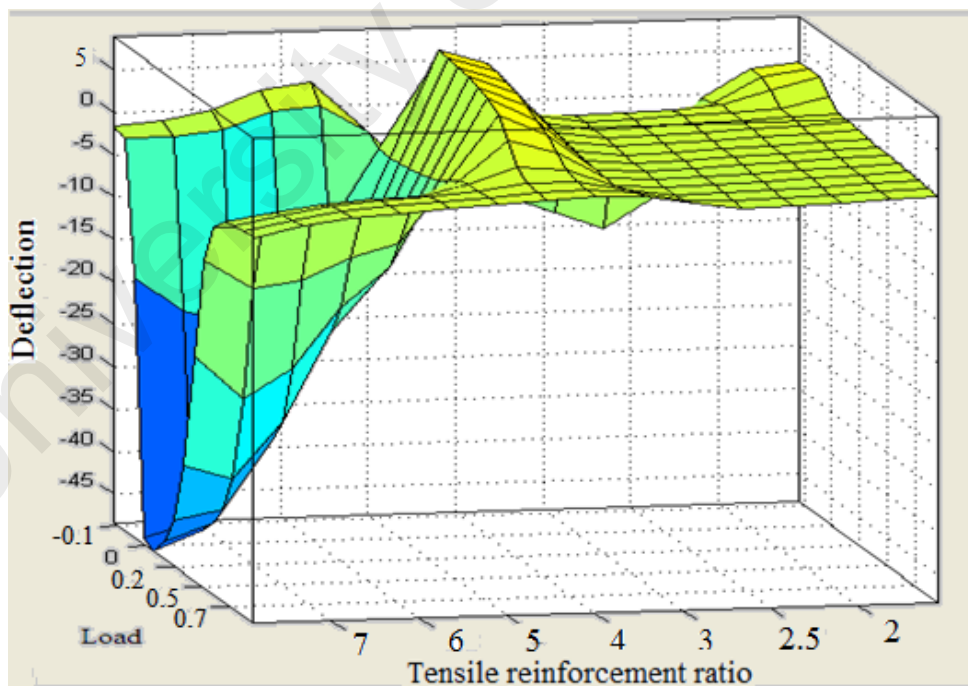


Figure 4.38: Fuzzy surface: Tensile reinforcement ratio and load vs. deflection prediction

4.2.3 Comparison of ANN and ANFIS in deflection prediction

As shown in Tables 4.17 and 4.18, the MSE values from ANN and ANFIS are respectively 40 and 10 times smaller than values from classical LR. R values from ANN and ANFIS for test data are 0.9931 and 0.9991, which are close to a value of 1 – the highest degree of confidence. The difference in the results from these comparative methods is more obvious for the test set. The results also show that ANN and ANFIS operate better than LR for linear data. This is evident from the comparison of MSE and R values for the testing and learning sets due to the nonlinearity of the both models. Thus LR is not able to accurately model nonlinear data. ANN and ANFIS show different prediction patterns in the training and testing sets. ANN has been trained better than ANFIS; ANN shows smaller MSE than ANFIS, less than 5 times with a greater R value. This confirms that ANN is more flexible in training data compared to ANFIS. In terms of incomplete data, ANFIS clearly has proper response to unseen data and can generate smaller MSE and larger R values. Overall, compared to the ANN's multilayer perception, ANFIS is a better choice for the modelling of deep beams.

4.2.4 Application and comparison of ANN, ANFIS and LR in predicting the strain in the tie section of concrete deep beams

4.2.4.1 Introduction

Ties are the elements within a STM that carry tension, and are generally confined to reinforcing or pre-stressing steel. The geometry of a tie is therefore much simpler. The tie is geometrically confined to elements that can carry high tensile forces, and the allowable force is generally given as a fraction of the yield force.

Appropriate attention must be given to the anchorage of ties. If the yield force of a tie is expected at any point in the STM, proper anchorage must be provided beyond this point. The necessary anchorage requirement for ties has been recently studied (Thompson, 2002).

In the ACI code provision, the main load-carrying mechanism in the STM approach consists of single diagonal struts between the loading and the support point (refer to Figure 4.39).

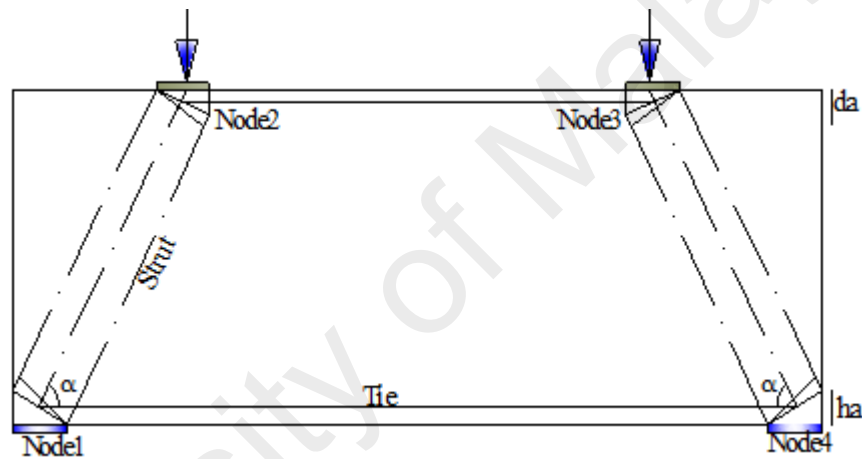


Figure 4.39: Strut and tie model for design using appendix A of the ACI code

The most commonly accepted STM used in deep beam design are the tied arch or truss models depending on the a/d of the beam. The tied arch model is predominantly used in the design of short beams with an a/d less than 1.0, on the assumption that the load is transferred directly from the load point to the support through the formation of a concrete strut. The horizontal component of each strut at the support is set in equilibrium by a horizontal tie extending the full length of the beam (Figure 4.39); it is assumed that the tie force in the model is constant throughout the span. To ensure this

constant tie force, the longitudinal bar forming the ties must be anchored at the face of the node over each support. This is to develop the yield stress and prevent bond failure.

4.2.4.2 Experimental results

Figures 4.40 to 4.44 show the strain distribution along the tie section of the deep beam tested. G.m represents the amount of strain at the mid-span of tie section, and G.s indicates the amount of tie strain near the support of the deep beam (refer to Figures 3.17 to 3.24).

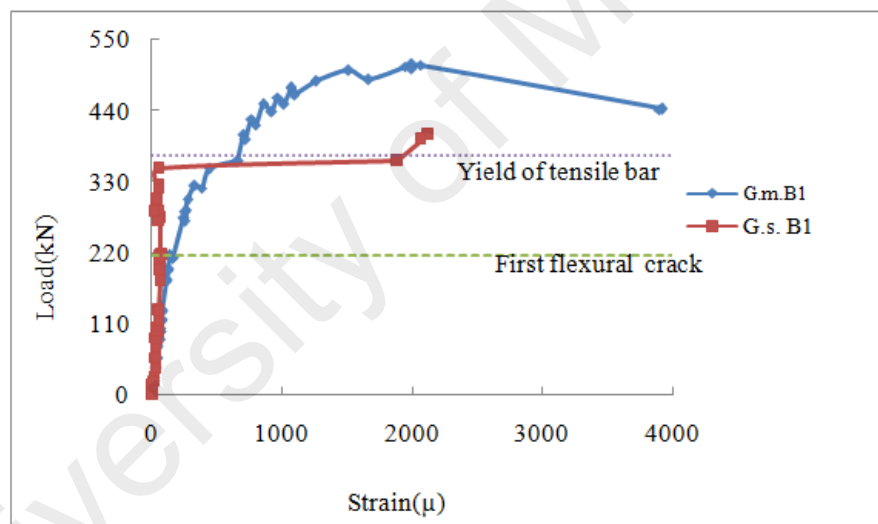


Figure 4.40: Strain variation along the tie section of B1

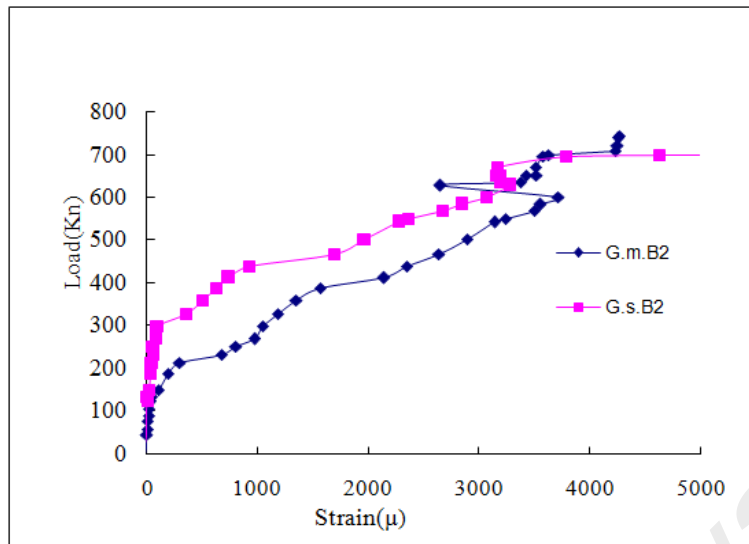


Figure 4.41: Strain variation along the tie section of B2

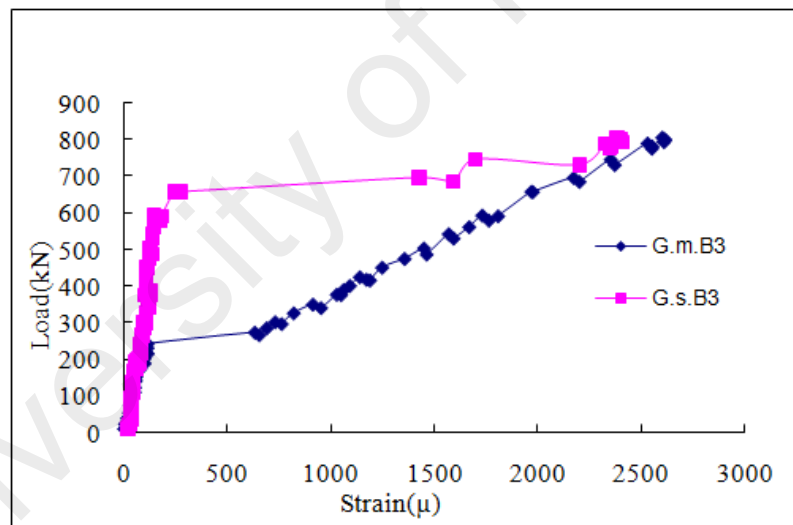


Figure 4.42: Strain variation along the tie section of B3

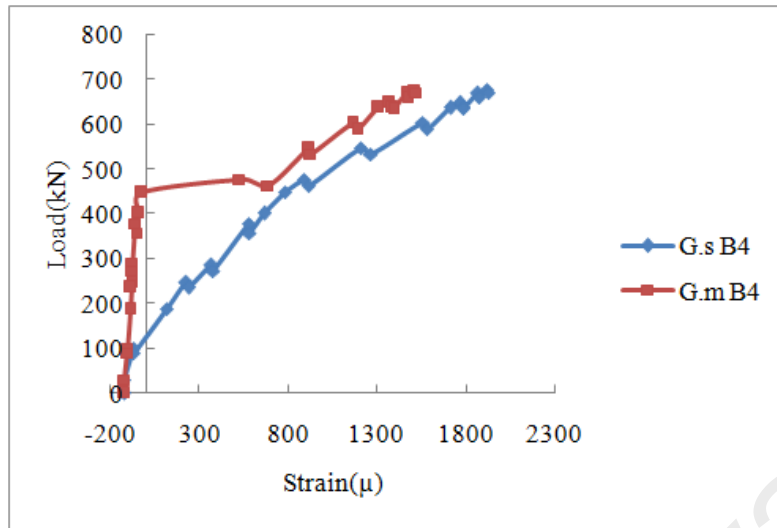


Figure 4.43: Strain variation along the tie section of B4

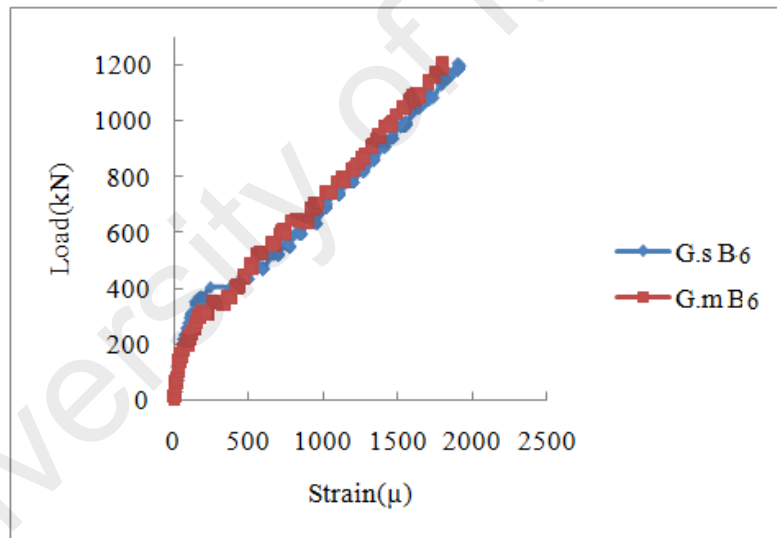


Figure 4.44: Strain variation along the tie section of B6

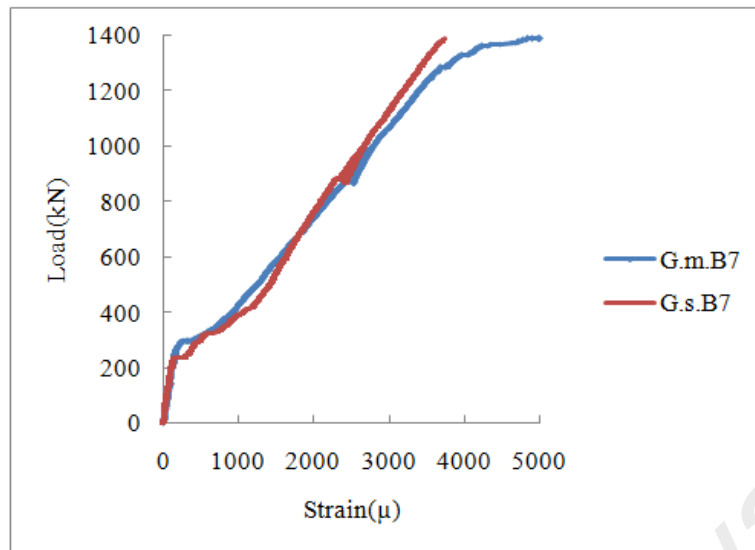


Figure 4.45: Strain variation along the tie section of B7

As seen, the strain variation along the tie section of a deep beam is not linear and shows complexities in behaviour that converge with an increase in the load applied.

4.2.4.3 The best learning function and optimum architecture of MLFFNN

To optimise the architecture of the network, 50 nets were examined. First a MLFFNN was constructed with two hidden layers, in which 20 and 15 neurons were considered for the first and second layers respectively. Also, the tangent hyperbolic (tansig) and linear (purlin) transfer functions were used for the hidden layers and the output layer respectively. This MLFFNN structure was independently trained 8 times to find the best type of BP. In the experiments, for each type of BP including “Trainlm”, “Traingd”, “Traingdm”, “Traingda”, “Traingcf”, “Trainoss”, “Trainrp” and “Traingdx”, the network was trained in 25 runs with initial random weights. The results of the abovementioned experiments are summarised in Tables 4.19 and 4.20. In these tables, for each trained network, the MSE and the correlation coefficient ‘R’ for the learning and test sets were

computed. The average of the MSE and R values over 25 independently initialised networks, the maximum and minimum values of MSE and R, and the average training time for each type of BP function are summarised and compared in Tables 4.19 and 4.20.

Table 4.19: Performance of different types of BP in tie strain prediction

		Traingdm		Traingda		Traingd		Traingdx	
		learn	test	Learn	test	learn	test	learn	test
MSE	Max	2.07	2.13	8.47	1.04	1.34	1.56	1.35	1.46
	Min	2.47	2.76	2.62	3.21	1.23	1.81	4.28	4.33
	Avg	4.23	4.31	5.18	6.58	3.38	4.80	8.07	8.32
Correlation(R)	Max	0	0	1	0	0	0	0	0
	Min	-1	-1	1	1	1	1	0	0
	Avg	0	0	1	1	1	1	0	0
Time	9.7		23.68		126.11		6.41		

Table 4.20: Performance of different types of BP in tie strain prediction

		Trainrp		Trainoss		Trainlm	
		learn	test	learn	test	learn	test
MSE	Max	1.13	1.35	4.01	6.54	1.71	1.03
	Min	1.94	1.93	5.29	7.37	1.31	1.69
	Avg	5.20	5.90	1.59	2.14	1.06	1.60
Correlation(R)	Max	1	1	1	1	1	1
	Min	1	1	1	1	0.9987	0.9977
	Avg	1	1	1	1	0.9996	1
Time	31.998		28.18		84.37		

The results are reported for 25 independently initialised weights. The best selection is based on the maximum average correlation coefficient value or the minimum average MSE value. Therefore by this definition, the function “Trainlm” is selected as the best function for the training of MLFFNN for the remainder of the experiments.

The best architecture was found by testing the different number of hidden layers and neurons in each hidden layer. In this order, R and MSE measures were used to determine the best architecture. First, an MLFFNN was tested with one hidden layer to determine the best number of neurons; various numbers of neuron between 1 to 30 are examined. Figures 4.46 and 4.47 summarise the results of the MSE and R values for this step.

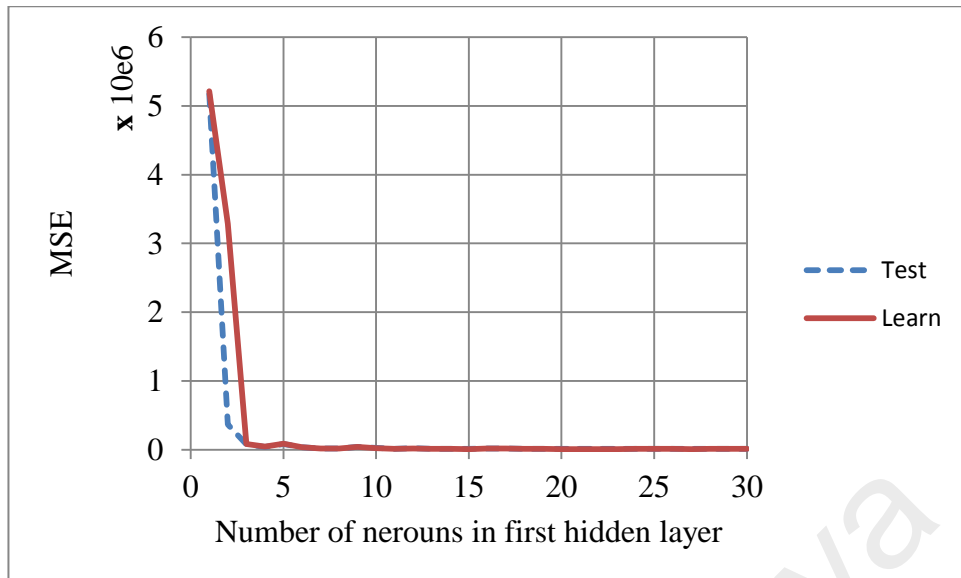


Figure 4.46: MSE value for different numbers of neuron in the first hidden layer

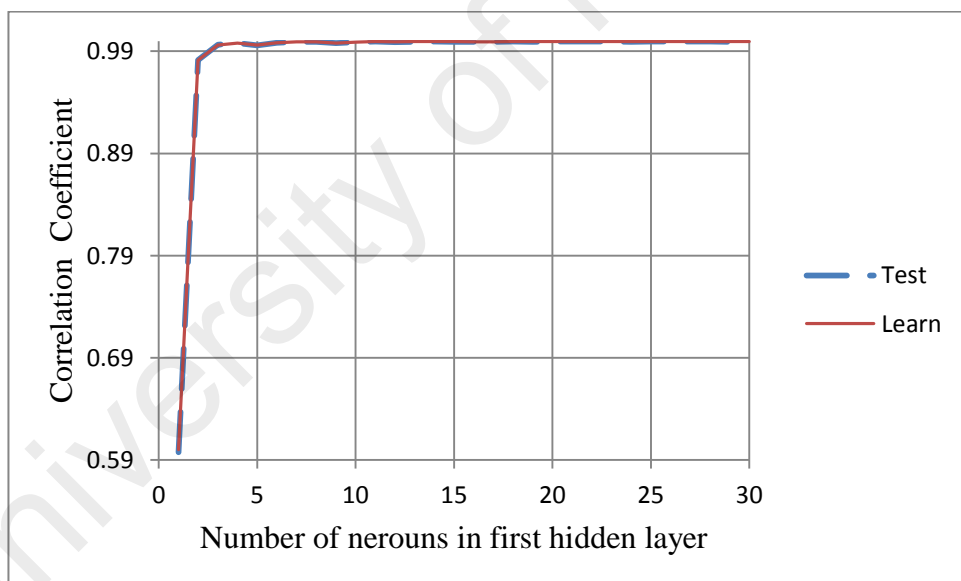


Figure 4.47: R value for different numbers of neuron in the first hidden layer

Figures 4.46 and 4.47 show that having more than 11 neurons results in an acceptable model. Subsequently, to determine the best number of neurons for the second layer, a MLFFNN was constructed with two hidden layers in which the numbers of neuron in the first hidden layer is fixed at 11 and the numbers of neuron in the second hidden

layer varies from 1 to 15. Figures 4.48 and 4.49 summarise the MSE and R values for this step.

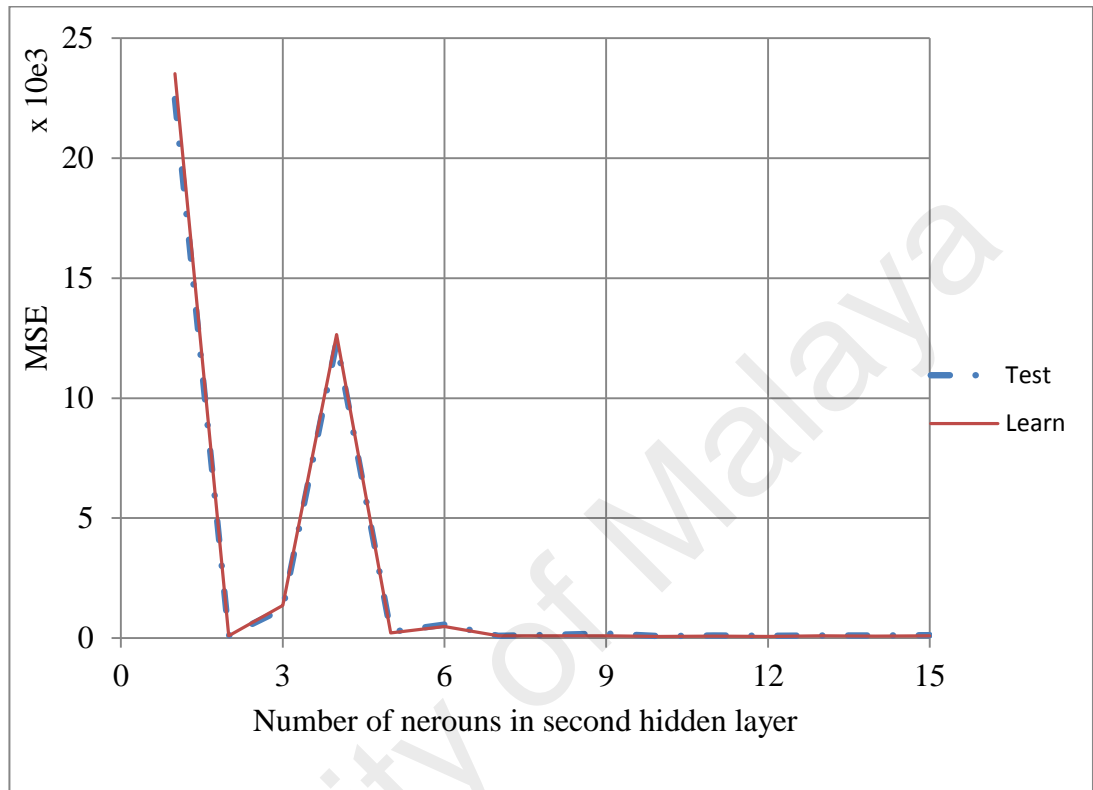


Figure 4.48: MSE values for different numbers of neuron in the second hidden layer

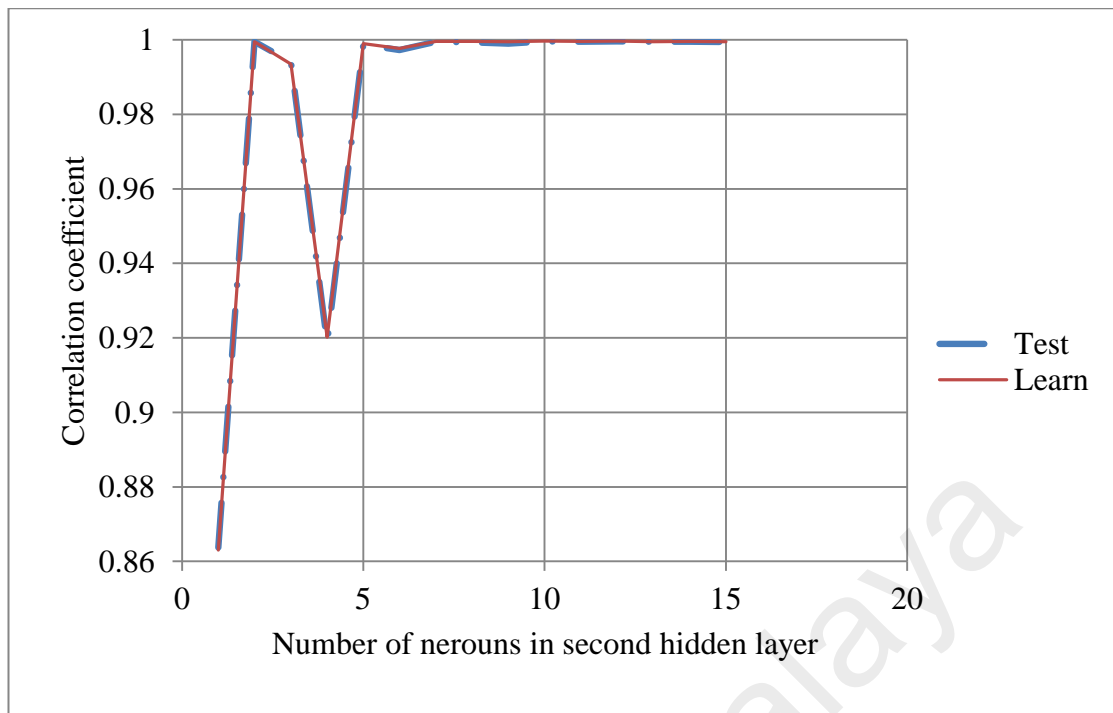


Figure 4.49: R values for different numbers of neuron in the second hidden layer

Figures 4.48 and 4.49 show that the architecture including 10 neurons in the second hidden layer provides the best results. Therefore the optimum network is described in Table 4.21.

Table 4.21: Optimum network specification

Subject	Definition
Structure	10-11-10-1
Transfer function (hidden-layer)	Tangent hyperbolic (tansig)
Transfer function (output-layer)	Linear (purlin)
Learning function	trainlm

LR analysis is carried out to establish a relationship between the output and input data for the proposed ANN.

Table 4.22 summarises the MSE and R results obtained using the proposed method and the LR separately for training and testing data. The neural network was trained 25 times using independent initial weight values and the average values of MSE and R are presented in Table 4.22.

Table 4.22: Comparison of MSE and R values from ANN and LR

Methods	Training Set			Testing set		
	Instances	MSE	R	Instances	MSE	R
Linear regression	3018	82252	0.9605	755	89898	0.9550
ANN	3018	874.86	0.9996	755	977.49	0.9995

As noted, the MSE values from ANN are approximately 94 times for training data and 92 times for test data smaller than the values from classical LR. Furthermore, the R values from ANN for the test data is 0.9995, which is indicative of very high degree of confidence.

The results obtained from the experiments show that the difference between these two comparative methods is more obvious for the test set. Figure 4.50 shows the tie strain prediction performance provided by LR and ANN for the test data. The horizontal and vertical axes present the actual and predicted data respectively.

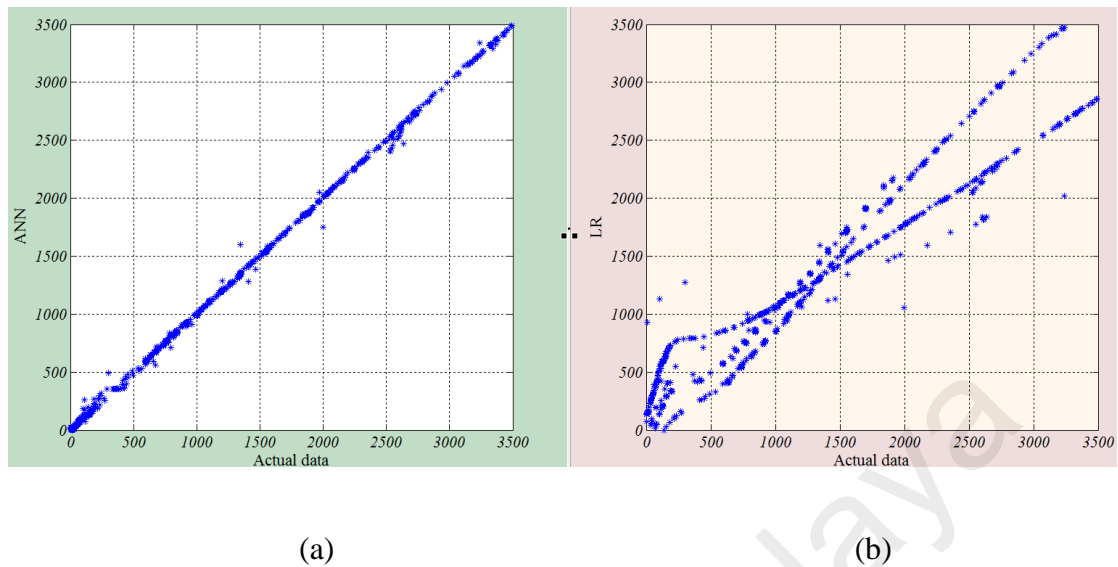


Figure 4.50: Tie strain prediction performance from (a) ANN, (b) LR

Precise modelling should result in a direct linear relation between the actual and predicted data. Figure 4.50 reveals that the proposed ANN method is highly accurate and precise compared to the classical LR for the strain prediction in the tie section of HSSCC deep beams.

4.2.4.4 Developing the ANFIS model for the prediction of strain in tie section of deep beam

To implement ANFIS the MATLAB programming language version R2010a is used. A Genfis2 function based on subtractive clustering method is used to generate the FIS structures. Determining the best structure with the appropriate membership function parameters involved two processes: learning and testing. Through the learning process, first the membership functions of the inputs are generated using subtractive clustering. Then the membership function parameters are tuned using a back-propagation algorithm

in combination with a recursive least squares method followed by the testing step where the generalisation capability of the generated model is checked. To decrease the MSE obtained by this method, the number of membership functions was gradually increased by lowering the range of the influence of cluster centres in a step by step and trial and error manner.

To evaluate the comparative methods, the MSE and Correlation Coefficient/Pearson Coefficient (R) values are used in this study. LR is an excellent, simple and yet effective scheme used for prediction of domains with numeric attributes. The linear models function as building blocks for more complex learning tasks. LR analysis is carried out to establish a relationship between the output and input data for the proposed ANFIS model.

Table 4.23 summarises the MSE and R results obtained using the proposed method and the LR for training and testing data separately.

Table 4.23: Comparison of MSE and R values from ANFIS and LR

Methods	Training Set			Testing set		
	Instances	MSE	R	Instances	MSE	R
Linear regression	3018	83781	0.9595	755	84087	0.9592
ANFIS	3018	778.3	0.9996	755	607.18	0.9997

As noted, the MSE values from ANFIS are approximately 107 times smaller than values from classical LR. Furthermore, the R values from ANFIS for the test data is 0.9997 which is a value close to 1. The results obtained by the experiments show that the

difference in the two comparative methods is more obvious for the test set. Figure 4.51 shows tie strain prediction performance provided by LR and ANFIS for the test data. The horizontal and vertical axes present the actual and predicted data, respectively. Precise modelling should result in a direct linear relation between the actual and predicted data. Figure 4.51 reveals that the proposed ANFIS method is highly accurate and precise compared to the classical LR for the tie strain prediction of HSSCC deep beams.

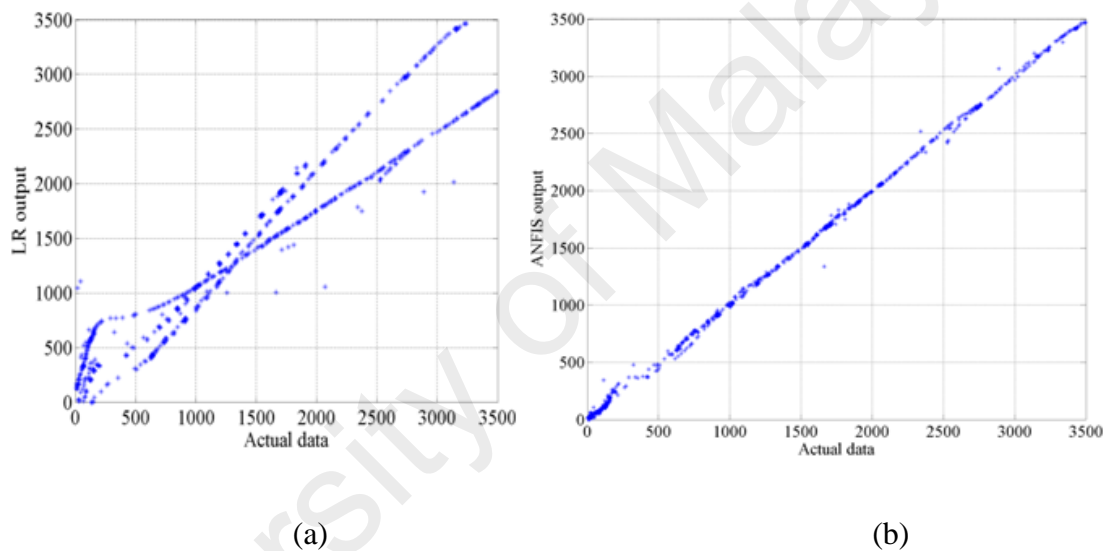


Figure 4.51: Tie strain prediction performance from a) LR, b) ANFIS

The relation between input variables and output variable can be visualised with the modelled fuzzy surfaces shown in Figures 4.52 and 4.53. A GUI tool allows the examining of the output surface of a FIS model. GUI provides a visual impression of the possible combinations of the two input variables and the output in 3-D. This is a fast visual method to analyse the amount of tie strain in deep beams. The FIS gives mathematical solution to determine the strain of a tie section based on data such as tensile reinforcement ratio vs. yield strength and tensile reinforcement ratio vs. load.

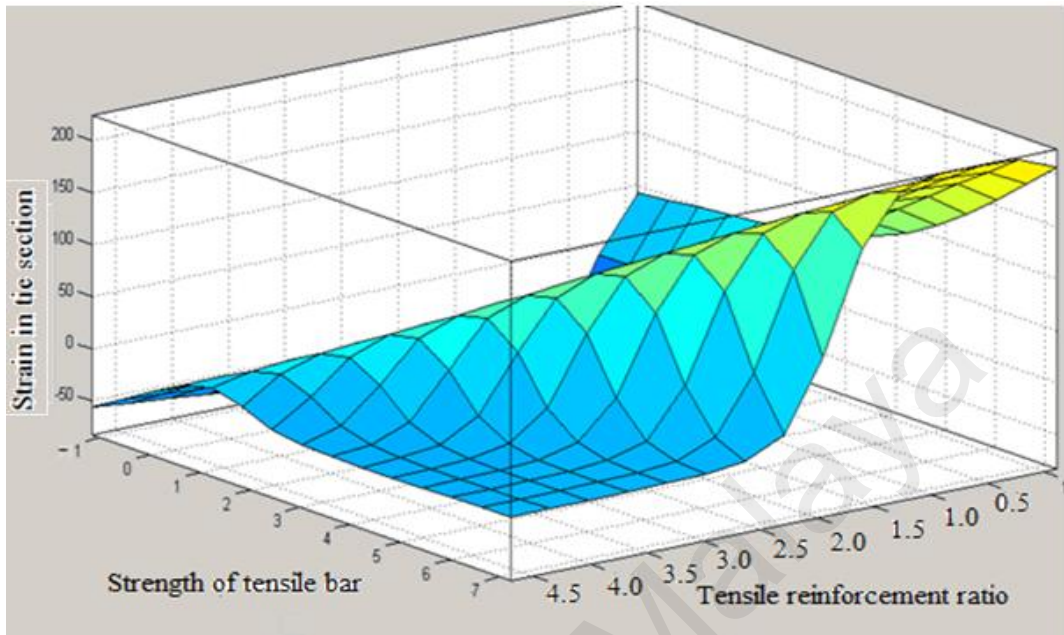


Figure 4.52: Fuzzy surface: Tensile reinforcement ratio and yield strength of tensile bar vs. strain in tie prediction

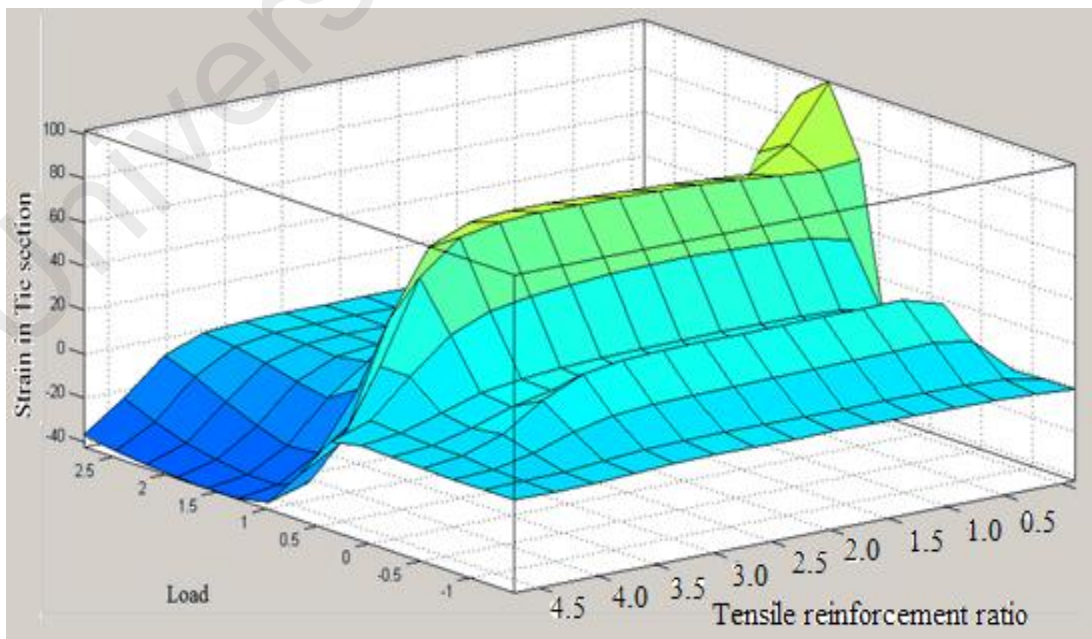


Figure 4.53: Fuzzy surface: Tensile reinforcement ratio and load vs. strain in tie prediction

The input-output surfaces shown in the figures above are nonlinear and monotonic surfaces that illustrate how the ANFIS model will respond to varying the values in the 'strain in tie section' prediction.

Tables 4.22 and 4.23 show that ANN and ANFIS operate better than LR for linear data. This is evident from the comparison of MSE and R values for testing and learning sets due to the nonlinearity of the both models. Thus LR is not able to accurately model nonlinear data.

The MSE values from ANFIS and ANN in the training set are approximately 107 and 138 times smaller than the LR values respectively. Furthermore, the R values from ANFIS for the test data is 0.9997 which is indicative of a high degree of confidence. The R values from ANFIS for the test data is higher than from ANN, while for the training sets the R values from ANFIS and ANN are the same.

ANFIS has been trained better than ANN; ANFIS shows smaller MSE than ANN in both the training and testing sets. This confirms that ANFIS is more flexible in training and testing the data compared to ANN. Also in terms of incomplete data, ANFIS clearly has a proper response to unseen data and can generate smaller MSE and larger R values. Overall, compared to the ANN's multilayer perception, ANFIS is a better choice for the modelling of strain in the tie section of a deep beam.

4.3 Application of ANFIS in shear strength prediction of deep beams

Experimental data from published works by Pal & Deswal (2011), Zhang & Tan (2010) and Yang et al (2003) for reinforced deep beams were used to study the effectiveness of ANFIS in the prediction of shear strength. They included experimental data from 139

reinforced deep beams of which 19 were HSC reinforced deep beams from Tan et al (1995), 52 from Smith and Vantsiotis (1982), 35 from Kong et al(1970), 21 from Zhang and Tan (2010) and 12 from Yang et al (2003). The complete set of 139 data is provided in Tables 4.24, and the shear strength unit is kN.

Table 4.24: Datasets of published works

l/d	d/b _w	a/d	f _c	f _{yh}	f _{yv}	p _h	p _s	p _v	V
19 High strength deep beam(KH Tan, Kong, Teng, & Guan, 1995)									
2.15	4.209	0.27	0.0588	0.5048	0.3752	0	0.0123	0.0048	675
3.23	4.209	0.27	0.0516	0.5048	0.3752	0	0.0123	0.0048	630
4.30	4.209	0.27	0.0539	0.5048	0.3752	0	0.0123	0.0048	640
5.38	4.209	0.27	0.0573	0.5048	0.3752	0	0.0123	0.0048	630
2.15	4.209	0.54	0.056	0.5048	0.3752	0	0.0123	0.0048	468
3.23	4.209	0.54	0.0457	0.5048	0.3752	0	0.0123	0.0048	445
4.30	4.209	0.54	0.0539	0.5048	0.3752	0	0.0123	0.0048	500
5.38	4.209	0.54	0.053	0.5048	0.3752	0	0.0123	0.0048	480
2.15	4.209	0.81	0.0512	0.5048	0.3752	0	0.0123	0.0048	403
3.23	4.209	0.81	0.044	0.5048	0.3752	0	0.0123	0.0048	400
2.15	4.209	1.08	0.0482	0.5048	0.3752	0	0.0123	0.0048	270
3.23	4.209	1.08	0.0441	0.5048	0.3752	0	0.0123	0.0048	280
4.30	4.209	1.08	0.0468	0.5048	0.3752	0	0.0123	0.0048	290
5.38	4.209	1.08	0.048	0.5048	0.3752	0	0.0123	0.0048	290
3.23	4.209	1.62	0.0506	0.5048	0.3752	0	0.0123	0.0048	220
4.30	4.209	1.62	0.0446	0.5048	0.3752	0	0.0123	0.0048	190
5.38	4.209	1.62	0.0453	0.5048	0.3752	0	0.0123	0.0048	173
4.30	4.209	2.16	0.0411	0.5048	0.3752	0	0.0123	0.0048	150
5.38	4.209	2.7	0.0428	0.5048	0.3752	0	0.0123	0.0048	107
52 Normal strength deep beam(Smith & Vantsiotis, 1982)									
2.67	2.990	1.00	0.0205	0.4835	0.4835	0	0.0194	0	140
2.67	2.990	1.00	0.0209	0.4835	0.4835	0	0.0194	0	136
2.67	2.990	1.00	0.0187	0.4835	0.4835	0.0023	0.0194	0.0028	161
2.67	2.990	1.00	0.018	0.4835	0.4835	0.0045	0.0194	0.0028	149
2.67	2.990	1.00	0.0161	0.4835	0.4835	0.0068	0.0194	0.0028	141
2.67	2.990	1.00	0.0206	0.4835	0.4835	0.0068	0.0194	0.0028	171
2.67	2.990	1.00	0.0211	0.4835	0.4835	0.0091	0.0194	0.0028	184
2.67	2.990	1.00	0.0217	0.4835	0.4835	0.0023	0.0194	0.0063	175
2.67	2.990	1.00	0.0198	0.4835	0.4835	0.0045	0.0194	0.0063	171
2.67	2.990	1.00	0.0203	0.4835	0.4835	0.0068	0.0194	0.0063	172
2.67	2.990	1.00	0.0191	0.4835	0.4835	0.0091	0.0194	0.0063	162
2.67	2.990	1.00	0.0181	0.4835	0.4835	0.0023	0.0194	0.0125	161
2.67	2.990	1.00	0.0192	0.4835	0.4835	0.0045	0.0194	0.0125	173

‘Table 4.24, continued’									
2.67	2.990	1.00	0.0208	0.4835	0.4835	0.0068	0.0194	0.0125	179
2.67	2.990	1.00	0.0199	0.4835	0.4835	0.0091	0.0194	0.0125	168
3.08	2.990	1.21	0.0217	0.4835	0.4835	0	0.0194	0	149
3.08	2.990	1.21	0.0221	0.4835	0.4835	0.0023	0.0194	0.0024	148
3.08	2.990	1.21	0.0201	0.4835	0.4835	0.0045	0.0194	0.0024	144
3.08	2.990	1.21	0.0208	0.4835	0.4835	0.0068	0.0194	0.0024	141
3.08	2.990	1.21	0.0195	0.4835	0.4835	0.0091	0.0194	0.0024	154
3.08	2.990	1.21	0.0192	0.4835	0.4835	0.0023	0.0194	0.0042	129
3.08	2.990	1.21	0.019	0.4835	0.4835	0.0045	0.0194	0.0042	131
3.08	2.990	1.21	0.0175	0.4835	0.4835	0.0068	0.0194	0.0042	126
3.08	2.990	1.21	0.0218	0.4835	0.4835	0.0068	0.0194	0.0042	150
3.08	2.990	1.21	0.0198	0.4835	0.4835	0.0091	0.0194	0.0042	145
3.08	2.990	1.21	0.0162	0.4835	0.4835	0.0023	0.0194	0.0063	131
3.08	2.990	1.21	0.0204	0.4835	0.4835	0.0023	0.0194	0.0077	159
3.08	2.990	1.21	0.019	0.4835	0.4835	0.0045	0.0194	0.0077	159
3.08	2.990	1.21	0.0192	0.4835	0.4835	0.0068	0.0194	0.0077	155
3.08	2.990	1.21	0.0207	0.4835	0.4835	0.0091	0.0194	0.0077	166
3.08	2.990	1.21	0.0171	0.4835	0.4835	0.0023	0.0194	0.0125	154
3.67	2.990	1.50	0.0207	0.4835	0.4835	0	0.0194	0	116
3.67	2.990	1.50	0.0192	0.4835	0.4835	0.0023	0.0194	0.0018	119
3.67	2.990	1.50	0.0219	0.4835	0.4835	0.0045	0.0194	0.0018	124
3.67	2.990	1.50	0.0227	0.4835	0.4835	0.0068	0.0194	0.0018	131
3.67	2.990	1.50	0.0218	0.4835	0.4835	0.0091	0.0194	0.0018	123
3.67	2.990	1.50	0.0199	0.4835	0.4835	0.0023	0.0194	0.0031	124
3.67	2.990	1.50	0.0192	0.4835	0.4835	0.0045	0.0194	0.0031	104
3.67	2.990	1.50	0.0193	0.4835	0.4835	0.0045	0.0194	0.0031	116
3.67	2.990	1.50	0.0204	0.4835	0.4835	0.0068	0.0194	0.0031	125
3.67	2.990	1.50	0.0208	0.4835	0.4835	0.0091	0.0194	0.0031	124
3.67	2.990	1.50	0.021	0.4835	0.4835	0.0023	0.0194	0.0056	141
3.67	2.990	1.50	0.0166	0.4835	0.4835	0.0045	0.0194	0.0056	125
3.67	2.990	1.50	0.0183	0.4835	0.4835	0.0068	0.0194	0.0056	128
3.67	2.990	1.50	0.019	0.4835	0.4835	0.0091	0.0194	0.0056	137
3.67	2.990	1.50	0.0196	0.4835	0.4835	0.0023	0.0194	0.0077	147
3.67	2.990	1.50	0.0186	0.4835	0.4835	0.0045	0.0194	0.0063	129
3.67	2.990	1.50	0.0192	0.4835	0.4835	0.0045	0.0194	0.0077	153
3.67	2.990	1.50	0.0185	0.4835	0.4835	0.0068	0.0194	0.0077	153
3.67	2.990	1.50	0.0212	0.4835	0.4835	0.0091	0.0194	0.0077	160
4.83	2.990	2.08	0.0195	0.4835	0.4835	0	0.0194	0	47
4.83	2.990	2.08	0.0161	0.4835	0.4835	0.0023	0.0194	0.0042	88
35 Normal strength deep beam(F. Kong, Robins, & Cole, 1970)									
1.05	9.526	0.35	0.0215	0	0.028	0	0	0.0245	239
1.28	7.855	0.43	0.0246	0	0.028	0	0	0.0245	224
1.62	6.184	0.54	0.0212	0	0.028	0	0	0.0245	190
2.22	4.513	0.74	0.0212	0	0.028	0	0	0.0245	164
3.53	2.842	1.18	0.0217	0	0.028	0	0	0.0245	90
1.05	9.526	0.35	0.0192	0	0.303	0	0	0.0086	249
1.28	7.855	0.43	0.0186	0	0.303	0	0	0.0086	224

‘Table 4.24, continued’									
1.62	6.184	0.54	0.0199	0	0.303	0	0	0.0086	216
2.22	4.513	0.74	0.0228	0	0.303	0	0	0.0086	140
3.53	2.842	1.18	0.0201	0	0.303	0	0	0.0086	100
1.05	9.526	0.35	0.0226	0.28	0	0.0245	0	0	276
1.28	7.855	0.43	0.0210	0.28	0	0.0245	0	0	226
1.62	6.184	0.54	0.0192	0.28	0	0.0245	0	0	208
2.22	4.513	0.74	0.0219	0.28	0	0.0245	0	0	159
3.53	2.842	1.18	0.0226	0.28	0	0.0245	0	0	87
1.05	9.526	0.35	0.0220	0.303	0	0.0086	0	0	242
1.28	7.855	0.43	0.0210	0.303	0	0.0086	0	0	201
1.62	6.184	0.54	0.0201	0.303	0	0.0086	0	0	181
2.22	4.513	0.74	0.0220	0.303	0	0.0086	0	0	110
3.53	2.842	1.18	0.0226	0.303	0	0.0086	0	0	96
1.05	9.526	0.35	0.0186	0.28	0.28	0.0061	0	0.0061	240
1.28	7.855	0.43	0.0192	0.28	0.28	0.0061	0	0.0061	208
1.62	6.184	0.54	0.0201	0.28	0.28	0.0061	0	0.0061	173
2.22	4.513	0.74	0.0219	0.28	0.28	0.0061	0	0.0061	127
3.53	2.842	1.18	0.0226	0.28	0.28	0.0061	0	0.0061	78
1.05	9.526	0.35	0.0261	0.303	0	0.0051	0	0	308
1.28	7.855	0.43	0.0251	0.303	0	0.0061	0	0	266
1.62	6.184	0.54	0.0261	0.303	0	0.0077	0	0	245
2.22	4.513	0.74	0.0261	0.303	0	0.0102	0	0	173
3.53	2.842	1.18	0.0251	0.303	0	0.0153	0	0	99
1.05	10.026	0.35	0.0251	0.303	0	0	0	0	253
1.05	10.026	0.35	0.0261	0.303	0	0.0017	0	0	300
1.05	10.026	0.35	0.0251	0.303	0	0.0034	0	0	260
1.05	10.026	0.35	0.0213	0.303	0	0.0068	0	0	264
1.05	10.026	0.35	0.0213	0.303	0	0.0085	0	0	297
21 Deep beams(Zhang & Tan, 2010)									
2.82	2.22	0.56	31.4	0	0	0	0.0100	0	446.9
3.78	3.47	0.54	31.4	0	0	0	0.0098	0	535.1
2.7	3.47	0.54	31.4	0	0	0	0.0098	0	479.2
1.97	4.28	0.55	31.4	0	0	0	0.0100	0	596.8
1.71	5.84	0.53	31.4	0	0	0	0.0090	0	582.1
3.94	2.22	1.13	31.4	0	0	0	0.0100	0	192.1
3.94	2.22	1.13	31.4	0	0	0	0.0100	0	311.6
3.78	3.47	1.08	31.4	0	0	0	0.0098	0	375.3
3.066	4.28	1.09	31.4	0	0	0	0.010	0	271.5
3.066	4.28	1.09	31.4	0	0	0	0.010	0	330.3
2.78	5.84	1.07	31.4	0	0	0	0.009	0	543.9
2.82	2.22	0.56	78.5	0	0	0	0.010	0	733.0
3.78	3.47	0.54	78.5	0	0	0	0.0098	0	823.2
1.97	4.28	0.55	78.5	0	0	0	0.010	0	1010.4
1.71	5.84	0.53	78.5	0	0	0	0.009	0	1029
3.94	2.22	1.13	78.5	0	0	0	0.010	0	498.8

‘Table 4.24, continued’.									
3.94	2.22	1.13	78.5	0	0	0	0.010	0	385.1
3.78	3.47	1.08	78.5	0	0	0	0.0098	0	573.3
3.06	4.28	1.09	78.5	0	0	0	0.010	0	338.1
3.06	4.28	1.09	78.5	0	0	0	0.010	0	360.6
2.78	5.84	1.07	78.5	0	0	0	0.009	0	769.3
12 Deep beams(Keun-Hyeok Yang, Chung, Lee, & Eun, 2003)									
3.35	3.912	1.10	0.0259	0	0.426	0	0.0125	0.00470	99.5
3.30	3.950	1.10	0.0274	0	0.426	0	0.0128	0.00330	186.5
3.27	4.010	1.10	0.0283	0	0.370	0	0.0122	0.00420	427.0
3.32	3.930	1.10	0.0287	0	0.455	0	0.0120	0.00455	775.0
3.34	3.925	1.10	0.0274	0	0	0	0.0125	0	85.0
3.27	5.740	1.10	0.0324	0	0	0	0.0115	0	135.5
3.23	8.125	1.10	0.0248	0	0	0	0.0128	0	155.5
3.24	11.57	1.10	0.0306	0	0	0	0.0126	0	241.5
3.34	3.925	1.10	0.0274	0	0	0	0.0125	0	85.0
3.30	3.950	1.10	0.0283	0	0	0	0.0128	0	167.0
3.27	4.010	1.10	0.0287	0	0	0	0.0122	0	360.5
3.32	3.930	1.10	0.0293	0	0	0	0.0120	0	672.0
2.82	2.220	0.56	31.400	0	0	0	0.0100	0	446.9

The dataset of the different parameters used in ANFIS are presented in Table 4.25.

Table 4.25: Different parameters of the eight HSSCC deep beams used in ANFIS

Input Parameters									Output
L/d	f_c	d/b_w	a/d	f_{yh}	f_{yv}	ρ_h	ρ	ρ_v	V

where:

L/d = effective span to effective depth ratio

f_c = concrete cylinder strength

d/b_w = effective depth to breadth ratio,

a/d = shear span to effective depth ratio

f_{yh} = yield strength of horizontal reinforcement,

f_{yv} = yield strength of vertical web reinforcement,

ρ_h = horizontal web reinforcement ratio

ρ = longitudinal reinforcement to area of concrete ratio

ρ_v = vertical web reinforcement (qv) ratio when shear strength (V) was used as the output.

The data set was first normalised using the Gaussian normalisation technique. Then 80% of this normalised data was randomly chosen as the training data and the remaining 20% as the testing data. ANFIS models with different parameters (total of nine) as inputs were implemented using MATLAB version R2010a.

The Genfis2 function based on a subtractive clustering method is used to generate the FIS structures.

Table 4.26 summarises the MSE and R results obtained using the proposed method and the LR separately using the training and testing data.

Table 4.26: Comparison of MSE and R values in the ultimate shear prediction of deep beams using ANFIS and LR

Methods	Training Set			Testing set		
	Instances	MSE	R	Instances	MSE	R
Linear regression	111	0.3135	0.8286	28	0.4672	0.7248
ANFIS	111	0.0025	0.9987	28	0.4334	0.7751

It is noted that the MSE value from ANFIS is approximately 125 times smaller for the training set and 7% smaller for the testing set than values from LR. The R values from ANFIS for the testing data is 0.7751 and for training set is 0.9987, while both are more than the corresponding value in LR.

Figure 4.54 shows the ultimate shear prediction performance from LR and ANFIS for the testing data; the horizontal and vertical axes represent the actual and predicted data respectively. Precise modelling would result in a direct linear relation between the actual and predicted data.

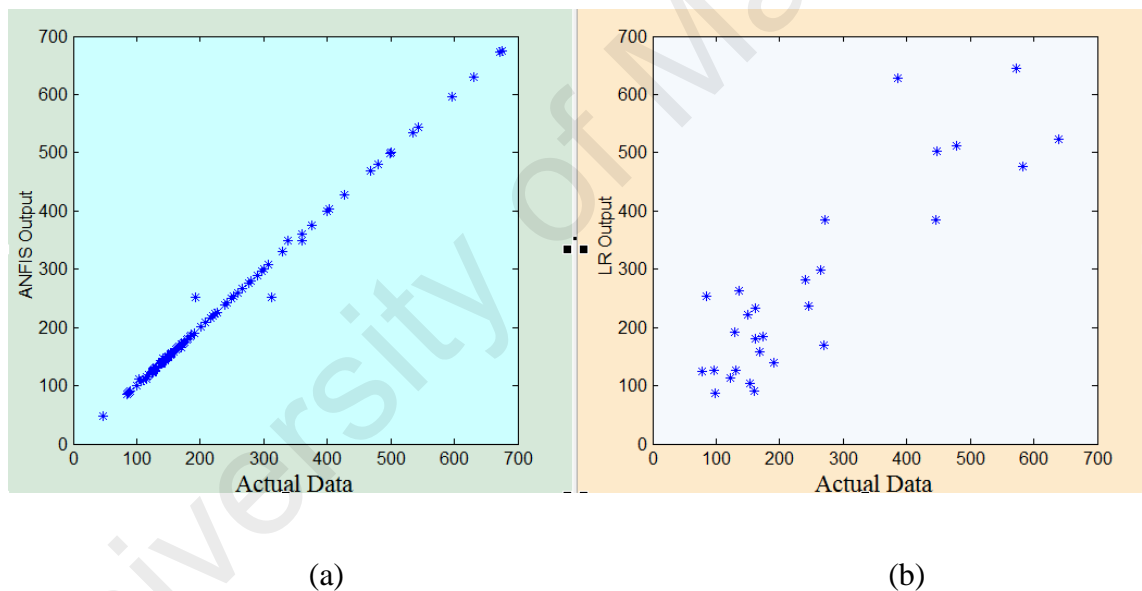


Figure 4.54: Ultimate shear prediction performance from a) ANFIS, b) LR

Figure 4.54 also reveals that the ANFIS method is highly accurate and more precise compared to LR for the ultimate shear prediction of deep beams.

5. NONLINEAR FINITE ELEMENT ANALYSIS

5.1 Introduction

FE modelling is used to analyse the test results reported in Chapter 4. The models were used to help in the prediction of strain at different points of concrete deep beams. The commercial program ABAQUS was used. ABAQUS is a suite of software applications for FE analysis and computer-aided engineering.

5.2 Material Properties

5.2.1 Concrete

The concrete model in ABAQUS can be employed with 2-D or 3-D solid elements. The basic characteristics of the concrete model are as follows:

- 1- Compression crushing failure at the extreme compression fibres at high compressive stresses.
- 2- Strain softening from compression crushing failure to an ultimate strain at which the material fails.
- 3- Tension failures at relatively small tensile stresses.

The tensile and compression failures are governed by stress strain envelopes.

Consideration of the case of biaxial stress states is conducted by employing the stress strain envelope proposed by Kupfer et al. (1969), as shown in Figure 5.1.

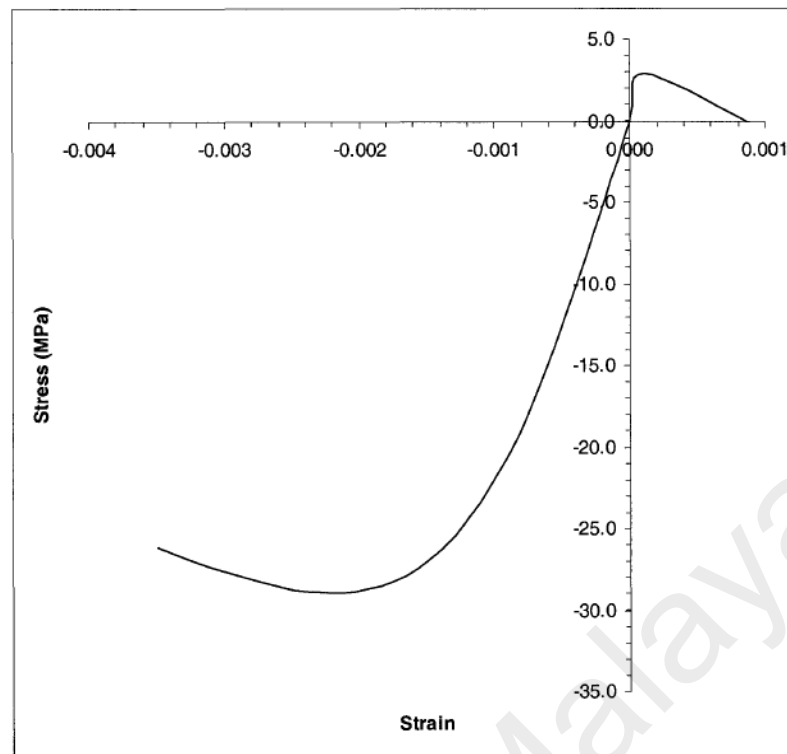


Figure 5.1: Concrete stress-strain curve used in the FE analysis

5.2.2 Steel

The steel reinforcement properties were modelled using the results of the tensile tests presented in Figure 3.3 and Table 3.1. The material model can be used with beam elements.

There are three methods for modelling reinforcement in a reinforced concrete member. These methods are known as disturbed, embedded and discrete and are shown in Figure 5.2.

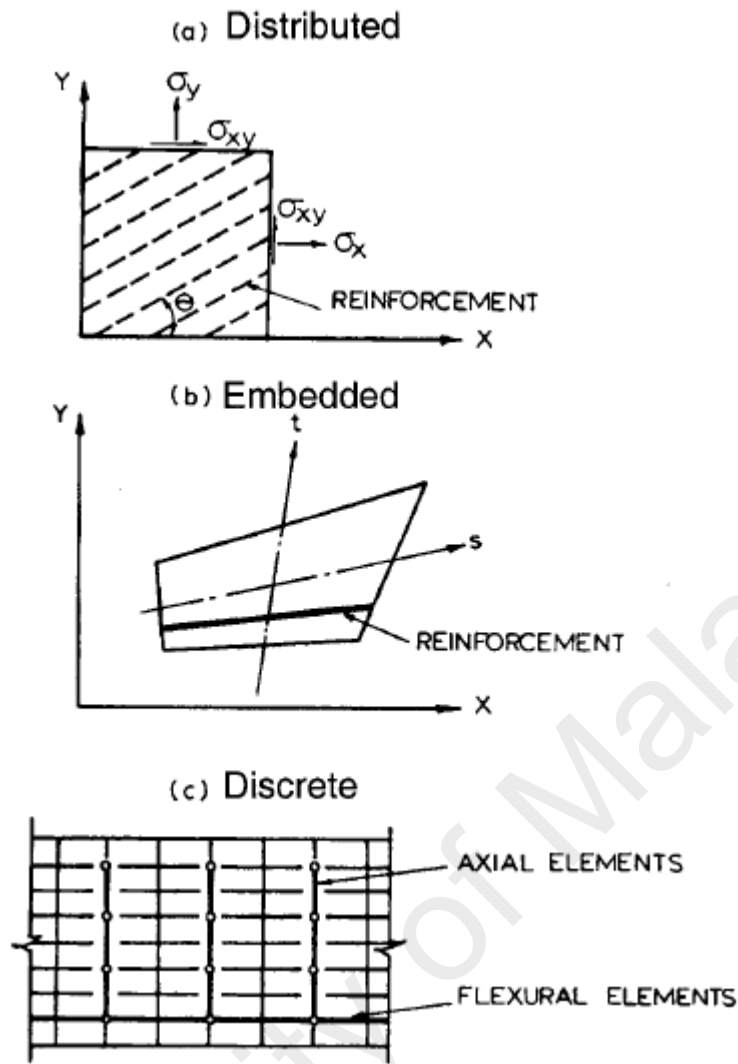


Figure 5.2: Methods of steel reinforcement modelling in concrete (Kupfer et al. (1969))

The disturbed method assumes that the steel is disturbed over the concrete element with a particular orientation. A composite concrete-reinforcement constitutive is used.

With the discrete method, axial force elements are assumed to be pin connected with two degrees of freedom at the nodal points. The one-dimensional reinforcement elements are superimposed on the two-dimensional FE mesh used to model the concrete.

An embedded method may be used with higher order isoperimetric concrete elements. In this case the reinforcement is considered to be an axial member in the isoperimetric element. A perfect bond is assumed between the concrete and steel.

In this study, a discrete reinforcement method is used.

5.3 Elements

5.3.1 Plane stress element

ABAQUS FE software is able to model kinematic assumptions such as plane stress, plane strain, generalised plane strain and 3-D plane stresses. The deep beams were modelled using eight node 3-D elements. This element is shown in Figure 5.3.

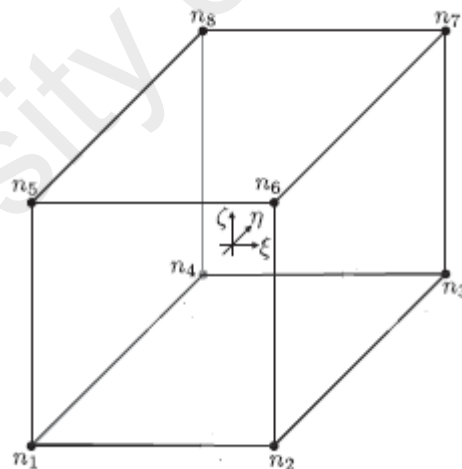


Figure 5.3: Eight node three-dimensional element

5.3.2 Beam element

ABAQUS is able to employ linear and quadratic beam elements. The steel reinforcement was modelled using beam elements. This element was used for all longitudinal, horizontal and vertical reinforcement. Figure 5.4 shows a two node beam element.

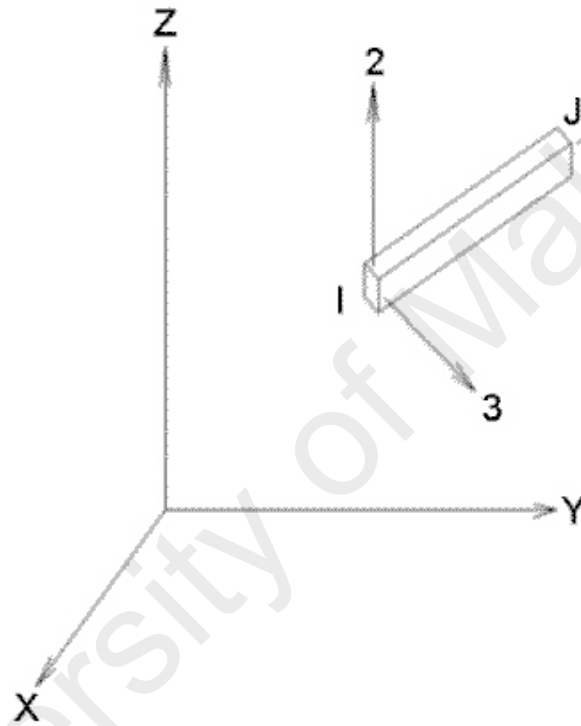


Figure 5.4: Two node beam element used to model the steel reinforcement

5.4 Finite Element Models

Although all beams were modelled, only three series are presented here. Three of the beams with different failure modes are chosen for FE modelling. In beam B1, all horizontal, vertical and tensile bars were of normal steel strength (NSS), while in beam

B2 only the tensile reinforcement was high-strength steel (HSS). In beam B8 all horizontal, vertical and tensile reinforcement was HSS.

Beam B1 and B2 were modelled using 7200 nodes, 5831 plane stress elements and 897 two node beam elements. Beam B6 was modelled using 7200 nodes, 5831 plane stress elements and 1020 two node beam elements. The concrete elements used were 8 node plane stress elements; the steel was modelled with beam elements. The FE models used are shown in Figure 5.5.

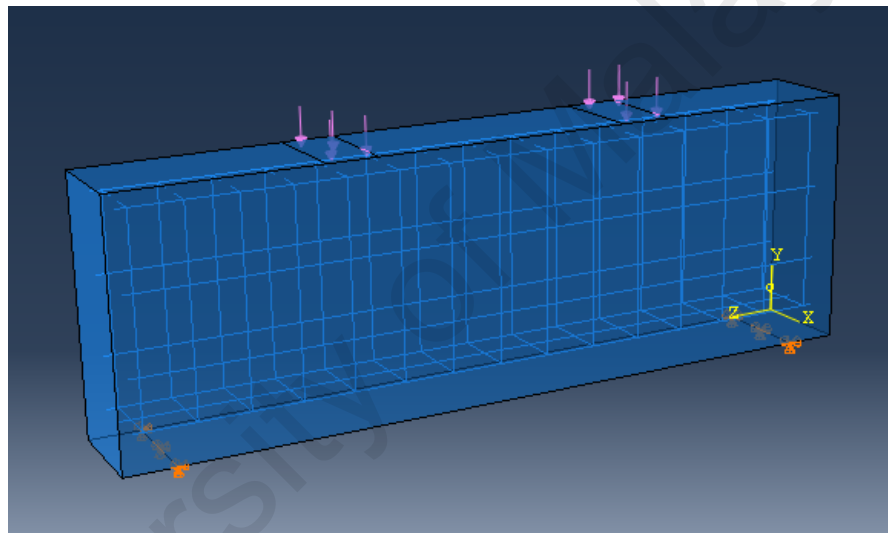


Figure 5.5: FE modelling

5.5 Finite Element Results

The FE model for beams B1, B2 and B6 predicted a failure load of 603 kN, 811 kN and 1318 kN respectively. These FE modelling results compare very well with the observed failure at 510.8 kN, 743.8 kN and 1950.7 kN for beams B1, B2 and B6 respectively. The comparisons of real and FE results of load-deflection graphs at the mid-span of beam lengths are shown in Figures 5.6, 5.7 and 5.8 for beams B1, B2 and B6 respectively.

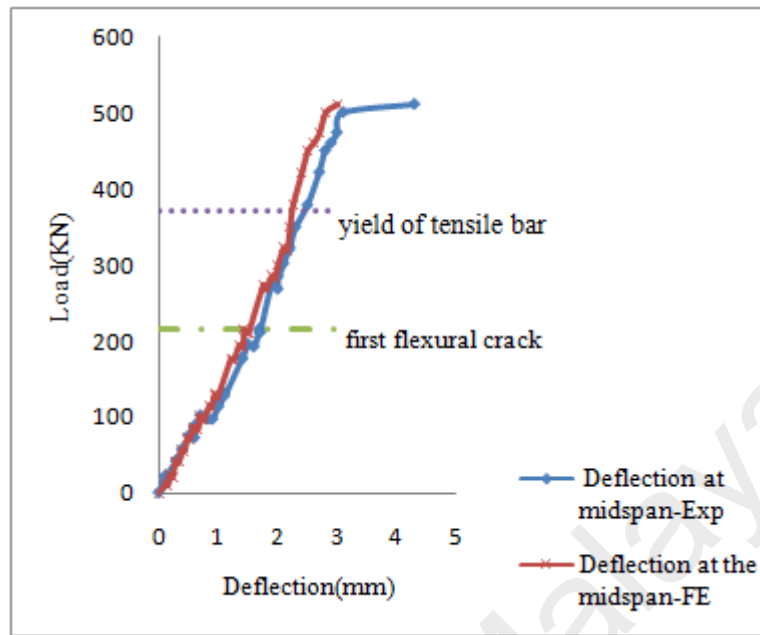


Figure 5.6: Comparison of experimental and FE analysis of deflection for beam B1

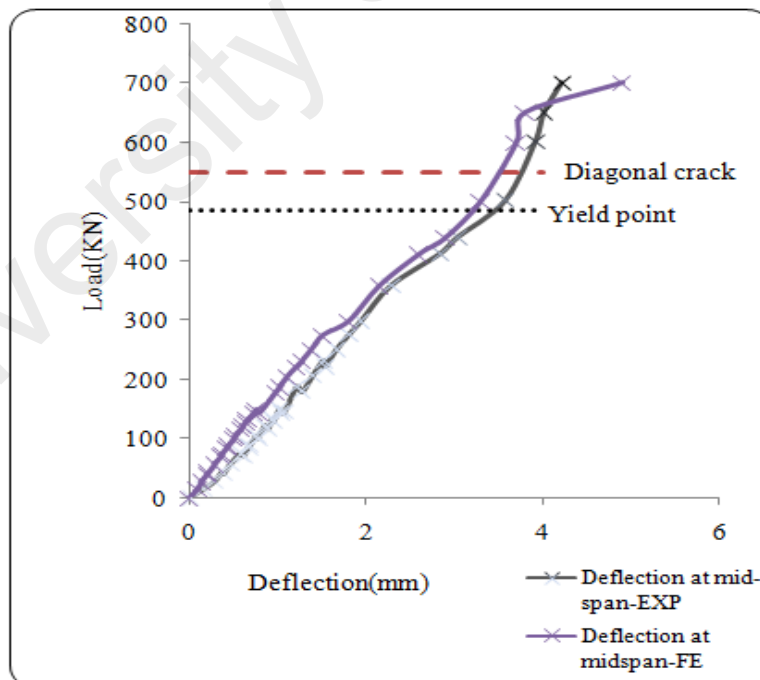


Figure 5.7: Comparison of experimental and FE analysis of deflection for beam B2

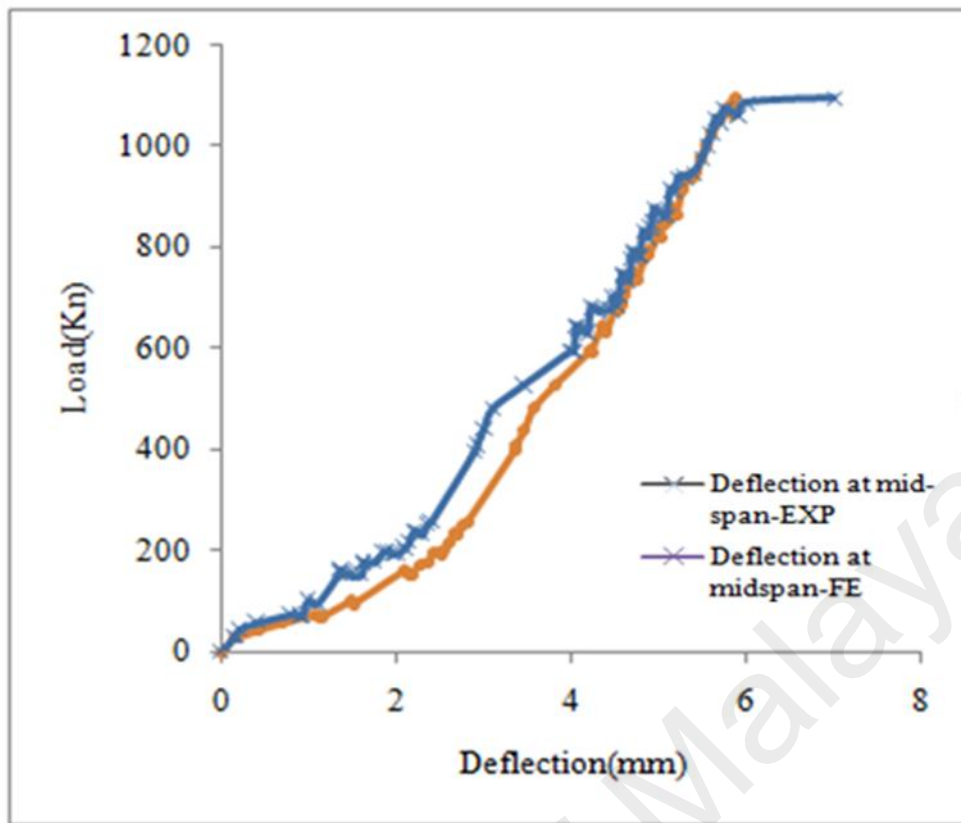


Figure 5.8: Comparison of experimental and FE analysis of deflection for beam B6

Contour plots for the deflection of deep beam tested are shown in Figures 5.9 to 5.13.

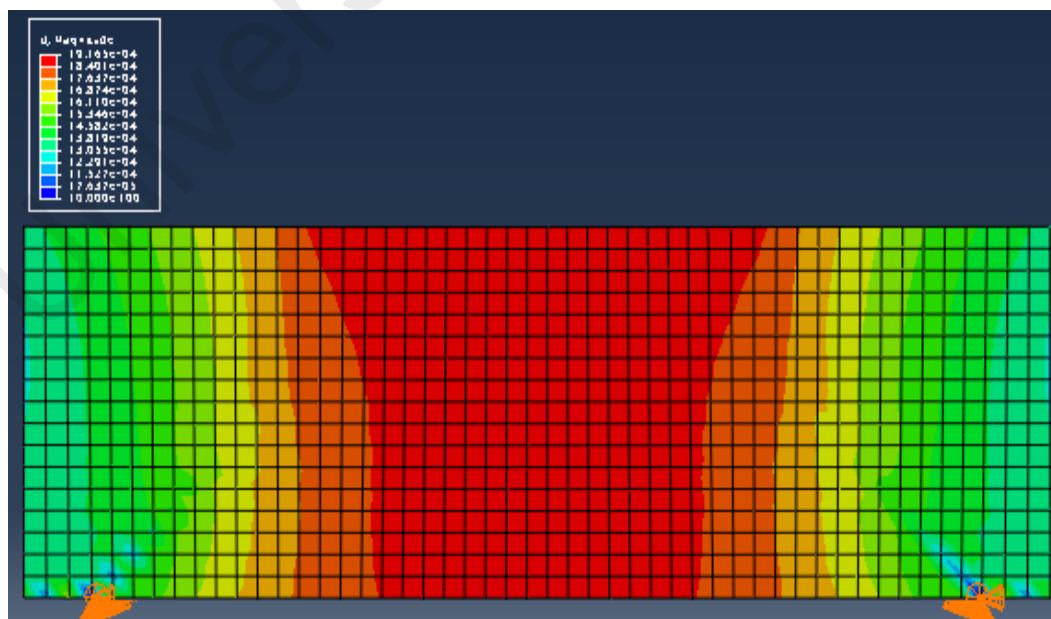


Figure 5.9: Deflection of beam B1 as determined by FE analysis at a loading of 215 kN

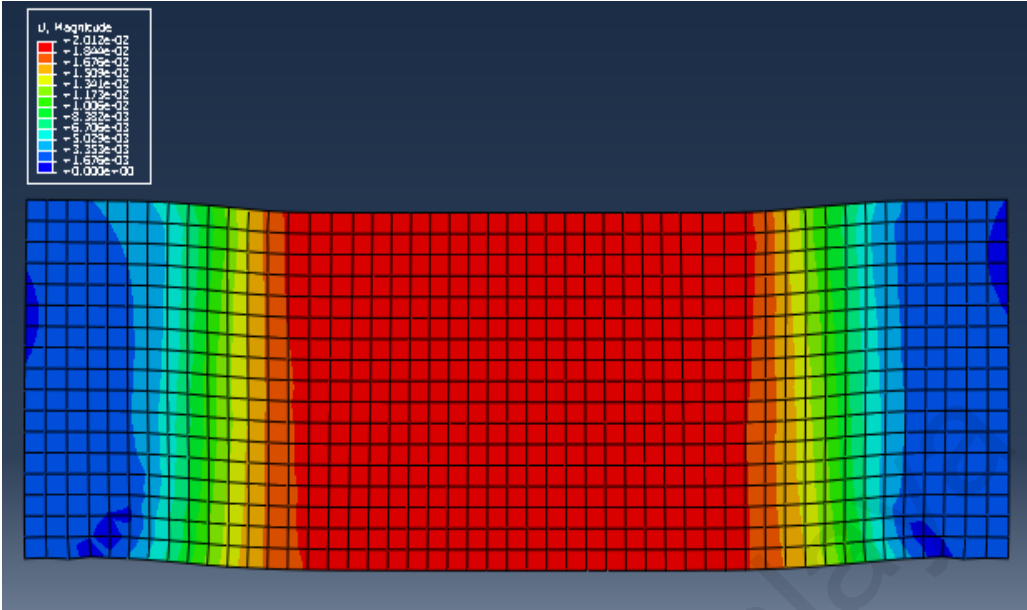


Figure 5.10: Deflection of beam B1 as determined by FE analysis at a loading of 402

kN

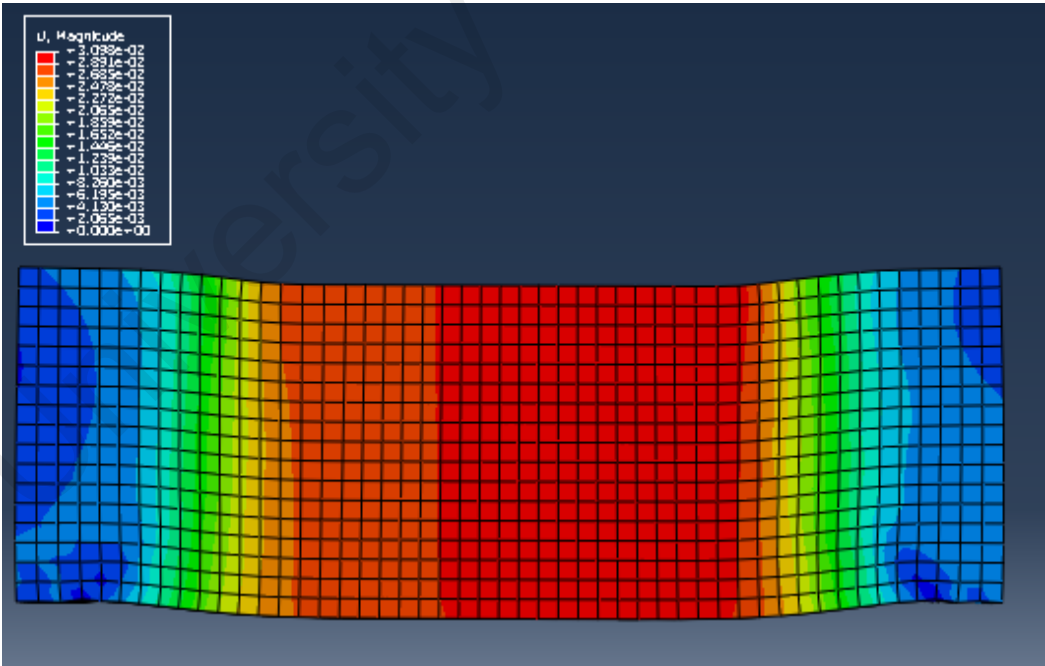


Figure 5.11: Deflection of beam B1 as determined by FE analysis at a loading of 510

kN

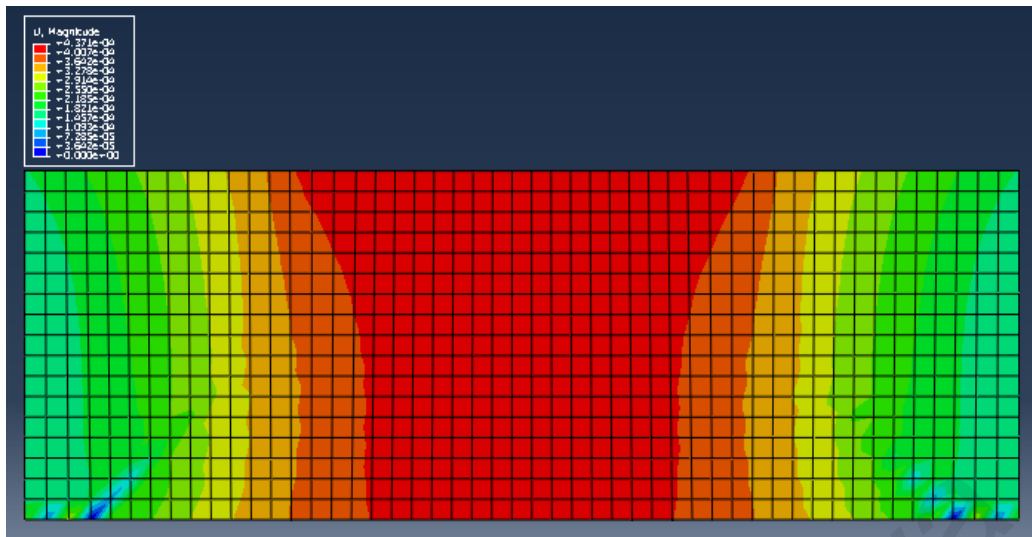


Figure 5.12: Deflection of beam B2 as determined by the FE analysis at a loading of 743 kN

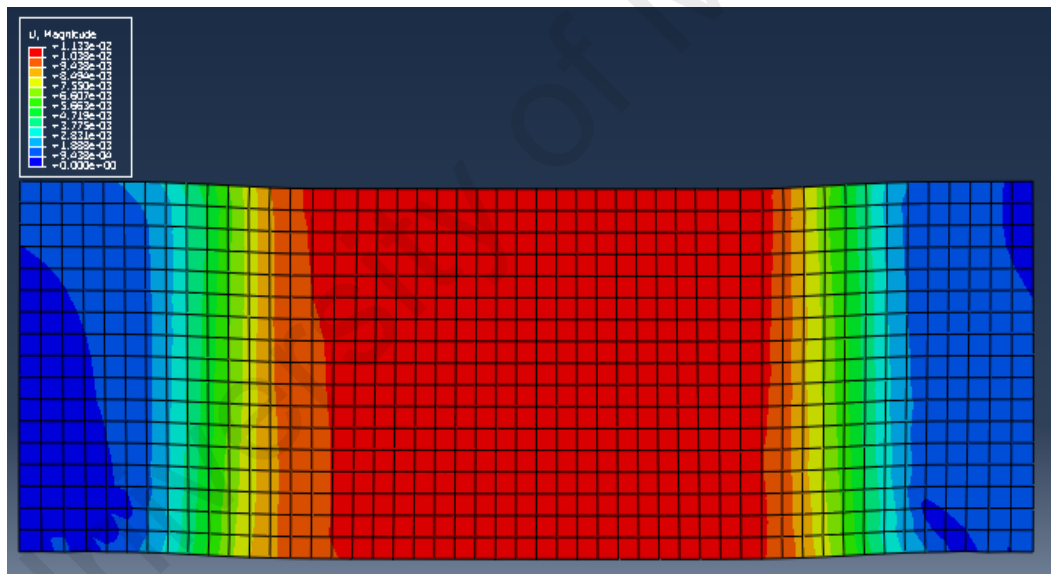
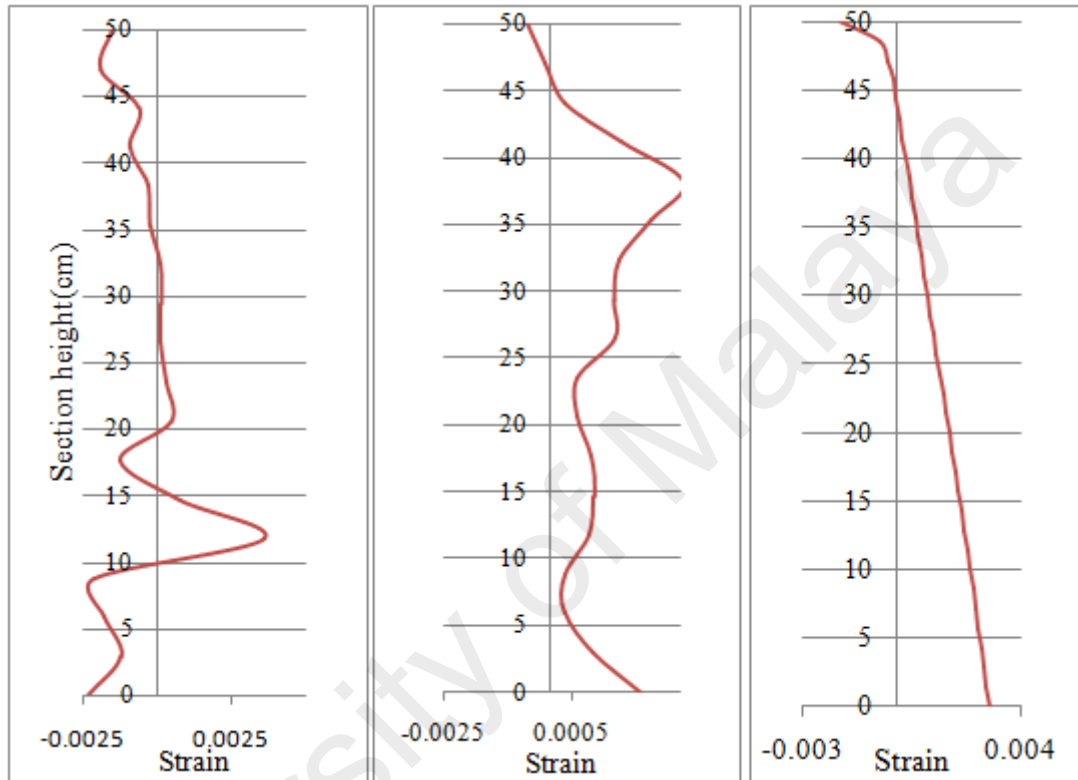


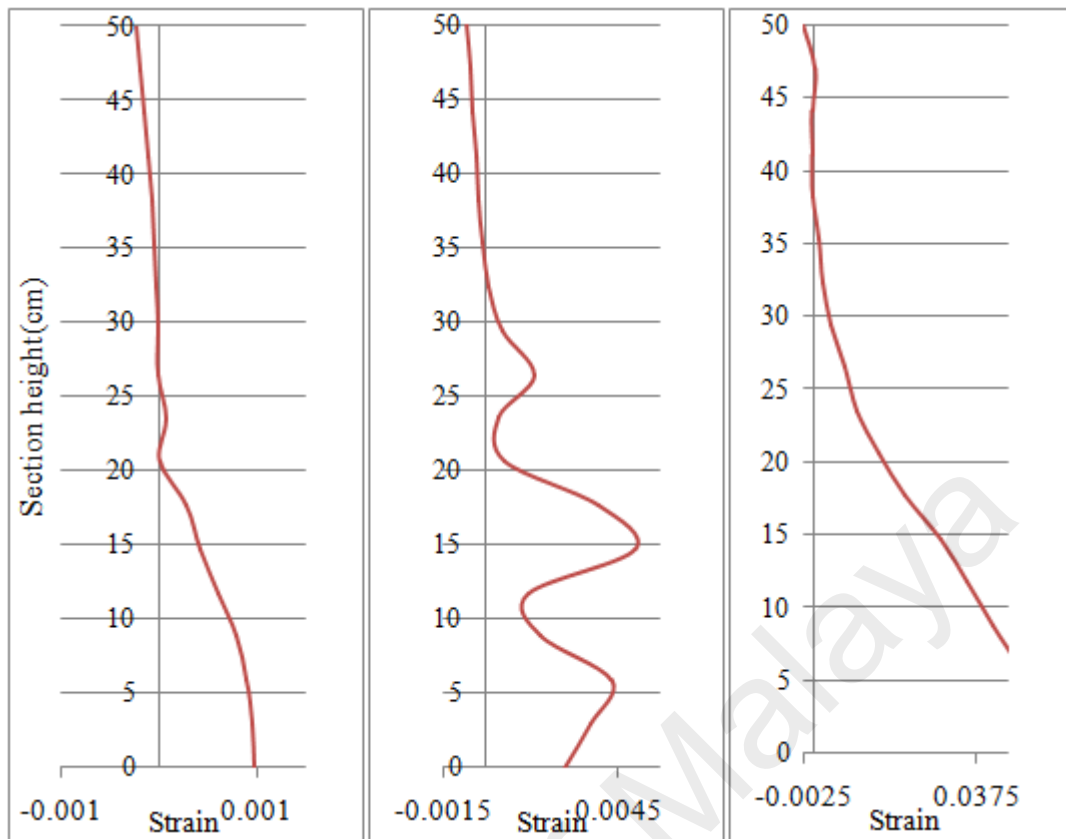
Figure 5.13: Deflection of beam B6 as determined by the FE analysis at a loading of 1100 kN

Plots of the strain variations determined by the FE analysis along the section height at the mid length and neutral axis depth (N.A.D) variations of beams B1, B2 and B6 are shown in Figures 5.14, 5.15 and 5.16 respectively.



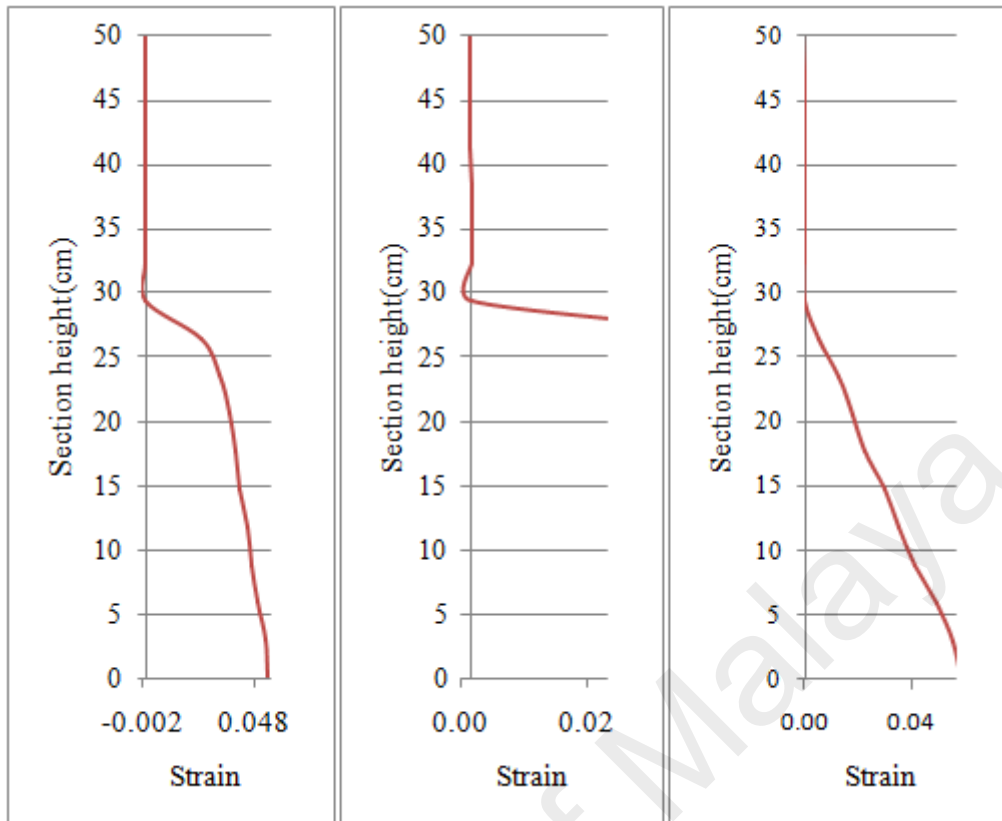
a) First crack b) Specified load (P=401KN) c) Ultimate load

Figure 5.14: NAD variations at mid-span at different loading stages for beam B1 using FE modelling



a) First crack b) Specified load (P=500KN) c) Ultimate load

Figure 5.15: NAD variations at mid-span at different loading stages for beam B2 using FE modelling



a) First crack b) Specified load (P=800KN) c) Ultimate load

Figure 5.16: NAD variations at mid-span at different loading stages for beam B6 using FE modelling

Counter plots of compressive stresses are shown in Figures 5.17 to 5.21 for increasing loads. The development of the compression strut is clearly shown in these figures. These results support the concept of the strut and tie modelling of deep beams.

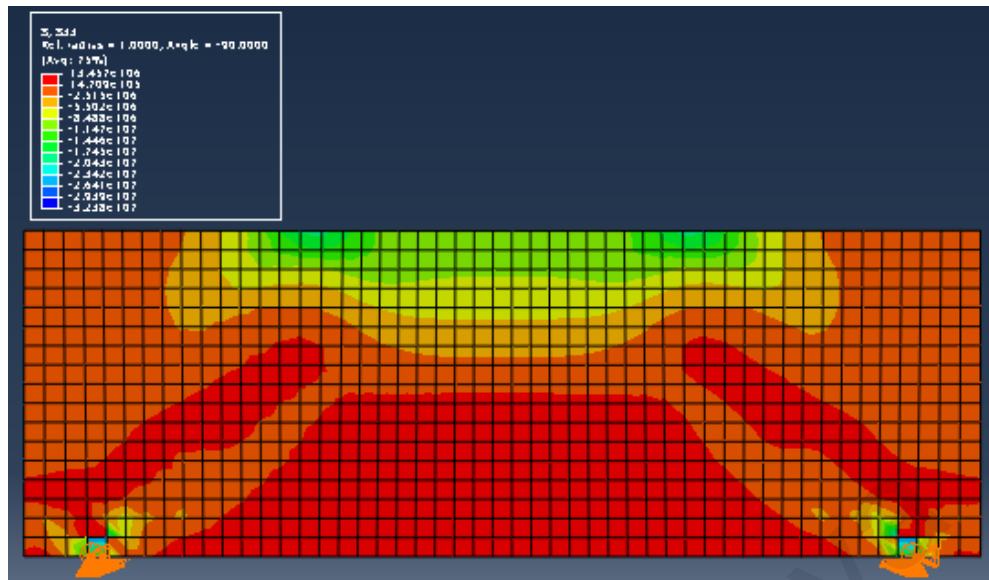


Figure 5.17: Compressive stresses at a loading of 215.8 kN for beam B1

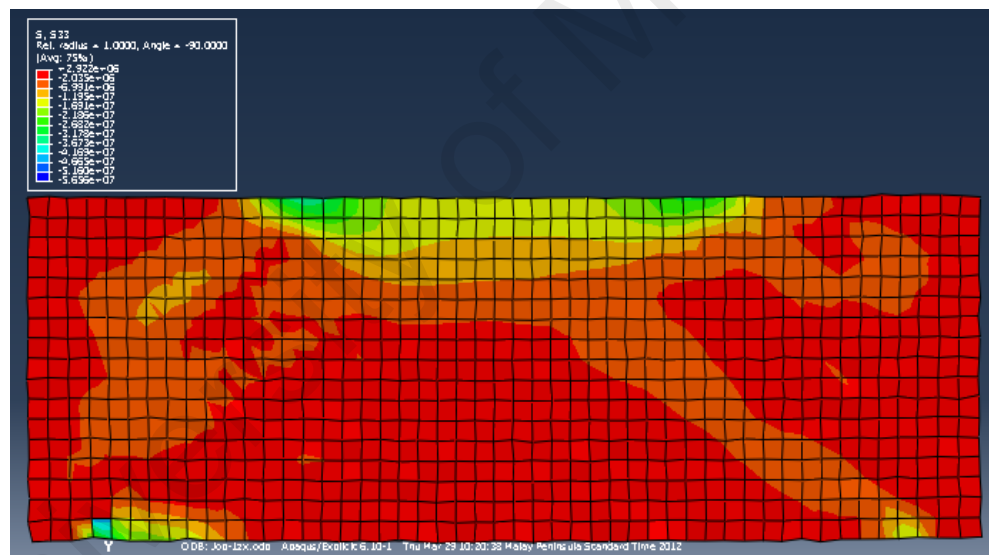


Figure 5.18: Compressive stresses at a loading of 401 kN for beam B1

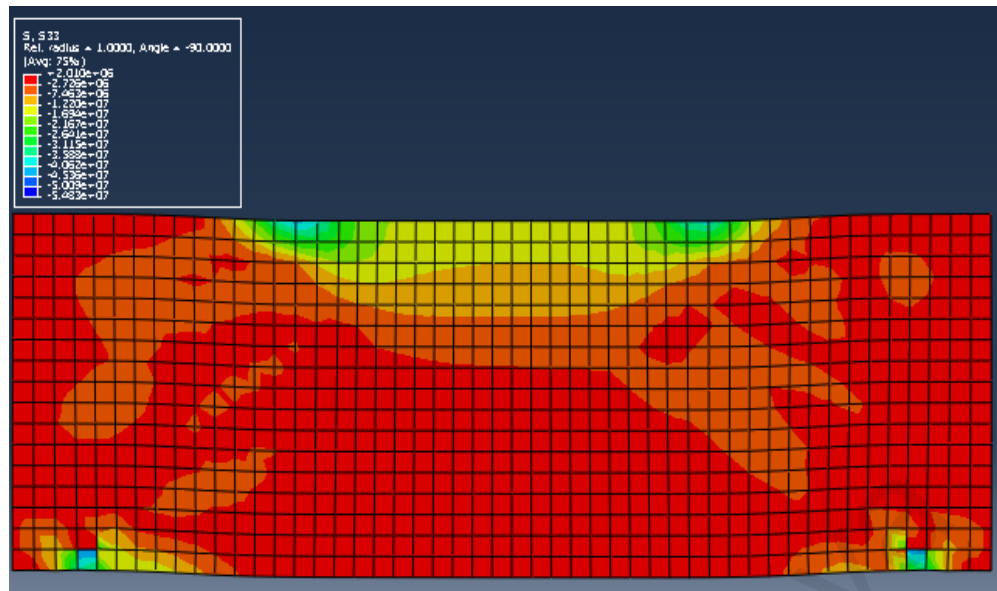


Figure 5.21: Compressive stresses at a loading of 1100 kN for beam B6

5.6 Summary

This chapter will first examine the validity of the FE models, then the strain distribution and strain variation will be studied using the results from the models.

Before conclusions can be drawn from the FE models, it is necessary to determine their validity. Table 5.1 lists the calculated capacity of the test samples as determined by the ABAQUS FE models.

Table 5.1: Comparison of experimental and FE measured values of the failure loads of the test samples

Beams	$P_{u_{exp}}$ (kN)	$P_{u_{FE}}$ (KN)	$\frac{P_{u_{exp}}}{P_{u_{FE}}}$
B1	510.8	603	0.85
B2	743.7	811	0.92
B3	806.9	848	0.95
B4	677.6	703	0.96
B5	661.6	726	0.91
B6	1206.1	1318	0.92
B7	1633.0	1750	0.93
B8	1950.7	2128	0.92

As can be seen from this table, the models accurately predicted the ultimate capacity of the test samples. Ultimate capacity by itself is not sufficient in determining the overall accuracy of the model; other factors must also be checked. Thus deflection graphs were drawn comparing the experimental model with the ABAQUS predictions. As can be seen in Figures 5.6, 5.7 and 5.8, the deflection predicted for the deep beam samples compared well with the actual recorded deflection. This is an excellent indication that the models are behaving in a similar manner to the experimental results.

Figures 5.14 to 5.16 show the variation in strain and N.A.D. predicted by FE analysis, and Figures 4.1, 4.2 and 4.6 show the variation in strain and N.A.D. recorded from the strain gauges applied to the test samples. As can be seen from these graphs, the predicted N.A.D. and strain variation are in good agreement with those recorded and

analysed from test results, indicating that the beams were modelled correctly and that the behaviour of the FE model is similar to that of the test samples.

Comparison of the FE modelling results and experimental results leads us to believe that the FE analysis is accurately modelling the test beams. The following summary is the results of the FE modelling of the deep beams tested.

As can be seen from the comparison of the experimental and FE modelling of the strain variation and deflection of the deep beams tested, the ABAQUS FE modelling software accurately represents the test samples.

The strain distribution along the height of mid-span section is nonlinear with more than one neutral axis depth; however it changes to almost linear with one neutral axis depth at the ultimate load. The strain in the extreme compression fibre is less than 0.0025 and it is less than 0.002 in the compression strut trajectory used by the Canadian code provision. Comparison of the failure load predicted by FE modelling and experimental values shows that the FE modelling predicts a value of 15% more than the experimental value in the beam with a tensile reinforcement ratio less than the minimum one suggested by the design code. This comparison is less than 10% in the other deep beams tested.

7.0 References:

ACI Committee 363, 1984”State-of-the-Art Report on High Strength Concrete”, ACI Journal, 81(4),364-399.

ACI Committee 318, 1995,“ Building Code Requirements for Reinforced Concrete“, (ACI 318-95) and Commentary, American Concrete Institute, Detroit.

ACI Committee 318, 2005, “Building Code Requirements for Reinforced Concrete (ACI 318-05) and Commentary (ACI 318R-05)” American Concrete Institute, Farmington, Hills, Mich.,430pp.

ACI Committee 318, 2008, “Building Code Requirements for Structural Concrete (ACI 318-08) and Commentary (ACI 318R-08)”. American Concrete Institute, Farmington Hills, MI: ACI.

Adeli, H. (2001). Neural Networks in Civil Engineering,1989-2000. Comput-Aided Civil Infrastruct Eng, 16(1), 26-42.

Ahmad, S. H., & Shah, S. P. (1985). Structural Properties of High Strength Concrete and Its Implications for Precast Prestressed Concrete. PCI Journal, 30(4-6), 92-119.

Alavi , N., Nozari , V., Mazlounzadeh , S. M., & Nezamabadi-pour, H. (2010). Irrigation water quality evaluation using adaptive network-based fuzzy inference system. Paddy Water Environ 8(3), 259-266.

Ansley, M. H. (2002). Investigation into the Structural Performance of MMFX Reinforcing. Tallahassee, Florida: MMFX Steel corporation.

Arabzadeh, A., Aghayari, R., & Rahai, A. R. (2011). Investigation of experimental and analytical shear strength of reinforced concrete deep beams. *International Journal of Civil Engineering*, 9(3), 207-214.

Ashour, A., & Yang, K. H. (2008). Application of plasticity theory to reinforced Concrete deep beams: a review. *Magazine of Concrete Research*, 60(9), 657-664.

Ashour, S. A. (2000). Effect of Compressive Strength and Tensile Reinforcement Ratio on Flexural Behaviour of High-Strength Concrete Beams. *Engineering Structures*, 22(5), 413-423.

Bechtoula, H., Kono, S., & Watanabe, F. (2009). Seismic performance of high strength reinforced concrete columns. *Structural Engineering and Mechanics, An Int'l Journal* 31(6).

Bilgehan, M. (2011). Comparison of ANFIS and NN models-With a study in critical buckling load estimation. *Applied Soft Computing* 11 (4), 3779-3791.

Bilgehan, M., & Turgut, P. (2010). Artificial neural network approach to predict compressive strength of concrete through ultrasonic pulse velocity. *Res. Nondestruct. Eval*, 21(1), 1-17.

Braestrup, M. W., & Nielsen, M. P. (1983). Plastic methods of analysis and design. In Handbook of Structural Concrete, eds Kong, F.K., Evans, R.H., Cohen, E. and Roll, F. Ch.20. London: Pitman.

British Standard Institution, 1985. (BS 8110: Part 1. Code of Practice for Design and Construction). Structural Use of Concrete (Part 1 ed.). London.

Caglar, N. (2009). Neural network based approach for determining the shear strength of circular reinforced concrete columns. Construct Build Mater, 23(10), 3225-3232.

CEB-FIP model code 1978, "Comité Euro-International du Béton/Fédération Internationale de la Précontrainte". Model Code for Concrete Structures, CEB-FIP, Paris.

Chemrouk, M., & Kong, F. K. (2004a). High strength concrete continuous deep beams- with web reinforcement and shear-span variations. Advances in Structural Engineering, 7(3), 229-243.

Chemrouk, M., & Kong, F. K. (2004b). Diagonal cracking and ultimate shear strength of slender high strength concrete deep beams. Advances in Structural Engineering, 7(3), 217-228.

Chow, L., Conway, H. D., & George, W. (1952). Stress in deep beam. Proceedings, ASCE, 78(127).

- CIRIA Guide 2. (1977). "Construction Industry Research and Information Association. The design of deep beams in reinforced concrete". Ove Arup & Partners London
- Cladera, A., & Mari, A. R. (2004). Shear design procedure for reinforced normal and high strength concrete beams using artificial neural networks. Part I: beams without stirrups. *Eng Struct*, 26(7), 917-926.
- Cladera, A., & Mari, A. R. (2004). Shear design procedure for reinforced normal and high strength concrete beams using artificial neural networks. Part II: beams with stirrups. *Eng Struct*, 26(7), 927-936.
- Collins, M. P., & Mitchell, D. (1986). A Rational Approach to Shear Design- The 1984 Canadian Code Provisions. *ACI Journal*, 83(6), 925-933.
- Canadian Standard Association, 1994. "Design of concrete structures for buildings" CAN3-A23.3-M94, Rexdale, Ontario.
- Canadian Standard Association, 2004. " CAN/CSA 23.3-04 Design of concrete structures," CSA, Rexdale, Canada.
- Darwin, D., Browning, J., Van nguyen, T., & Locker, J. C. (2002). mechanical and corrosion properties of high strength, high chromium reinforcing steel for concrete. final report. South Dakota: Departement of Transportation.
- Davis, L. (1991). *Handbook of Genetic Algorithms*: Van Nostrand Reinhold Company

De Paiva, H., & Siess, C. (1965). Strength and Behavior of Deep Beams. ASCE Structural Journal, 91(10), 19-41.

Dischinger, F. (1932). Beitrag zur Theorie der Halbscheibe und des wandartigen Trägers. Assoc. of Bridge and Struct, 1(69).

El-Hacha, R., & Rizkalla, S. (2002). Fundamental Material Properties of MMFX Steel Rebars", Research report (No. RD-02-04 submitted to MMFX Corp): Constructed Facilities Laboratory (CFL), North Carolina State University (NCSU).

Flood, I., & Kartam, N. (1994). Neural networks in civil engineering, principle and understanding. ASCE J Comput Civil Eng, 8(2), 131-148.

Flood, I., Muszynski, L., & Nandy, S. (2001). Rapid analysis of externally reinforced concrete beams using neural networks. Comput Struct, 79(17), 1553-1559.

Garay-Moran J.d.D & Lubell A.S. (2008). behaviour of concrete deep beam with high strength reinforcement. Alberta: University of Alberta.

Geer, E. (1960). Stresses in deep beams. Proceedings, Symposia in Pure Mathematics, 56(39), 651-671.

González, M. a. P., & Zapico, J. L. (2008). Seismic damage identification in buildings using neural networks and modal data. Computers and Structures, 86(3-5), 416-426.

- Hakan Arslan, M. (2010). An evaluation of effective design parameters on earthquake performance of RC buildings using neural networks. *Engineering Structures*, 32(7), 1888-1898.
- Hashemi, S. H., Maghsoudi, A. A., & Rahgozar, R. (2008). Flexural ductility of reinforced HSC beams strengthened with CFRP sheets. *Structural Engineering and Mechanics, An Int'l Journal*, 30(4).
- Haykin, S. (1998). *Neural Networks-A Comprehensive Foundation*. New York: Mcmillan College Publishing.
- Hola, J., & Schabowicz, K. (2005). New technique of nondestructive assessment of concrete strength using artificial intelligence. *NDT&E Int*, 38(4), 251-259.
- Iravani, S. (1996). Mechanical Properties of High-Performance Concrete. *ACI Material Journal*, 93(4), 16-26.
- Jang, J. R., Sun, C. T., & Mizutani, E. (1997). *Neuro-Fuzzy and Soft Computing: A Computational Approach to Learning and Machine Intelligence*. Upper Saddle River, NJ, USA Prentice-Hall
- Jang, J. S. R. (1993). Adaptive network based fuzzy inference system. *IEEE Transactions Systems, Man and Cybernetics*, 23(3), 665-685.
- Kang, F., Li, J., & Xu, Q. (2009). Structural inverse analysis by hybrid simplex artificial bee colony algorithms. *Computers and Structures*, 87(13-14), 861-870.

- Kani, G. (1966). Basic facts concerning shear failure. American Concrete Institute, ACI Journal of the Prestressed Concrete Institute, 63(6), 675-692.
- Kao, C. Y., & Hung, S. L. (2003). Detection of structural damage via free vibration responses generated by approximating artificial neural networks. Computers & Structures, 81(28-29), 2631-2644.
- Khaloo, A.R. and Hoseini, A.(2005). Seismic performance of high-strength concrete columns strengthened with CFRP. Canadian Journal of Civil Engineering., 32(3), 569-578.
- Khaloo, A.R. and Kim, N. (1996). Mechanical properties of normal to high-strength steel fiber reinforced concrete. cement, concrete, and aggregates (ASTM Journal)., 18(2), 92-97.
- Khaloo, A.R. and Ghodrati Amiri, G.R. (1995). Moment-curvature analysis of confined concrete flexural members. Asian Jrnl. of Structural Eng., 1(2), 103-127.
- Kong, F., Robins, P., & Cole, D. (1970). Web reinforcement effects on deep beams. ACI struct J, 67(73), 1010-1017.
- Kong, F. K. (2003). Reinforced concrete deep beams (Vol.). new york: taylor&francis book, inc.
- Kong, F. K., & Singh, A. (1972). Diagonal cracking and ultimate loads of lightweight concrete deep beams. Proc. Am. Concr. Inst, 69(8), 513.

Kupfer, H., Hilsdorf, H. K., & Rusch, H. (1969). Behavior of concrete under biaxial stresses.

Lai, S., & Serra, M. (1997). Concrete strength prediction by means of neural network. *Construct Build Mater*, 11(2), 93-98.

Lambotte, H., & Taerwe, L. R. (1990). Deflection and Cracking of High Strength Concrete Beams and Slabs. Paper presented at the High Strength Concrete, Second International Symposium, Farmington Hills.

Lautour, O. R. D., & Omenzetter, P. (2009). Prediction of seismic-induced structural damage using artificial neural networks. *Engineering Structures*, 31(2), 600-606.

Lee, S. C. (2003). Prediction of concrete strength using artificial neural networks. *Eng Struct*, 25(7), 849-857.

Leonhardt, F., & Walther, R. (1966). *Wandartige Trager (Deep Beams)*. : Deutscher Ausschuss fur Stahlbeton Bulletin. Wilhelm Ernst and Sohn (Berlin).

Lu, W. Y., Hwang, S. J., & Lin, I. J. (2010). Deflection prediction for reinforced concrete deep beams. *Computers and Concrete*, 7(1).

Malhas, F. A. (2002). Preliminary Experimental Investigation of the Flexural Behavior of Reinforced Concrete Beams Using MMFX Steel. MMFX Steel Corporation, 55.

- Mamdani, E., & Assilian, S. (1975). An experiment in linguistic synthesis with a fuzzy logic controller. *Int J Man Mach Stud*, 7(1), 1-13.
- Mashreia, M. A., Abdulrazzaqb, N., Abdallac, T. Y., & Rahmand, M. S. (2010). Neural networks model and adaptive neuro-fuzzy inference system for predicting the moment capacity of ferrocement members *Engineering Structures*, 32(6), 1723-1734.
- Masri, S., Smyth, A., Chassiakos, A., Cauthey, T., & Hunter, N. (2002). Application of neural networks for detection of changes in nonlinear system. *J Eng Mech, ASCE*, 126(7), 666-676.
- Mazlounzadeh, S. M., Shamsi , M., & Nezamabadi-pour , H. (2010). Fuzzy logic to classify date palm trees based on some physical properties related to precision agriculture. *Precision Agric* 11(3), 258-273.
- Mendel, J. M. (1995). Fuzzy logic systems for engineering: a tutorial. *Proc. IEEE* 83(3), 345-377.
- Mohammadhassani, M., Jumaat, M. Z., Ashour, A., & Jameel, M. (2011a). Failure modes and serviceability of high strength self compacting concrete deep beams. *engineering failure analysis*, doi:10.1016/j.engfailanal.2011.08.003.
- Mohammadhassani, M., Jumaat, M. Z., Chemrouk , M., Maghsoudi, A. A., Jameel , M., & Akib, S. (2011b). An experimental investigation on bending stiffness and neutral axis depth variation of over-reinforced high strength concrete beams. *Nuclear Engineering and Design*, 241(6), 2060-2067.

- Möller, B., Liebschera, M., Schweizerhofb, K., Matternb, S., & Blankenhornb, G. (2008). Structural collapse simulation under consideration of uncertainty - Improvement of numerical efficiency. *Computers and Structures*, 86(19-20), 1875-1884.
- Moody, K. G., Viest, I. M., Elstner, R. C., & Hognestad, E. (1954). Shear Strength of Reinforced Concrete Beams Part 2 - Tests of Restrained beams Without Web Reinforcement.
- Naderpour, H., Kheyroddin, A., & Amiri, G. G. (2010). Prediction of FRP-confined compressive strength of concrete using artificial neural networks. *Compos Struct*, 92(12), 2817-2829.
- Ni, H.-G., & Wang, J.-Z. (2000). Prediction of compressive strength of concrete by neural networks. *Cement Concrete Res*, 30(8), 1245-1250.
- Nielsen, M. P. (1971). On the Strength of Reinforced Concrete Discs. Copenhagen, Acta Polytechnica Scandinavica, Civil Engineering and Building Construction Series
- Oh, J. K., & Shin, S. W. (2001). Shear strength of reinforced high strength concrete deep beam. *ACI structural Journal*, 8(2), 164-173.
- Ozcan, F., Atis, C. D., Karahan, O., Uncuoglu, E., & Tanyildizi, H. (2009). Comparison of artificial neural network and fuzzy logic models for prediction of long-term compressive strength of silica fume concrete. *Adv Eng Software*, 40(9), 856-863.

- Pal, M., & Deswal, S. (2011). Support vector regression based shear strength modelling of deep beams. *Computers and Structures*, 89(13-14), 1430-1439.
- Park, J.-W., & Kim, S.-E. (2008). Force transfer mechanisms for reliable design of reinforced concrete deep beams. *Structural Engineering and Mechanics*, 30(1).
- Paulson, K. A., Nilson, A. H., & Hover, K. C. (1989). Immediate and Long-Term Deflection of High Strength Concrete Beams (No. 89-3). Ithaca: Department of Structural Engineering, Cornell University.
- Pimentel, M., Cachim, P., & Figueiras, J. (2008). DEEP-BEAMs with indirect supports: numerical modelling and experimental assessment. *Computers and Concrete, An Int'l Journal*, 5(2).
- Rajagopalan, K. S., & Ferguson, P. M. (1968). Exploratory Shear Tests Emphasizing Percentage of Longitudinal Steel. *ACI Journal*, 65(8), 634-638.
- Rajasekaran, S., & Vijayalakshmi Pai, G. A. (2004). *neural Networks, Fuzzy Logic and Genetic Algorithms: Synthesis and Applications*: PHI Learning Pvt. Ltd
- Ramakrishnan, V., & Ananthanarayana, Y. (1968). Ultimate Strength of Deep Beams in Shear. *ACI Journal*, 65(2), 87-98.
- Rashid, M. A., & Mansur, M. A. (2005). Reinforced High-Strength Concrete Beams in Flexure. *ACI Structural Journal*, 102(3).

Ray, S. P. (1980). Behaviour and Ultimate Shear Strength of Reinforced Concrete Deep Beams With and Without Opening in Web. PhD THESIS. Unpublished PhD Indian Institute of Technology, Kharagpur, India.

Ray, S. P. (1982). A short review of literature on reinforced concrete deep beams with and without opening in web. J. Struct. Eng., India, 9(1), 5.

Ray, S. P., & Reddy, C. S. (1979). Strength of reinforced concrete deep beams with and without opening in web. Indian Concr. J, 53(9), 242.

Rigoti, M. (2002). Diagonal cracking in reinforced concrete deep beam-An experimental investigation. Concordia University, Montreal, Quebec, Canada.

Rogowsky, D. M., & MacGregor, J. G. (1986). Design of reinforced concrete deep beams. ACI Journal, 8(8), 49-58.

Rosales, M. B., Filipich, C. P., & Buezas, F. S. (2009). Crack detection in beam-like structures Engineering Structures, 31(10), 2257-2264.

Roth, M. J., Slawson, T. R., & Flores, O. G. (2010). Flexural and tensile properties of a glass fiber-reinforced ultra-high-strength concrete: an experimental, micromechanical and numerical study. Computers and Concrete, An Int'l Journal 7(2).

- Sakr, M. A., & Sakla, S. S. S. (2009). Long-term deflection of cracked composite beams with nonlinear partial shear interaction - A study using neural networks Engineering Structures, 31(12), 2988-2997.
- Sanad, A., & Saka, M. P. (2001). Prediction of ultimate strength of reinforced concrete deep beams by neural networks. ASCE J. Struct. Eng, 127(7), 818-828.
- Saridakis, K. M., Chasalevris, A. C., Papadopoulos, C. A., & Dentsoras, A. J. (2008). Applying neural networks, genetic algorithms and fuzzy logic for the identification of cracks in shafts by using coupled response measurements. Comput. Struct, 86 (11-12), 1318-1338.
- Schlaich, J., & Schäfer, K. (1991). Design and Detailing of Structural Concrete Using Strut-and-Tie Models. The Structural Engineer, 69(6), 113-125.
- Schlaich, J., Schafer, K., & Jennewein, M. (1987). Toward a Consistent Design of Structural Concrete. Journal of the Prestressed Concrete Institute, 32(3), 74-150.
- Selvam, V. K. M., & Tomas , k. (1987). Shear strength of concrete deep beam. Indian Concr. J, 61(8), 219-222.
- Seow, P E C and S Swaddiwudhipong.(2005). Failure surface for plain concrete and SFRC under multi-axial loads, a unified approach. Journal of Materials in Civil Engineering, 17 ,219-228.
- Shah, S. P., & Ahmad, S. H. (1998). High Performance Concrete: Properties and Application: McGraw Hill

- Shin, S. W. (1986). Flexural Behaviour Including Ductility of Ultra-High Strength Concrete Member. University of Illinois at Chicago, PhD thesis, Illinois.
- Smith, K. N., & Vantsiotis, A. S. (1982). Shear Strength of Deep Beams. American concrete institute(ACI), 79(3), 201-213.
- Sobhani, J., Najimi, M., Pourkhorshidi, A. R., & Parhizkar, T. (2010). Prediction of the compressive strength of no-slump concrete: a comparative study of regression, neural network and ANFIS models. Construct Build Mater, 24(5), 709-718.
- Swaddiwudhipong, S, E Harsono, J Hua, and Z S Liu. (2008). Reverse analysis via efficient artificial neural networks based on simulated Berkovich indentation. Engineering with Computers. 25 , 126-133.
- Takagi, T., & Sugeno , M. (1985). Fuzzy identification of systems and its applications to modeling and conml. IEEE Transon SMC, 35(1), 116-132.
- Tan, K., Kong, F., Teng, S., & Guan, L. (1995). High-strength concrete deep beams with effective span and shear span variations. ACI struct J, 92(37), 395-405.
- Tan, K., Kong, F., Teng, S., & Weng, L. (1997). Effect of web reinforcement on high-strength concrete deep beams. ACI Structural Journal, 94(5), 572-582.
- Tan, K., & Lu, H. (1999). Shear behavior of large reinforced concrete deep beams and code comparisons. ACI Struct J, 96(5), 836-845.

- Tang, C.-W., Chen, H.-J., & Tsong, Y. (2003). Modeling confinement efficiency of reinforced concrete columns with rectilinear transverse steel using artificial neural networks. *J Struct Eng* 129(6), 775-783.
- Thompson, M. K. (2002). The Anchorage Behavior of Headed Reinforcement in CCT Nodes and Lap Splices. Unpublished Doctoral Dissertation, University of Texas at Austin.
- Van Mier, J. G. M. (1986). Multiaxial strain-softening of concrete, Part I:Fracture, . *Materials and Structures* 19(111), 179-190.
- Vassilopoulos, A. P., & Bedi, R. (2008). Adaptive neuro-fuzzy inference system in modelling fatigue life of multidirectional composite laminates. *Comp. Mater. Sci*, 43(4), 1086-1093.
- Vijay, P. V., GangaRao, H. V. S., & Prachasaree, W. (2002). Bending Behavior of Concrete Beams Reinforced with MMFX Steel Bars: West Virginia University.
- Watstein, D., & Mathey, R. G. (1958). Strains in beams having diagonal cracks. *ACI Journal*, 55(12), 717-728.
- Yang, K.-H., Chung, H.-S., & Ashour, A. F. (2007). Influence of section depth on the structural behaviour of reinforced concrete continuous deep beams. *Magazine of Concrete Research*, 59(8), 575-586.

Yang, K.-H., Chung, H.-S., Lee, E.-T., & Eun, H.-C. (2003). Shear characteristics of high-strength concrete deep beams without shear reinforcements. *Engineering Structures*, 25,doi:10.1016/S0141-0296(03)00110-X, 1343–1352.

Yeh, I. C. (1999). Design of high-performance concrete mixture using neural networks and nonlinear programming. *J Comput Civil Eng*, 13(1), 36-42.

Yilmaz, I., & Kaynar, O. (2011). Multiple regression, ANN (RBF, MLP) and ANFIS models for prediction of swell potential of clayey soils. *Expert Systems with Applications*, 38(5), 5958-5966.

Zadeh, L. A. (1965). Fuzzy sets. *Inform. Control*, 8(3), 338-353.

Zhang, N., & Tan, K.-H. (2010). Effects of support settlement on continuous deep beams and STM modeling. *Engineering Structures*, 32(2), 361-372.